MECHANICAL STRAIN-MEDIATED SYNDECAN REGULATION AND ITS EFFECTS ON ADHESION OF VASCULAR SMOOTH MUSCLE CELLS

A Dissertation
Presented to
The Academic Faculty

By

Mathéau A. Julien

In Partial Fulfillment
of the Requirements for the Degree
Doctor of Philosophy in Bioengineering

Georgia Institute of Technology

May 2005

MECHANICAL STRAIN-MEDIATED SYNDECAN REGULATION AND ITS EFFECTS ON ADHESION OF VASCULAR SMOOTH MUSCLE CELLS

Approved by:

Dr. Elliot L. Chaikof, Advisor
School of Biomedical Engineering
Georgia Institute of Technology
Department of Surgery
Emory University School of Medicine

Dr. Andrew P. Kowalczyk
Department of Dermatology
Emory University School of Medicine

Dr. Andrés J. García, Co-Advisor
School of Mechanical Engineering
Georgia Institute of Technology

Dr. W. Robert Taylor
Department of Medicine
Emory University School of Medicine

Dr. Zorina S. Galis
School of Biomedical Engineering
Georgia Institute of Technology

Date Approved: January 14, 2005

DEDICATION

To my loving and understanding wife Pam,

who had absolutely no idea what she was getting herself into.

And to my son Kéleb,

who provided inspiration through bright-eyed smiles during the final push.

ACKNOWLEDGMENTS

I would like to express my deep appreciation to my thesis advisor, Dr. Elliot Chaikof, for the important role he played during this stage of my career and life. His knowledge, support, and guidance were crucial to my educational experience. I would also like to thank my advisor at Georgia Tech, Dr. Andrés García, for his attention to detail, which helped mold me into a better scientist. In addition, I appreciate the time and effort of the rest of my thesis committee and their interest in my area of study. Special thanks go to Dr. John Chon, Dr. Michelle Houston, and Lisa Cargo for their instruction and assistance as I embarked on my thesis research, to Drs. Wanxing Cui, Shyam Rele, Xue-Long Sun, and Karthik Nagapudi for making daily life in the lab enjoyable, and to Peiyi Wang for helping me work through the final experiments. I would be remiss not to acknowledge Dr. Suri Iyer for never allowing me to take anything too seriously. I also extend my appreciation to Beverly Noe, who was always willing and able to help…with anything, and to Valerie, whose bark is definitely worse than her bite.

I would like to thank my fellow lab members, past and present, for bringing fresh perspectives to my graduate work, and I also appreciate the patience and helpfulness of the various neighboring labs whose time, expertise, and equipment I often seemed to make my own.

Lastly, much gratitude is extended to my family, both old and new, for their profound impact on my life, and for being such good sports by nodding at the appropriate times after making the mistake of asking me to explain my thesis work.

TABLE OF CONTENTS

LIST OF TABLES

LIST OF FIGURES

LIST OF ABBREVIATIONS

ACE	Angiotensin Converting Enzyme
ADAM	A Disintegrin and Metalloprotease
ANOVA	Analysis of Variance
AP-1	Activator Protein 1
APP	β-Amyloid Precursor Protein
ATIII	Antithrombin III
bFGF	Basic Fibroblast Growth Factor
BSA	Bovine Serum Albumin
CHO	Chinese Hamster Ovary
cpm	Counts per Minute
CS	Chondroitin Sulfate
DEAE	Diethylaminoethyl
DMEM	Dulbecco's Modification of Eagle's Medium
ECM	Extracellular Matrix
EGF	Epidermal Growth Factor
ELISA	Enzyme-Linked Immunosorbent Assay
ERK	Extracellular Signal-Regulated Mitogen-Activated Protein Kinase
FACS	Fluorescence-Activated Cell Sorting
FAK	Focal Adhesion Kinase
FBS	Fetal Bovine Serum
FGF	Fibroblast Growth Factor
FN	Fibronectin
GAG	Glycosaminoglycan
GAPDH	Glyceraldehyde-3-Phosphate Dehydrogenase
GFP	Green Fluorescent Protein
GlcA	Glucuronic Acid
GlcNAc	N-Acetyl Glucosamine
GPI	Glycosyl Phosphatidylinositol
HPODE	13-hydroperoxy-9,11-octadecadienoic acid
HRP	Horseradish Peroxidase
HS	Heparan Sulfate
HSPG	Heparan Sulfate Proteoglycan
ICAM-1	Intercellular Adhesion Molecule-1
IdoA	Iduronic Acid
IP	Immunoprecipitation
JNK	c-Jun NH_2-terminal Kinase
LDL	Low Density Lipoprotein
LPL	Lipoprotein Lipase
MAP	Mitogen-Activated Protein
MAPKAPK	MAP Kinase-Activated Protein Kinase
MEK	MAP Kinase Kinase
MEKK	MAP Kinase Kinase Kinase

MMP	Matrix Metalloproteinase
MOI	Multiplicity of Infection
MWCO	Molecular Weight Cut-Off
PBS	Phosphate Buffered Saline
pfu	Plaque Forming Units
PKC	Protein Kinase C
PTCA	Percutaneous Transluminal Coronary Angioplasty
PVDF	Polyvinylidene Fluoride
RCF	Relative Centrifugal Force
RNA	Ribonucleic Acid
RNAi	RNA Interference
RPA	Ribonuclease Protection Assay
RTK	Receptor Tyrosine Kinase
SA	Surface Area
SAPK	Stress-Activated Protein Kinase
SD	Surface Density
SEM	Standard Error of the Mean
siRNA	Short Interfering RNA
SMC	Smooth Muscle Cell
TCA	Trichloroacetic Acid
TNFα	Tumor Necrosis Factor Alpha
UV	Ultraviolet Light
VCAM-1	Vascular Cell Adhesion Molecule-1
VEGF	Vascular Endothelial Growth Factor
vWF	von Willebrand Factor

SUMMARY

An injured vascular system has a substantial impact on an individual's overall health, and an understanding of the mechanisms that underlie blood vessel pathophysiology is required for the development of rational and effective treatment strategies. The phenotypic modulation of smooth muscle cells (SMC) during vascular injury, characterized by altered adhesion, migration and synthetic behavior, plays an important role in the eventual outcome. Specifically, the ability of SMCs to adhere to and remodel their extracellular environment via regulation of the syndecan class of cell adhesion molecules dictates the response of the vascular wall to local injury. The effect of *in vitro* syndecan-4 regulation on SMC adhesion was investigated through the use of a glass microsphere centrifugation assay, and an antisense-mediated reduction in gene expression was found to correlate with decreased adhesive strength. Regulation of syndecan-1, syndecan-2, and syndecan-4 gene expression was observed experimentally by mechanical strain of SMCs. Using real-time polymerase chain reaction (PCR), the kinetics of both static and cyclic mechanical strain were found to modify the gene expression in a time and strain magnitude-dependent manner unique to each syndecan. In particular, the responses of syndecan-4 were acute, but transient, while the evolution of syndecan-1 and syndecan-2 regulation was delayed by comparison. Mechanical strain also modulated syndecan-4 protein expression and ectodomain shedding, as measured by Western immunoblotting, and this effect was found, through selective inhibition, to be at least in part dependent on mitogen-activated protein (MAP) kinase signaling. In particular, intact extracellular signal-regulated MAP kinase (ERK) 1/2 and c-Jun NH_2-

terminal kinase / stress-activated protein kinase (JNK/SAPK) signaling pathways were found to be required for the observed strain-induced shedding. These findings offer a better understanding of syndecan function in response to mechanical strain and suggest potential new mechanisms by which physical forces may modulate vascular SMC behavior and regulation during normal physiology, pathologic conditions, and engineered arterial substitute development.

CHAPTER 1

INTRODUCTION

1.1 Specific Aims

Coordinated changes in smooth muscle cell (SMC) adhesion and migration are fundamental methods of vascular wall adaptation to many forms of physiologic and pathologic stress. While a variety of molecular events underlie these cellular responses, cell surface heparan sulfate proteoglycans (HSPG) are especially important through their interactions with heparin-binding molecules that either reside permanently or appear transiently in and near the vascular wall. Recent evidence implicates the HSPG syndecan-4 as having a significant role in influencing vascular mesenchymal cell adhesion and migratory behavior that is associated with matrix reorganization[2-4]. This reorganization is primarily due to interactions with extracellular matrix (ECM) proteins.

The *central hypothesis* of the work described in this manuscript is that syndecan-4 expression and shedding is regulated by the local cellular mechanical environment. Secondly, these strain-induced alterations in syndecan-4 gene and protein expression are controlled by a mitogen-activated protein (MAP) kinase signal transduction cascade. We postulate that, through the regulation of these and other key intracellular signaling events, mechanical strain modulates cell surface syndecan-4 levels, and thereby alters cell-ECM adhesive interactions. Overall, this results in a paradigm for mechanical strain-induced regulation of vascular remodeling. This work is motivated by (1) investigations by us and others demonstrating the important role of cell surface HSPGs in cell adhesion and migration and (2) the capacity of both cell surface and shed syndecans to bind a variety of

growth and pro-inflammatory factors that can modulate a range of physiologic and disease-related responses in the vascular wall.

We believe that syndecan-4 plays a critical role in vascular biology through its interaction with ECM ligands; however, due in part to its relative non-specificity, elucidation of its diverse functions has historically proven to be a complex task. Nonetheless, there is clear evidence for its role in key elements of vessel injury response and remodeling. The *Specific Aims* of the project were (1) to investigate the manner in which mechanical stimuli regulate cell surface syndecan-4 in vascular SMCs, (2) to characterize the signaling mechanisms that are involved in strain-mediated changes in the expression and shedding of syndecan-4, and (3) to determine the extent to which regulation of syndecan-4 influences the strength of cell-substrate interactions during late phases of the adhesion process.

To accomplish our experimental objectives, the methodology presented in this dissertation utilized *in vitro* vascular SMCs as a model system. Well-characterized techniques were used to apply mechanical strain to the cells and to quantify the adhesive interaction between them and the ECM. Investigations were aimed at analyzing various levels of syndecan-4 regulation, allowing us to examine its influence in vascular SMC and ECM adhesive interactions. In select instances, syndecan-4 responses were compared to those of other syndecan family members expressed in SMCs, including syndecan-1 and syndecan-2. The following approaches were taken:

1.1.1 Investigation of the manner in which mechanical stimuli regulate cell surface syndecan-4 in vascular SMCs

Human aortic SMCs grown on flexible silicone membranes were used to define the ability of mechanical stimuli to ultimately influence cell surface syndecan-4 regulation. This involved determining gene and protein expression patterns, as well as ectodomain shedding. Additionally, comparative analyses to syndecan-1 and syndecan-2 were performed. To accomplish this we subjected the cells to clearly-defined strain protocols as *in vitro* models of relevant physiological events. We then examined the subsequent regulation of syndecan expression in order to evaluate the effect of these stimuli on that regulation.

1.1.2 Characterization of the signaling mechanisms involved in strain-mediated changes in the expression and shedding of syndecan-4

The extent and timescale in which mediators of mechanical strain-induced syndecan-4 protein expression and regulation occur were evaluated. In particular, we focused on the MAP kinase signal transduction pathways as potential mediators of this response, and made use of chemical and peptide inhibitors of specific enzymes required by these pathways. Our studies served to implicate multiple signaling pathways involved in syndecan-4 expression and shedding, and provided potential future targets for manipulation of these events.

1.1.3 Determination of the extent to which syndecan-4 regulation influences the strength of cell-substrate interactions during late phases of the adhesion process

Adhesive interactions between rat pulmonary artery SMCs and fibronectin-coated glass microspheres were characterized using a modified centrifugation methodology. By

employing the ability of this assay to exert the necessary detachment forces to a cell monolayer, we were able to determine how syndecan-4 modulates adhesion between the ECM and well-spread cells.

1.2 Background

1.2.1 Rationale

According to the Heart Disease and Stroke Statistics published by the American Heart Association, cardiovascular disease remains the primary cause of mortality in both women and men in the United States[5]. More than 945,000 cardiovascular-related deaths occurred in 2001 at a cost of greater than $350 billion in health expenditures and lost productivity. It claimed more lives than the next 5 leading causes of death combined. In particular, peripheral vascular disease affects 8 to 12 million Americans. The total number of surgical and non-surgical procedures has risen from 4.3 million in 1998 to over 5.9 million in 2001, and in the past 20 years, the number of cardiac catheterizations has increased 341 percent[6,7].

While these interventions consist of a variety of procedures, including balloon angioplasty, endarterectomy, and artificial bypass grafting, all involve some form of acute *mechanical* injury to the vascular wall, which in turn initiates a sequence of physiologic events necessary for lesion repair. Likewise, as a form of chronic mechanical injury, hypertension can also initiate events that contribute to changes in the structure of the vessel wall, leading to increased susceptibility to atherosclerosis, aneurysm formation, and plaque disruption[8,9]. Significantly, recent evidence in the field of cardiovascular bioengineering has uncovered an important role for mechanical

stimulation in the development of a robust tissue-engineered blood vessel[10-15]. Thus, restenosis after acute local injury, hypertension-induced remodeling, and the tissue engineering of an arterial substitute through mechanical conditioning in a bioreactor are examples of processes in which cells alter tissue architecture in a manner that is influenced, in part, by their responses to changes in their local biomechanical environment.

1.2.2 Vascular Wall Mechanics

The uniquely complex environment of the vascular system is largely due to its dynamic chemical and mechanical environment. In addition to the transport-related consequences of unsteady flow of a non-Newtonian fluid, the cells which comprise the blood vessels are subject cyclic and non-uniform stresses[16]. If the artery were a classic pressure vessel, governed by LaPlace's and Hooke's laws, a fairly simple relationship between transmural blood pressure and wall stretch would exist:

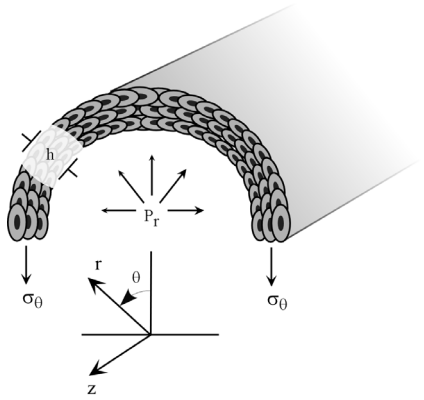

Figure 1. Simplified view of vascular hemodynamics. The drawing above represents an artery, bisected along its longitudinal axis. If modeled as an open-ended, thin-walled pressure vessel, transmural pressure (P_r) results in principal stresses in the r and θ directions.

$$\varepsilon_\theta = \sigma_\theta / E = (P * R)/(h * E) \tag{1.1}$$

where ε_θ is circumferential strain; σ_θ is circumferential (hoop) stress; P is transmural pressure; R is vessel radius; h is wall thickness; E is Young's modulus. Although this equation is only applicable for infinitesimal strains of a thin-walled, linear elastic cylinder, it demonstrates the general effect of local hemodynamics and vessel geometry on the state of stress in the vascular wall. The force that actually causes the vessel wall to expand causes an outwardly directed radial stress, which can be completely described in terms of circumferential deformation. In other words, a given mean arterial pressure results in a certain level of stress in the wall, and the actual strain depends on the modulus, or wall stiffness. The circumferential stress is mediated by intercellular connections, and it is a result of the production of longitudinal forces between cells during vasomotion[17]. Despite this description, the dynamic interaction between blood flow, blood pressure, and wall mechanics in the native artery is neither simple nor straightforward.

The vascular wall exhibits complex material properties, including nonlinearity, spatial heterogeneity, anisotropy, and viscoelasticity. In addition, the presence of residual axial and circumferential stresses, perivascular tethering, and basal muscular tone make it difficult to analyze and theoretically model. Moreover, the properties of the vessel wall vary along the vascular tree. Large and medium-sized arteries behave differently than capillary vessels, which in turn behave differently than low pressure veins. Nevertheless, several simplifying assumptions can still be employed and have been shown by others to allow for reasonably accurate estimation of the local physiologic stresses and strains, i.e. the micromechanical environment, experienced by the individual

cells in the vessel wall (reviewed by Humphrey)[18]. First, the geometric symmetry of the vessel allows it to be considered as cylindrically orthotropic[19]. Studies have also shown that principal stresses exist mainly in the circumferential (tensile) and radial (compressive) directions. Additionally, due in part to the presence of residual stress, mechanical function follows histological form, as the artery can be considered to be composed of two separate, homogeneous layers – media and adventitia, resulting in constant stress distribution in each layer[20-24].

In addition to the stresses of normal hemodynamics, cells in the vascular wall are subjected to abnormal stresses due to pathologic states, as well as acute injury during clinical interventions. When transmural blood pressure is chronically elevated, the mechanical environment becomes the primary determinant of both intimal hyperplasia and medial thickening. Since stresses are functions of the vessel wall geometry, a mechanism naturally exists by which the affected cells can counterbalance hydrodynamic effects by initiating responses that may ultimately change lumen diameter, wall thickness, and compliance. This occurs primarily through cell proliferation, apoptosis, migration, and remodeling of the ECM. Similarly, one of the most commonly induced injuries occurs as a result of balloon catheterization, in which acute vessel expansion is accomplished by direct compression of the wall constituents. Despite its therapeutic benefits, angioplasty results in endothelial denudation, fracture and dissection of atherosclerotic plaque, overstretch of the non-diseased wall, and extrusion of fluid from the lesion[25-27]. Accordingly, this type of injury elicits a subsequent cellular reaction, leading to a characteristic wound healing and remodeling response. On a cellular level, there exists a coordinated process of SMC and fibroblast differentiation, adhesion, and

migration, while on a molecular level, cell surface and soluble proteins are regulated both spatially and temporally. If these events are deficient, the vessel wall, in principle, can become weakened and may be susceptible to aneurysmal degeneration. More commonly however, these responses are overactive; and in turn, scar formation and restenosis occur, as is often the case following vascular graft implantation or angioplasty, with the potential for failure of the clinical intervention.

1.2.3 The Extracellular Matrix and Remodeling

Many living tissues change their mass, metabolism, and deposition / re-uptake of ECM proteins in response to changes in mechanical stress[28]. Matrix remodeling is a process common to many reparative vascular events, including post-angioplasty restenosis, transplant vasculopathy, and the outward remodeling that occurs in conjunction with a developing atherosclerotic plaque[29]. It is the term given to the process of synthesis, degradation, and rearrangement of ECM components to maintain homeostasis, and it involves both transient and permanent changes in tissue architecture, such as basement membranes, basal laminae, and interstitial stroma[30]. In fact, the ECM has been described as "homeostatic" due to the tight regulation of its components and the influence this action has on mesenchymal cell behavior[29,31]. This behavior is determined by a combination of interactions with both other cells and the ECM. The ECM is composed of fibrillar and non-fibrillar constituents, including collagen, elastin, glycoproteins such as fibronectin and laminin, and proteoglycans such as perlecan and versican[1,32,33]. The composition of this matrix has a profound impact on the type of cellular interactions that take place. It also determines the tensile strength and resilience

of the tissue. Mesenchymal cells, for their part, interact with each other through the association with their local ECM. For example, they bind matrix proteins, secrete growth factors, and release cytokines and proteases, thereby altering the surrounding chemical, and remodeling the surrounding mechanical, environment.

Such vascular wall remodeling is a critical event in the pathophysiology of atherogenesis, restenosis, and in the development of a tissue-engineered vascular graft[34-37]. When a tissue is induced to undergo any type of structural change, it does so largely through a rearrangement of its ECM composition. While it is clear that in many cases the events are adaptive in nature and serve to counterbalance injury, in other cases these events are either inadequate or lead to undesirable conditions. For example, compensatory dilation under the influence of prolonged hypertension can result in aneurysm formation. Ultimately, the role of the cellular components is to maintain a functional balance.

Of particular interest in cardiovascular bioengineering is the occurrence of this balancing act during wound repair and tissue engineering. Both require extensive remodeling events, including provisional matrix deposition, tissue or wound contracture, and eventual re-epithelialization; these events also involve cell activation, adhesion and migration. Glagov et al., who introduced the concept of compensatory remodeling in the coronary arteries, demonstrated that this process allows the lumen area to remain constant as atherosclerotic disease progresses[38]. The accepted reason for this is that the total vessel diameter increases to compensate for the lumen encroachment. Controlled remodeling events hold particular significance in the tissue engineering of an arterial substitute, which typically includes re-population and organization of appropriate cellular

components, matrix deposition, and tissue contracture. Regardless of the specific stimulus or response, a model for vascular remodeling includes four generalized events: (1) recognition of changes in either the ECM, the flow environment, or mechanical properties of the arterial wall; (2) intracellular transduction of these signals and communication to adjacent and nearby cells; (3) expression and release of paracrine mediators which alter cellular activity; and (4) resultant structural changes in the vessel wall[39-41]. Therefore, in this model the ultimate effectors of specific vascular remodeling events are the resident cells in direct physical proximity to the responsible stimulus.

1.2.4 Cellular Basis for Vascular Remodeling

Among the cellular components in the vessel wall, a great deal of work has been aimed at elucidating the role of the endothelium[17,42-44]. Its role in sensing shear stress, mechanical stretch, and the chemical composition of the blood, using a variety of specialized receptor mechanisms, as well as its transduction of these signals, has underscored its importance in vascular biology. However, the role of the underlying medial and adventitial mesenchymal constituents is considerably less well characterized.

Two classes of mesenchymal cells are of particular interest with respect to vascular wall remodeling. In the vascular wall, these cells include SMCs and adventitial fibroblasts. In response to injury, SMCs undergo a change from a quiescent and contractile to a synthetic phenotype. This is followed by migration into the sub-endothelial neointima, where these cells synthesize, deposit, and organize ECM components. These cells are the primary sources of collagens, elastic fibers, and proteoglycans[35,45].

Arterial injury also appears to induce the proliferation and transmigration of myofibroblasts into the sub-endothelium, which may in turn lead to lumenal stenosis[46-49]. Myofibroblasts are derived from fibroblasts that have become activated, and are identified most commonly by their expression of α-smooth muscle actin. Originating in the adventitia, they also deposit collagen, as well as migrate into the neointima. Migrating cells produce ECM-degrading enzymes and plasminogen activators to facilitate their movement, similar to the fibroblasts that degrade connective tissue in the dermis after skin damage[50-52]. Just as this cellular activity alters the extracellular environment, cell proliferation, differentiation, adhesion, migration, and changes in shape are in turn dictated in part *by* the ECM. Evidence is accumulating that the cells are exquisitely sensitive to the composition of their local microenvironment[53,54]. For example, Koyama et al. suggest that a polymerized collagen substrate alters cyclin-dependent kinase 2-dependent cell cycle progression through regulation of integrin signaling[55]. Ichii et al. have also demonstrated that polymerized collagen suppresses a number of genes associated with integrin-dependent migration of SMCs[56]. The sensitivity of cells to their microenvironment is primarily dictated by the cell surface receptors which, among others, include integrins and syndecans.

1.2.5 Syndecan Structure and Function

A widespread and evolutionarily conserved class of molecules that resides on the surface of all animal cells includes the HSPGs, which consist of two minor and two major families. The minor HSPGs – betaglycan and CD44 – contain heparan sulfate (HS) chains only under certain conditions. On the other hand, the major HSPGs – glypicans

and syndecans – always have covalently attached HS chains[1]. The glypicans are anchored to the plasma membrane via a glycosylphosphatidyl inositol (GPI) linkage, whereas the syndecans are type I transmembrane proteins.

It has been proposed that the main function of syndecans is to modulate ligand-dependent activation of integrin receptors at the cell surface[57]. Recent evidence, however, has shown that this view is incomplete. Syndecans, first described by Sanderson and Bernfield[58], have been shown to function in capacities ranging from growth factor and cytokine cell surface localization and binding[59,60] to intracellular signaling complex assembly, and they appropriately have their roots in the Greek word syndein, meaning "to bind together"[61]. In addition, studies have even demonstrated a role in nuclear transcriptional activity[62].

The various functions of the syndecan family members are undoubtedly governed by their individual structures, and despite the fact that each syndecan has a slightly different role in cellular function , the syndecans can be considered as two subfamilies[1]. Syndecan-1 (CD138) and syndecan-3 (N-syndecan) represent one subfamily, while syndecan-2 (fibroglycan) and syndecan-4 (ryudocan, amphiglycan) represent the other. All four syndecans share some common general features (see Figure 2A). They are HSPGs, and therefore consist of a core protein decorated with pendant, disaccharide-laden glycosaminoglycan (GAG) chains. The core protein consists of a short, highly conserved cytoplasmic domain, a single-pass transmembrane domain, and a variable ectodomain. The cytoplasmic domain is composed of two invariant (C1 and C2) domains and one variable (V) domain, and contains regions for phosphorylation, binding of cell scaffolding proteins, and interaction with the actin cytoskeleton. The transmembrane

domain aids in syndecan oligomerization, and localizes syndecans within discrete aggregates in the membrane, such as focal adhesions[63-65]. The ectodomains contain regions for attachment of GAG chains, which are typically HS and chondroitin sulfate (CS). The basic chemical structure of HS is depicted in Figure 2B.

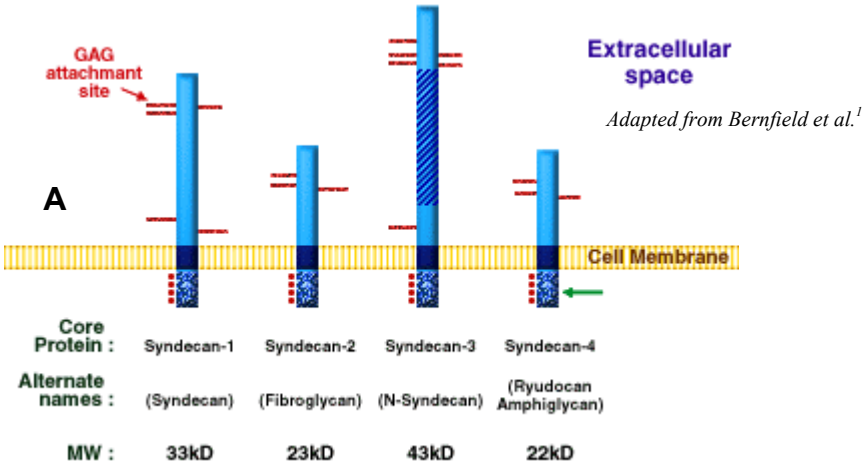

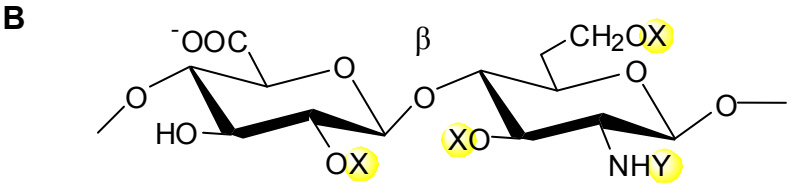

X=H, SO_3^-
Y=H, Ac, SO_3^-

Heparan Sulfate

Figure 2. Syndecan core protein (A) and heparan sulfate structure (B).

The differences between the syndecans lie in some key specifics. Structurally, the V region of the cytoplasmic domain and a majority of the ectodomain vary for each family member. For example, an adhesion site has been demonstrated within the syndecan-4 ectodomain only[66,67], and unlike the other family members, it has a high affinity for membrane phospholipids. In addition, the ectodomains are variable in length. While all syndecans have GAG attachment sites near the N-terminus which typically bind HS, syndecan-1 and syndecan-3 also have sites near the plasma membrane for CS binding. The distribution of each syndecan is also unique. Syndecan-1 is expressed early during embryonic development, as well as in epithelia, mesenchymal tissue, and B cells of the immune system. Syndecan-3 is expressed in neuronal and musculoskeletal tissues. Syndecan-2 is distributed in neuronal cells as well, but also in mesenchymal and hepatic tissue. Lastly, syndecan-4 has been detected in a wide variety of cell types[65,68]. As a result of these variations in developmental and tissue distribution, the family of syndecans enables cells to interact in numerous capacities throughout the body.

The physiologic activity of many proteins depends on or is enhanced by interactions with heparan sulfates[69]. For example, syndecan ectodomain shedding is important in sequestering soluble ligands and reducing the number of remaining available cell surface receptors[70,71]. Also, heparan sulfates serve as a means in which several microbial pathogens can gain entry into host cells[65]. Additionally, shed syndecan-1 ectodomains have been implicated in regulating the proteolytic activity of acute wound fluid[72]. The objective of this thesis was to demonstrate that certain functions of syndecans may play a role in strain-mediated responses of the vascular wall.

Given the evidence for HSPG interactions with numerous matrix proteins[73-75], and

assembly into focal adhesions[63,76-79], our lab has sought to determine the role of small heparin-binding peptides in cell adhesion phenomena *in vitro*, and we have demonstrated that soluble peptides interfere with syndecan-ECM interactions, and thereby reduce cell-substrate adhesive strength[80,81]. In our previous work, PAC-1 immortalized rat pulmonary artery cells were treated with heparin-binding peptides derived from fibronectin or von Willebrand Factor (vWF), and our results demonstrated that these oligopeptides reduced the relative centrifugal force (RCF) corresponding to 50% cell detachment (RCF_{50}), a quantitative measure of cell-substrate adhesion, in a dose-dependent manner. We have also demonstrated in an *in vivo* model that syndecan-4 gene and protein expression were regulated in a temporally and spatially specific manner after balloon injury of the rat carotid artery[82]. Furthermore, ongoing research in our lab is also investigating the association between atherosclerosis and syndecan localization within the vascular wall *in vivo*.

1.3 Significance

Our interest in the role of syndecan-4 in adhesion and vascular remodeling is motivated by the results of previous workers in the field. Specifically, the work of Bernfield, Tumova, Couchman, and others have recently described roles of HSPGs in cell adhesion and migration[1-3,76,83-86]. Likewise, Horowitz, Oh, and others have elucidated many of the mechanisms in which HSPGs regulate intracellular signaling[75,87-93]. Improvements in the quantitative techniques for analyzing single cell[94,95] and population-based[81,96-98] adhesion to the extracellular matrix has allowed for the appreciation of subtle differences in discrete stages of the adhesion process. Efforts geared toward thwarting

the remodeling behavior of SMCs in vivo or enhancing that same behavior during development of a bioartificial vascular graft have numerous implications.

CHAPTER 2

REGULATION OF SYNDECAN-4 HAS IMPLICATIONS ON CELL-SUBSTRATE ADHESIVE INTERACTIONS

Cell-matrix adhesions, typically characterized as physical links between the extracellular matrix and internal actin cytoskeleton, are necessary for both the movement of cells and the generation of traction forces that effect matrix remodeling. In particular, focal adhesions, involving actin, α-actinin, talin, vinculin, paxillin, and tensin were originally described as regions of close contact (10-15 nm)[99,100]. They are thought to represent a general form of interaction between cytoskeletal proteins, integrins and other adhesion receptors, and the substratum. It has recently become clear that regulation of focal adhesion formation, and the interaction of adhesion receptors with the actin cytoskeleton via intracellular scaffolding proteins, are critical to the control of cell migration. Our aim was to employ a glass microsphere centrifugation assay, which is a modified form of the commonly used centrifugal detachment assay, to quantify cell-ECM adhesive interactions. Using an antisense-containing adenoviral vector to down-regulate specific protein translational activity, we then assessed the functional role of syndecan-4 on these interactions. We postulated that this modulation of syndecan-4 would lead to decreased adhesive forces.

2.1 Background and Significance

2.1.1 Biological Importance of Cell Adhesion

Cellular adhesive interactions are crucial to the proper functioning of cells, tissues

and organisms. From embryonic cell migration in the developing fetus to leukocyte rolling and margination in the cellular defense against infection, intercellular and cell-ECM adhesive interactions help to guide cell movement and direct cell function. In addition to its part in normal physiology, cell adhesion plays a role in many pathologic conditions, including tumor metastasis[101] and atherosclerosis[102].

Current knowledge recognizes integrin-ligand binding as the principal means of cell-ECM adhesion[103,104]. Through their interaction with the actin cytoskeleton and the recruitment of cytoplasmic proteins into focal adhesion complexes, integrins play a critical role in the cell's interaction with its extracellular environment. Despite this fact, other cell adhesion molecules, including cadherins, selectins, and the immunoglobulin superfamily class of receptors, play important roles in cellular interactions with other cells and with their environment, and only fairly recently has the ubiquitous and evolutionarily conserved syndecan family of HSPGs received adequate recognition for its role in cell-ECM interactions.

2.1.2 Syndecan-4 and Adhesion

As a result of their structure, HSPGs, including syndecan-4, interact with the heparin-binding sites of a number of small peptides and macromolecules. These include fibronectin (FN), interstitial collagens, antithrombin III, epidermal growth factors, microbial peptides, chemokines, and lipoprotein lipase, among others[1]. Recent evidence supporting the hypothesis that syndecan-4 is an important regulator of cell adhesion includes work by Couchman and others. Cell surface heparan sulfates have been shown to be necessary for the development of focal contacts[105] due to the intracellular signaling

that follows the interaction between surface HSPGs and their ligands. Studies have demonstrated syndecan-4 localization to focal adhesions in several cell types, in which this proteoglycan helps direct focal adhesion assembly[63,77,78,84]. Also, syndecan-4 overexpression in Chinese hamster ovary (CHO) cells leads to increased focal adhesion assembly, while truncation of the cytoplasmic V region leads to reduced cell spreading and focal adhesion formation[3].

In this regard, syndecan-4 has been shown to co-localize with β_1 and β_3 integrins within focal adhesions[3,63,76], and although syndecan-4 may not always be necessary for focal contact formation[106], it does appear to play a key role in cell adhesion, as well as cell spreading, clustering of adhesion receptors, and stress fiber formation. Notably, syndecan-4 has recently been shown to directly mediate the β_1-integrin-dependent binding, spreading, and focal adhesion formation to the cystein-rich domain of a disintegrin and metalloprotease (ADAM) 12[83,107]. Additionally, syndecan-4 has been associated with important signal transduction cascades, such as activation of protein kinase C (PKC), that underlie many of these cellular events[75,91]. For example, upon cell binding to fibronectin via $\alpha_5\beta_1$ integrins[108], syndecan-4 molecules accumulate, possibly due to adjacent GAG-binding domains on the FN monomer[109,110] and oligomerize via their cytoplasmic domains, leading to the formation of focal adhesions[77,105]. Thus, as a co-receptor for both soluble and insoluble ligands, and through organization of subplasmalemmal scaffolding proteins, including vinculin and α-actinin, syndecan-4 can induce changes in actin cytoskeletal organization[57,111-113]. For these reasons, the syndecan-4 core protein and their highly sulfated pendant chains were the targets of our experimental strategy.

Atherosclerotic lesions occur when SMCs migrate toward the lumen, proliferate, and secrete ECM components, including collagen, fibrin and proteoglycans. The plasticity of SMC phenotype allows for them to become synthetic during remodeling in response to changing hemodynamic conditions; however, this is often undesirable during the development of an atherosclerotic lesion and post-angioplasty restenosis[114]. Taken together, the experimental background discussed above suggested that targeting syndecan-4 expression would be a useful approach to identifying the significance of this putative mediator of cell adhesion. Furthermore, previous studies by García and others have demonstrated that cell detachment assays are sensitive methods to determine the cell-substrate adhesive interactions[98]. Since a critical component of SMC migration involves alterations in their adhesion, we employed this type of assay in order to assess the involvement of syndecan-4 in SMC atherogenic potential.

2.1.3 Methods of Analysis

The purpose of using an antisense construct-containing adenoviral vector was to eliminate syndecan-4 expression at the messenger ribonucleic acid (mRNA) level. We postulated that the presence of single-stranded mRNA in the antisense configuration would bind to native syndecan-4 mRNA, sequestering it, and rendering it (1) unavailable for translation, and (2) prone to rapid degradation. The choice of an adenovirus as a means of transferring this antisense gene offered several advantages over other conventional vectors, such as retroviruses and electroporation. Unlike many retroviral systems, adenoviral vectors have the potential for clinical application. Moreover, the likelihood of phenotypic variants and the development of substantial compensatory

mechanisms often seen in knockout models are diminished. A limitation of adenoviral systems, however, is that the transfection is transient.

2.2 Materials and Methods

2.2.1 Cell culture

PAC-1 immortalized rat pulmonary artery SMCs were provided by Dr. Abraham Rothman (UCSD Medical Center, San Diego, CA). Though immortalized, these cells retain expression of important markers of SMC phenotype, including angiotensin II, norepinephrine, and α-thrombin receptors, and also SMC isoforms of α-actin, myosin heavy and regulatory light chains, α-tropomyosin, meta-vinculin, phosphoglucomutase, and calponin[115]. The cells were cultured using standard cell culture techniques. Growth medium consisted of M199 Medium (Invitrogen), supplemented with 10% FBS, L-glutamine (Mediatech), 100 U/L penicillin, 100 µg/L streptomycin, and 10 U/L amphotericin B (Mediatech). Quiescence medium consisted of growth medium, supplemented with 0.5% FBS. Cells were incubated at 37ºC, 5% CO_2, in a humidified atmosphere.

2.2.2 Recombinant Adenovirus Construction and Infection

Adenoviral vectors containing antisense syndecan-4 DNA in order to block the synthesis of syndecan-4 RNA were employed. Ribonuclease protection assay (RPA) was used to investigate the infection efficiency. The pAdTrack-CMV and pAdEasy-1 vectors[116], as well as E. coli BJ5183 cells were provided by Dr. Bert Vogelstein (Johns Hopkins University, Baltimore, MD). Generation of a recombinant syndecan-4 antisense

virus, containing a green fluorescent protein (GFP) reporter, and amplification in 293 cells were performed as described previously[116]. Briefly, a 691 bp Hind III/Not I fragment comprising full-length rat syndecan-4 cDNA was cut from a pcDNA3.1(+) plasmid and ligated into the pAdTrack-CMV shuttle vector to form pAdTrack-CMV/antisense. PAdTrack-CMV/antisense was linearized with Pme I and co-transformed with pAdEasy-1 into BJ5183 bacterial cells to achieve homologous recombination. Recombinant adenoviral constructs were isolated and transfected into 293 cells (Qbiogene, Carlsbad, CA) using a standard lipofectamine (Invitrogen) transfection. Seven to ten days post-transfection, virus was harvested by scraping and pelleting the transfected 293 cells, resuspending in sterile PBS, and freeze-thawing for 3 cycles. The cell debris was pelleted and the supernatant used to re-infect 293 cells for amplification. Virus was amplified for 4 cycles using the harvesting and re-infection process described above. Titration of the virus was performed by infecting 293 cells for 18 hours with serially-diluted viral stocks and counting positive cells through GFP fluorescence. Virus stock titers of 1.4 to 5.7×10^8 plaque forming units (pfu)/mL were retained and used for experiments.

For infection, cells were briefly incubated at 37ºC with a multiplicity of infection (MOI) of 10, representing the number of virus particles per cell, in Quiescence medium. After 1.5 hours, growth medium was added, and the cells were cultured for up to 24 hours. Cells were then detached with 0.5% Trypsin (Mediatech) and passaged into 10 cm and 96-well culture dishes. After the cells reached confluence they were either harvested for RNA quantification or used in the centrifugation adhesion assay.

2.2.3 RNA Analysis

To quantify syndecan-4 gene expression in PAC-1 cells, a ribonuclease protection assay (RPA) kit was used according to the manufacturer's instructions (Promega, Madison, WI; Ambion, Austin, TX). Briefly, total RNA was extracted by adding 3 mL TRIzol (Gibco BRL) to cells growing in a 100 mm culture dish. After 5 minutes, the cells were scraped from the dishes into microcentrifuge tubes. Following chloroform and isopropanol extractions, and rinsing with 75% ethanol, the RNA was re-suspended in RNase-free water. The RNA concentration was determined by measuring OD_{260}. Riboprobes (Table 1) were generated to the extracellular domains of rat syndecan-4 by sub-cloning the PCR product into the pCR vector system (Invitrogen). The vector was linearized, and corresponding sense and antisense probes were transcribed, using a T7 promoter in the presence of ^{32}P labeled UTP (Amersham). The target syndecan-4 mRNA was quantified by hybridizing 10 µg of the extracted mRNA with the radiolabeled probes and running the samples on a 5% polyacrylamide/8M urea gel. A commercially available Glyceraldehyde-3-Phosphate Dehydrogenase (GAPDH) RNA template (BD Biosciences – Pharmingen, San Jose, CA) was also radiolabebeled and used as an internal control. 10 µg of extracted RNA was used for each sample. BioMax MS autoradiography film was exposed to the resolved gels at -80ºC and used to visualize the position of the bands. Levels of RNA were quantified by densitometry using IP Lab Spectrum image analysis software.

Table 1. Oligonucleotide primer sequences for rat syndecan-4 riboprobes.

Primer	Sequence	PCR Size
Forward	5'- AGG CGA GTC GAT TCG AGA GA -3'	398 bp
Reverse	5'- TCA GAG CTG CCA AG ACCT CT -3'	398 bp

2.2.4 Surface Adsorption

The relationship between bulk solution and surface concentrations of heparin-binding peptides was quantified by radiolabeling the peptides with ^{125}I (NEN Life Science, Boston, MA) and adsorbing different concentrations to the surfaces of glass beads. The tyrosine-containing peptides were radiolabeled using IODO-Beads Iodination Reagent (Pierce Biotechnology, Rockford, IL) according to the manufacturer's instructions. Briefly, 1 mCi Na^{125}I per 100 μg target protein was oxidized and incorporated into the protein, using PBS pH 7.2 as the reaction buffer. The reaction was terminated by removing the beads from the mixture. Unincorporated ^{125}I was removed using a D-Salt Desalting Column (Pierce). The protein was precipitated by incubation in 10% trichloroacetic acid (TCA) for 45 minutes, followed by centrifugation at 16,000 x *g* and washing of the pellet twice with 10% TCA. The amount of radioactivity in the pellet was measured using a γ-counter (LKB-Wallac RiaGamma 1274, Wallac Oy, Finland). The protein concentration was determined using the Bradford method (Bio-Rad), and the specific activity (SA) in cpm/μg was then calculated and used for surface density (SD) determinations.

Cover slips (15 mm diameter) were used to determine adsorption onto glass. The discs were incubated with the ^{125}I-labeled protein, diluted 1:100 in unlabeled protein, and

incubated at 4ºC for 24 hours. The discs were then blocked with 1% BSA in PBS at room temperature for 45 minutes, and then washed with PBS. The adsorbed radioactivity of each disc was determined using a γ-counter. The protein concentration vs. SD was determined using the following equation (dilution = 100):

$$SD = \left(\frac{cpm}{SA * Area} \right) * (Dilution) \qquad (2.1)$$

2.2.5 Glass Microsphere Adhesion Assay

Cell-substrate adhesive strength was determined by employing a modified centrifugation assay (Figure 3). Details of this assay are described in Appendix A and elsewhere[117]. Briefly, human plasma FN was pre-adsorbed onto 30-50 μm glass microspheres (Polysciences, Warrington, PA) by incubating them in 100 μg/mL of the protein at 4ºC for at least 24 hours. The microspheres were then washed five times with PBS, blocked with 1% BSA in PBS for 45 minutes at room temperature, and washed three more times in PBS. At this point, the microspheres were suspended in serum-free medium (MCDB 104 Medium, Gibco BRL) supplemented with Supplement-X (10 mg/L insulin, 5.5 mg/L transferrin, 6.7 μg/mL sodium-selenite; Gibco BRL), 2 mM L-glutamine (Mediatech), 1 mM $CaCl_2$ and Penicillin/Streptomycin. PAC-1 cells were sub-cultured at an initial density of $3x10^5$ cells/mL into each of the 72 inner wells of a 96-well culture-treated strip plate (Corning, Corning, NY) and cultured in growth medium until 80% confluent (approximately 4 days). The cells were then quiesced for 24 hours, rinsed twice with PBS, and 200 μL of the microsphere suspension was placed in each

well on top of the cell monolayer. Selected cells were treated with sodium chlorate at this point. Chlorate, a competitive inhibitor of ATP-sulfurylase, results a loss of GAG sulfation. The result is that sulfated GAG-mediated interactions are eliminated. Up to 75 mM sodium chlorate has been used with smooth muscle cells without evidence of cytotoxicity[118-120]. The cells were incubated for 6 to 8 hours at 37ºC, after which the strip wells were detached in sets of two, placed inverted into a 12-well plate, filled with 0.01% BSA in PBS (Figure 3). Each plate was placed in a swing-bucket holder and centrifuged (Thermo EC, Waltham, MA), at designated speeds ranging from 500-3400 rpm (approximately 50-2500 x *g*) for one minute from the time maximum angular velocity was reached.

In this assay a range of detachment forces was applied to a population of matrix-coated glass microspheres, and the quantity of beads that adhered to the monolayer of cells upon inversion of the culture dish varied in a time-dependent manner. In plotting the percentage of adherent microspheres vs. the relative centrifugal force (*RCF*), the force value at which 50% of the microspheres detached could be determined and was designated as RCF_{50}. For example, the RCF_{50} was approximately 500 ± 100 x *g* for FN-coated glass microspheres that had been deposited and incubated for 6 hours on a monolayer of PAC-1 cells.

Different samples were centrifuged for 1 minute in increments of 500 rpm. Each well was then viewed at 40X magnification using an inverted microscope (Nikon, Melville, NY) with ambient visible light illumination. The reflection of the rounded microspheres provided adequate contrast with low background noise, and enabled precise image measurements. Since the area covered by the microspheres was proportional to the

total number attached to the cells, the fraction of glass microspheres remaining was determined by measuring the covered area, using IP Lab Spectrum image analysis software (Scanalytics, Fairfax, VA). The results were fit to the following symmetrical logistic model (Equation 2.2), using the Marquardt-Levenberg algorithm, where f is the percent adherent glass microspheres, f_0 is the percent adherent at zero force, b is the decay slope, and RCF was measured in gravitational units, g. The parameters b and RCF_{50} were then calculated:

$$f = \frac{f_0}{1 + \exp[b(RCF - RCF_{50})]} \tag{2.2}$$

2.2.6 Statistics and Data Analysis

Values are reported as mean ± standard error of the mean (SEM). Statistical analysis was performed using SigmaStat 3.0 software package (SPSS, Chicago, IL). Student's *t*-test was employed for individual comparisons, while analysis of variance (ANOVA) was employed, using the Tukey's method, for multiple pairwise comparisons among the treatments. A p value < 0.05 was considered statistically significant for all tests.

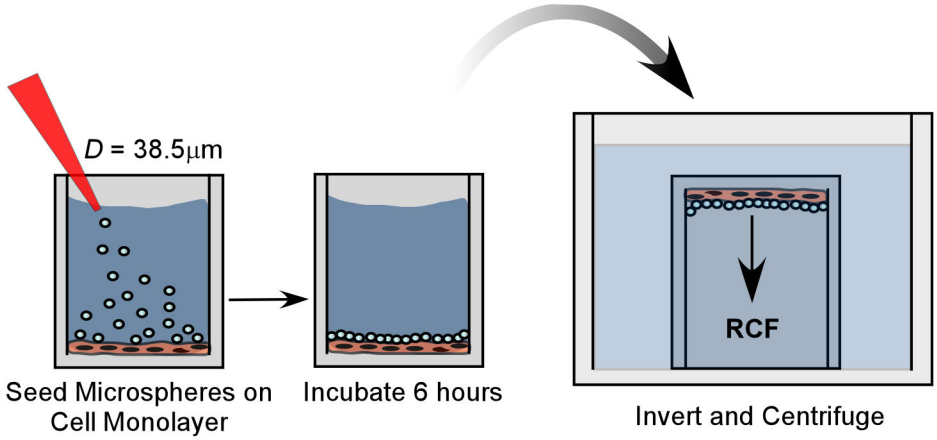

Figure 3. Scheme for cell adhesion experiments. PAC-1 cells were grown in 96-well strip plates. At confluence, glass microspheres, pre-adsorbed with FN, were placed onto the cell monolayer and incubated for 8 hours. The wells were then inverted and centrifuged in order to separate the microspheres from the cells, after which the area covered by the remaining microspheres was calculated.

2.3 Results

2.3.1 Centrifugation Assay is a Convenient Tool for Evaluating Cell-ECM Adhesion

The glass microsphere adhesion assay was used to quantify cell-substrate adhesiveness. This assay required that several assumptions be made: (1) the cells formed an intact monolayer on the polystyrene culture plate which could not be disrupted by the conditions imposed by the assay; and (2) the *substrate* under investigation was the surface of the glass microspheres, rather than the polystyrene culture plate, and as such, the strength of the cell-substrate interaction needed to be within the measurement limits of the assay. To test this, the cells were initially imaged after centrifugation at the maximum force of 2500 x *g*. We also imaged the cells after all microspheres themselves had initially adhered for 8 hours prior to centrifugation at 2500 x *g* (Figure 4). The fact that the cell monolayer remained intact following both conditions suggested that the adhesive interaction between the cells and the glass microspheres was within the working range of, and could therefore be evaluated by, this assay. Furthermore, the result suggested that the strength of adhesion between the cells and the culture plate was above this range.

2.3.2 Adhesive Strength is Influenced by Post-Translational Sulfation and Syndecan-4 Regulation

Prior evidence has demonstrated that N- and O-sulfation of the HS chains are necessary for many of the biological functions of HSPGs, including syndecans, and these substitutions greatly influence the binding affinity of HSPGs to soluble matrix proteins[73,121,122]. Our current experiments demonstrated this to be true for the role of

syndecan-4 in mediating cell-substrate adhesive interactions. Elimination of HS sulfation with sodium chlorate treatment reduced adhesive forces between the FN-coated glass microspheres and the SMC monolayer, as indicated by a reduction in RCF_{50} by 76% of untreated controls (Figure 5).

While the results with sodium chlorate implicated a critical role of sulfated biomolecules in SMC adhesion, they did not address the specific role of HSPGs or syndecan-4 in particular. To answer the question of whether syndecan-4 regulation influenced cell adhesion, we employed an adenovirus transfection strategy to interfere with syndecan-4 expression. The results demonstrated that the cells were cultured successfully after infection with an adenovirus MOI of 10. As shown in Figure 6A, the infection did not significantly alter the morphology of the cells, and they were able to form a confluent monolayer. Using GFP as a housekeeping indicator of infection with our adenoviral construct, Figure 6B and Figure 6C also demonstrate that the infection was sustained after a week in culture, which was the maximum duration that the cells were cultured prior to running the adhesion experiment. Once we demonstrated that transfection was stable and non-cytotoxic by our measurements, we quantified the level of syndecan-4 RNA produced by the transfected cells, and compared them with non-transfected controls (Figure 7). Using radiolabeled riboprobes to detect syndecan-4 and GAPDH RNA (inset), we found that the syndecan-4 RNA from these cells, after internal normalization to GAPDH RNA, was reduced by 78% of non-transfected controls.

To test the functional significance of this decrease in detectable syndecan-4 RNA, we compared (1) cells treated with the antisense genetic construct-containing adenovirus with (2) those treated with a null (empty vector) construct-containing adenovirus and (3)

normal, non-transfected controls (Figure 8). The results indicated that, regardless of the genetic contents of the adenoviral vector, a significant difference in cell adhesive behavior existed between transfected and non-transfected SMCs. The antisense construct-transfected cells displayed an adhesive strength that was reduced by 56 ± 2% of the non-transfected controls (p value < 0.001), while the null construct-infected cells also displayed reduced adhesive strength (26 ± 2% of the non-transfected controls; p value < 0.001). More importantly however, a significant difference existed between the antisense and null vectors (p value < 0.001). In other words, the decrease in SMC adhesive strength that was associated with the reduction of syndecan-4 RNA was two-fold greater than with the presence of the empty vector control alone. Taken together, these results indicate that there was a marginal nonspecific effect due to transfection with the null vector; however, a much greater reduction in adhesive strength was observed in cells in which syndecan-4 expression was lacking.

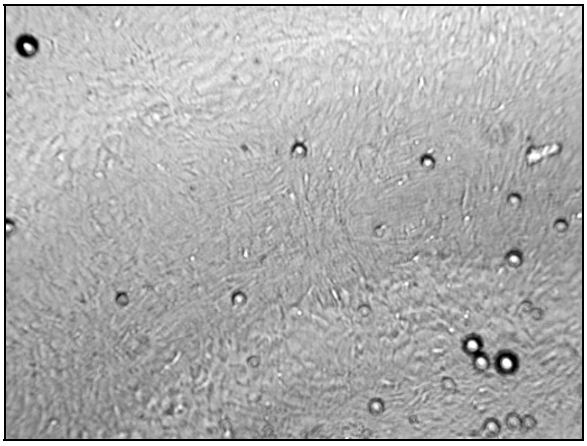

Figure 4. Demonstration that cell monolayer remained adherent to culture dish following adhesion assay. Cells were cultured in 96-well plates, and FN pre-adsorbed glass microspheres were incubated on the cells for 8 hours. The plates were then centrifuged at 2500 x *g* for 1 minute in order to completely remove the microspheres. 40X magnification.

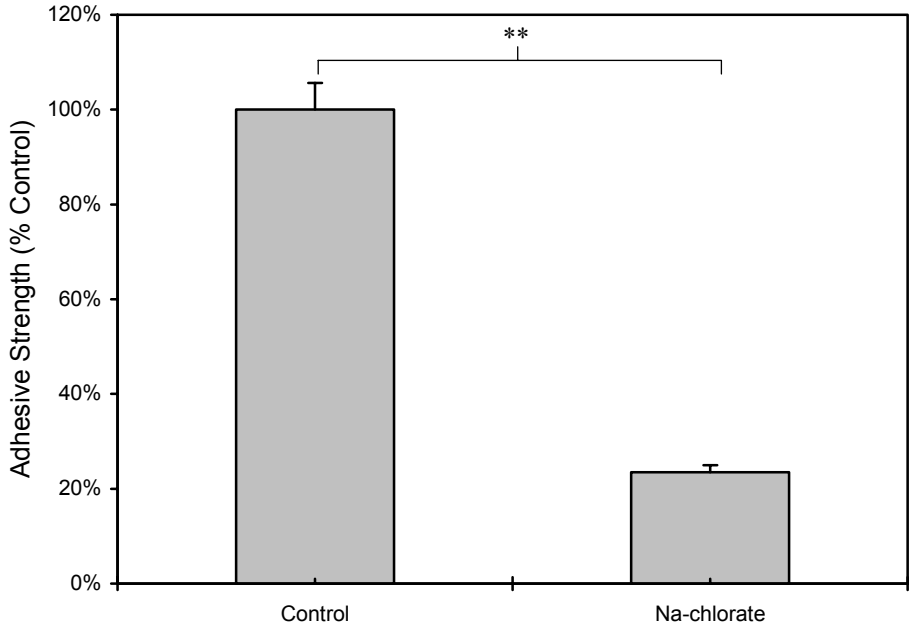

Figure 5. Decrease in adhesive strength due to treatment with sodium chlorate. At the time the glass microspheres were placed on the cells, sulfation of new GAG chains was inhibited by treatment with 30 mM sodium chlorate. Cell-substrate adhesive strength was determined by employing a glass microsphere centrifugation assay, in which a range of detachment forces were applied to a population of matrix-coated microspheres deposited onto a SMC monolayer. Adhesive strength was reduced by 76% compared to untreated controls. (**Indicates p value < 0.001, using the Student's t-test)

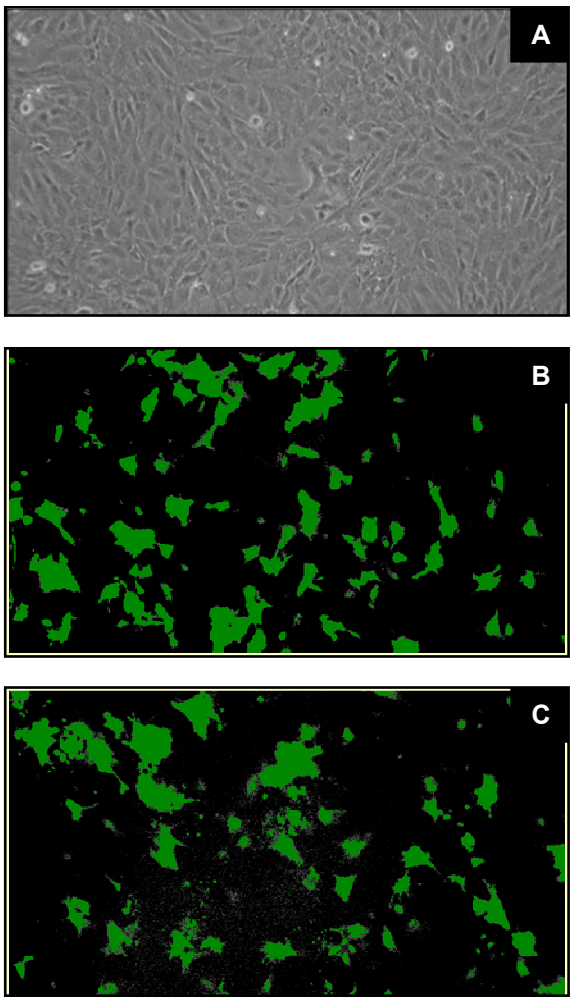

Figure 6. Evidence of adenovirus infection. Cells were viewed under at 100X magnification, using an inverted microscope with either a phase contrast (A) or an epifluorescence attachment (B and C). Adenovirus constructs carried a GFP reporter gene which allowed for the identification of transfected PAC-1 cells. After 20 hours (B) and seven days (C) in culture, infected cells were identified by GFP expression. The cells in all cases remained viable during the experiment (A).

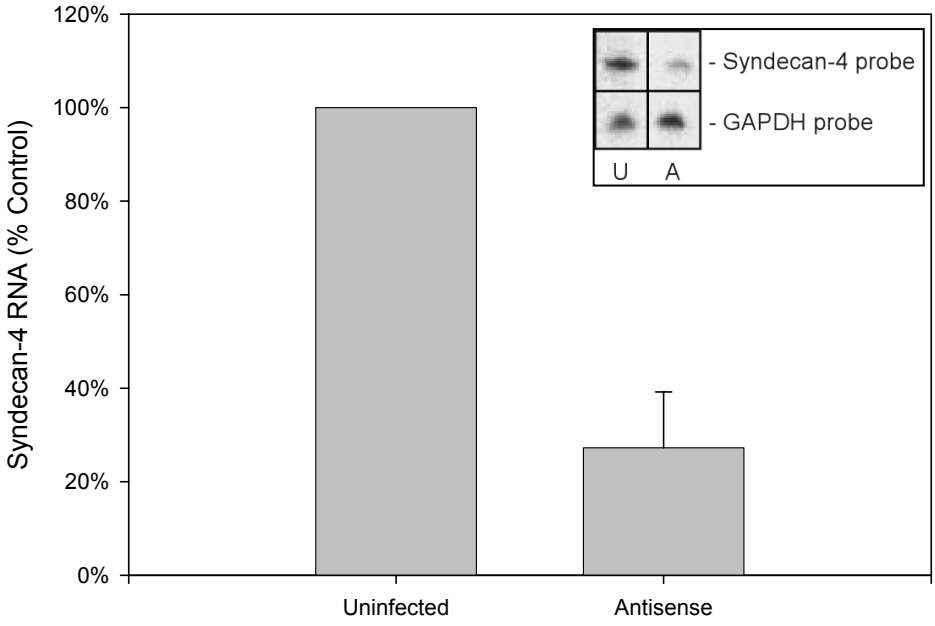

Figure 7. Reduction in syndecan-4 RNA after adenovirus infection. Cells were infected for 72 hours with a MOI of 10. Riboprobes were generated to the extracellular domains of rat syndecan-4 and corresponding sense and antisense probes were transcribed. The RNA was extracted, analyzed by RPA, and quantified by densitometry, using image analysis software. Measured RNA levels of the infected cells were reduced by 73%, compared to the uninfected controls. Inset: RPA results, indicating uninfected control (U) and antisense (A) RNA, detected with syndecan-4 and GAPDH (endogenous control) radioprobes. The results were obtained from at least three replicates.

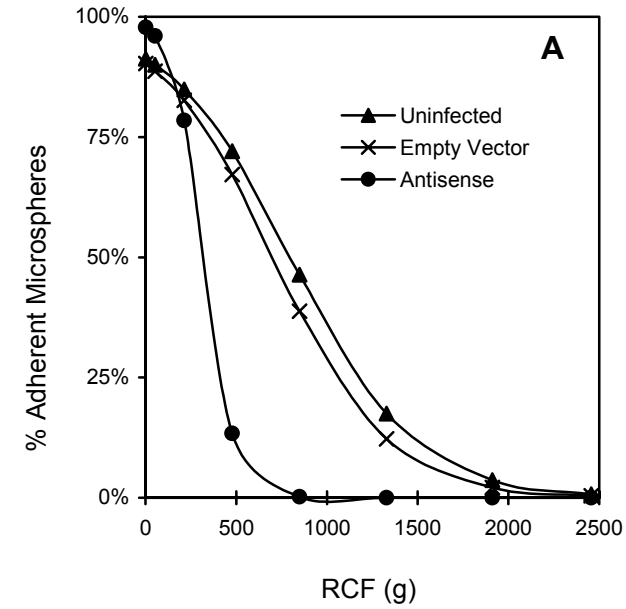

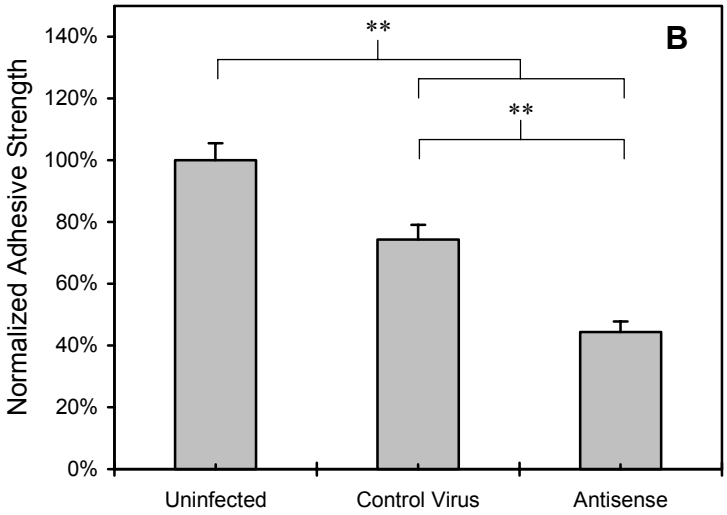

Figure 8. Decrease in adhesive strength as a result of a reduction in syndecan-4 RNA. Cells were either uninfected or infected with 10-30 MOI of adenovirus contructs containing a null (empty vector) or an antisense genetic construct. After one additional passage post-transfection, the cells were used in the centrifugation adhesion assay. Data were normalized to uninfected controls, and the results were obtained from at least three replicates. Differences between all groups are significant. ANOVA was performed, using Tukey's method for multiple pairwise comparisons. (**Indicates p value < 0.001)

2.4 Discussion

2.4.1 Syndecan-4 Regulation as a Means to Modify Cell Adhesion

Regulation of cell adhesion is a fundamental requirement for the normal function of cells in the blood vessel wall. SMCs, in particular, balance their adhesiveness and migratory characteristics based upon cues – chemical and mechanical – from their surrounding environment. These cues direct the cells to regulate the assembly, activity, and secretion of adhesion-related molecules, and to reorganize existing ECM components. Cell locomotion depends on a balance between cell adhesiveness and motility, which is directly affected by ECM composition and receptor density[104,123]. In particular, syndecan-4 has an established role in promoting the assembly of focal contacts, and subsequent cell adhesiveness. Through alterations in cell adhesion and locomotion, syndecan-4 regulation ultimately results in blood vessel remodeling, including restenosis and atherosclerotic plaque development.

The goal of our adhesion experiments was to examine the effectiveness of syndecan-4 regulation in the multi-step process of cell spreading and establishment of vascular SMC adhesive interactions. The highly sulfated pendant chains of syndecan-4 were the targets for our initial experiments using sodium chlorate. This chemical reversibly inhibits GAG sulfation, and therefore served as a first approximation of the importance of sulfated GAGs in general on the adhesion strength of spread cells. One recognized limitation of the sodium chlorate strategy was that sulfation inhibition was not restricted to GAGs, raising the possibility that unintended inhibition of sulfate-dependent cellular events may have confounded any observed alteration in adhesive strength. Despite this potential source of error, we noticed that the adhesion strength was indeed

reduced, and we were thus motivated to examine the effect that the highly sulfated syndecan-4 molecule in particular had on this process.

The studies outlined above also demonstrate the usefulness of our adenoviral system to selectively regulate syndecan-4 gene expression in order to examine its effects on cell adhesion. The use of an adenoviral vector as a means of specifically targeting syndecan-4 expression provided several advantages. In this system, sustained transfection for at least a week after the initial infection was verified by both the presence of GFP expression, indicating the presence of a co-transfected reporter gene, as well as RPA data showing reduced syndecan-4 mRNA. Additionally, the normal cytological appearance of the cells a week after transfection indicated that the cells remained viable. Unfortunately, verification of reduced syndecan-4 *protein* expression in the transfected cells was not possible due to the lack of a suitable anti-rat syndecan-4 antibody at the time of experimentation. However, in these adenovirus-infected cells, the marked reduction in adhesive strength in the presence of antisense construct beyond the effect of the null vector alone supported a role for syndecan-4 expression in adhesion generation. Despite the limitations of potent immunogenicity, an adenovirus system offers relative advantages over other transfection strategies, including the ability to shuttle large transgenes, replicate in high titer, and stably transfect target cells. Other transfection/transduction strategies, including electroporation, liposome-mediated, and retroviral methods suffer from variability, low efficiency, cell mortality, or safety concerns. An additional strategy is the use of genetic knockout models, where impaired wound healing has been demonstrated in both syndecan-1 and syndecan-4 knockout mice, each apparently due to separate processes[124-126]. However, despite recent success

using these models, genetic knockout methodologies often result in animals with an unpredictable phenotype, or who may not be viable or fertile.

2.4.2 Adhesion Assay Limitations

The assay employed in our experiments, though useful in its ability to measure cell-substrate adhesion, contained some inherent limitations. One limitation was that our measurements did not account for the fact that the *RCF* experienced by the cell monolayer varied during the experimental procedure, based on the time it took for the centrifuge to accelerate to (and decelerate from) the desired angular velocity. Although the target speed in each experiment was maintained for one minute, the duration of the acceleration and deceleration periods depended on the final speed. For example, the centrifuge required approximately 10 seconds before measuring 500 x *g*, while it required approximately 25 seconds before measuring 1500 x *g*.

In addition to this nonlinear acceleration, the detachment profiles of our FN pre-adsorbed glass microspheres at a constant *RCF* were likely nonlinear functions of time (Figure 9). Since a critical requirement of the assay was that, at a given *RCF*, each sample needed to be centrifuged for a length of time after which no additional microspheres detached from the cell monolayer, a one minute time period was chosen in order to allow for the microspheres to detach at all forces available in the assay. It was assumed that any additional amount of time would not yield a significant decrease in adherent microspheres.

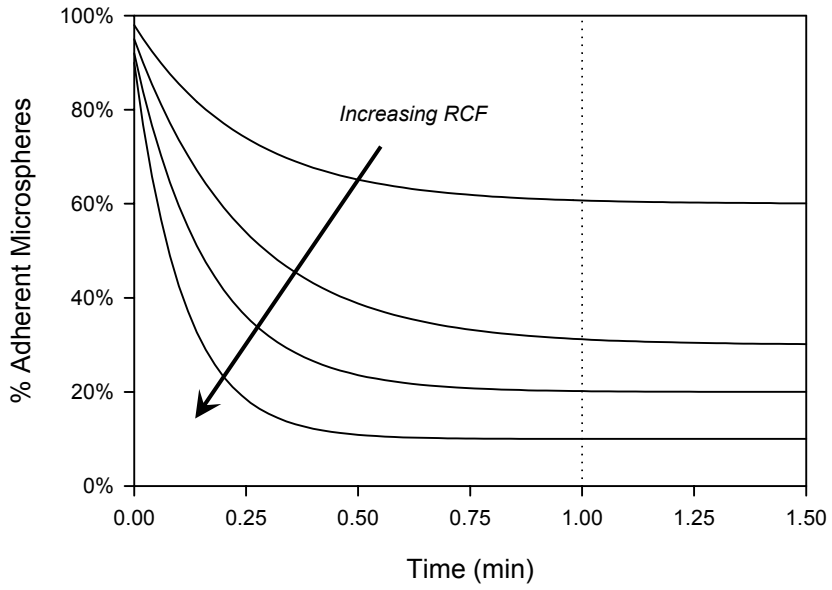

Figure 9. Predicted detachment profiles of FN pre-adsorbed glass microspheres adherent to a SMC monolayer. In our experiments, we assumed that for each applied *RCF* the percent adherent microspheres decreased as an undetermined, nonlinear function of time, but that by 1 minute (dotted line), no significantly additional detachment occurred for all samples. The arrow denotes detachment profiles at increasing maximal *RCF* values.

Another limitation of the selected assay was that it enabled the quantification of global, population-based, rather than single cell or receptor adhesion parameters. Unlike micromanipulation techniques, which are able to isolate the adhesive forces between a limited number of individual receptors, our assay applied a relatively uniform detachment force to all cells in a given experiment. Thus, potentially important cell-to-cell and even single receptor differences may have been underappreciated. In addition, a potential source of error could arise due to an effect of syndecan-4 regulation on other adhesion receptor expression and/or activity, resulting in changes in adhesion strength that were

not directly related to syndecan-4. An example of this has been demonstrated by the effects of syndecan-1 regulation in mammary epithelial cells[127]. In this system, down-regulation of E-cadherin occurred in concert with syndecan-1, resulting in altered cell-cell interactions.

Overall, our experimental system served as a simple and sensitive technique to assess well-established cell-ECM adhesive interactions on a defined substrate. As a functional assay, our strategy offered distinct advantages over other methods, including other types of centrifugation[96,128-130], micromanipulation[94,95,131-133], and hydrodynamic flow[97,98,134-140]. In other centrifugation assays, the maximum force generated is insufficient to detach well-spread cells. In micromanipulation assays, time, cost, and investigator variability limit the assay's usefulness and reliability. In hydrodynamic flow assays, the need for specialized equipment and the dependence of the applied force on cell morphology restrict the assay's widespread use and adaptability[141]. Despite the limitations of each, the various adhesion assays have been used to demonstrate the importance of cell adhesion in vascular biology[87,142,143]. For example, it has been shown that during periods of angiogenesis, physiologic remodeling, and responses to vessel injury, this process is particularly dramatic. SMCs and myofibroblasts alter their adhesive characteristics, proliferate, and migrate within the vessel wall[114,144,145], often leading to adverse events such as intimal hyperplasia and alterations in normal vascular hemodynamics.

CHAPTER 3

REGULATION OF SYNDECAN GENE EXPRESSION IS INFLUENCED BY MECHANICAL STRAIN

The local mechanical environment in the vascular wall regulates many functions of the resident cells. This fact is particularly evident in the medium and large arteries, where the magnitude of the hemodynamic fluctuations varies under different physiologic and metabolic conditions. Using vascular SMCs as a model system, our aim of was to use a well-characterized technique to mechanically strain the cells under controlled and reproducible conditions for the purpose of evaluating the transcriptional regulation of syndecan-4. As a means of comparison, we also investigated the regulation of other HSPGs expressed by SMCs, namely syndecan-1 and syndecan-2. We postulated that syndecans, increasingly well known for their involvement in cell-matrix interactions and growth factor signaling, were candidates for cyclic strain-induced modulation.

3.1 Background and Significance

3.1.1 Vascular Wall Mechanics and Physiologic Effects

Regulation of vascular hemodynamics takes place at several levels: self-regulation, central and autonomic control, and hormonal control. This regulation serves either to alter the flow of blood traveling within the vessel or to alter the mechanical properties of the wall itself. Several workers have modeled the mechanics of the arterial wall in terms of the stresses present during physiologic and pathologic loading[18,146,147]. These stresses include hydrostatic pressure, fluid shear, and circumferential tension; and

the nature and duration of these same stresses are potentially critical factors in the type and the extent of an injury outcome. In particular, periodic deformations, resulting from the cardiac cycle, are imparted on the constituents of the vessel wall and play a significant role in creating an optimal biomechanical microenvironment essential for normal cell function. Thus, it has become increasingly apparent that alterations in the local mechanical environment, both acute versus chronic, and static versus cyclic, may be important factors that initiate and modulate cellular responses to injury. In fact, cyclic strain has been shown to stimulate collagen synthesis by SMCs[148], activate extracellular signal-regulated mitogen-activated protein kinase (ERK) 1/2 [149], as well as induce intracellular trafficking and protein phosphorylation[150,151]. The stresses that accompany direct tissue injury activate SMCs and modulate gene expression and cell differentiation[152]. Thus, changes in the local mechanical environment of the vascular wall can induce the activation and transformation of SMCs from a quiescent to a synthetic phenotype, and we therefore found it necessary to analyze cellular responses to defined mechanical conditions.

Among the stresses transmitted to SMCs in the vascular wall during injury (Equation 1.1), for the purposes of this study, our model system focused our analysis on circumferential tension, and we evaluated the resulting regulation of syndecan-4 gene expression. Admittedly, an examination of the interplay of all of these mechanical elements will eventually provide the most significant insight into in syndecan-4 regulation; however, we chose three mechanical microenvironments which appear to be particularly relevant to the development of lesions within the vascular wall. First, an *acute increase in static tension* is produced during cardiopulmonary bypass for coronary

artery and cardiac valve repair[153], and during percutaneous transluminal coronary angioplasty (PTCA) and stenting procedures (increased *P and R*). Although not modeled in our studies, PTCA actually produces forces that are great enough in magnitude to stretch and even split components of the vessel wall[25-27,154]. Second, an *acute increase in cyclic tension* results during physical or metabolic conditions that transiently increase blood pressure (increased *P*). Finally, a persistent or *chronic increase in cyclic tension* may be manifest in clinical conditions such as untreated or poorly controlled hypertension or an aortic aneurysm (increased *R*), while a *chronic decrease in cyclic tension* may be associated with atherosclerosis, intimal hyperplasia, and restenosis (decreased *R*; increased *h* and *E*). In summary, the purpose of our *in vitro* model assay was to replicate specific examples of *in vivo* mechanical forces experienced by vascular SMCs and gain insight into syndecan regulation.

3.1.2 Cyclic strain device

Periodic hoop stress is the predominant force on cells in the media and adventitia of blood vessels[18]. Due to the transmural pressure across the vessel wall, this stress in turn results in radial and circumferential strains. The experiments outlined below were performed using SMCs grown on a FN-coated silicone elastomer, which could be subjected to mechanical tension. Previous strain devices principally employed uniaxial stretch of rectangular membranes or biaxial stretch of membranes of various geometries. These geometries were typically circular, and deformation of the membrane was induced by means of a platen-driven assembly or a pressure gradient. In order to circumvent the inherent problems of strain heterogeneity and anisotropy of the popular Flexercell Strain

Unit (Flexcell International Corp)[155-161], in-plane membrane stretch devices were developed. Schaffer et al. and Hung and Williams[162] were the first to describe the use of a type of device capable of applying equibiaxial (radial = circumferential) strain to a monolayer of cells[163]. We have previously used this device in our lab to recapitulate balloon angioplasty injury[164]. The mechanism of this device is in contrast to the commonly used vacuum pressure-driven ones. Until recently, these various pressure-driven devices were limited by non-uniform strain fields, resulting in a gradient of membrane stress with distance from the center of the plate. Notably, Chen et al. used a vacuum-driven device to impart 10% average strain at 1 Hz to cells growing on an elastic membrane. This level of strain has been shown to be relevant physiologically to that present in large arteries (aorta, carotid, femoral, brachial) [165,166]. For our purposes, we used a truly equibiaxial strain device as an *in vitro* correlate for the *in vivo* micromechanical environment of the native vessel[164].

3.1.3 Heparan Sulfate Proteoglycan / Syndecan Biology

The principal way cells sense changes in and communicate with their environment is through their cell surface receptors, and it has become well known that cells respond to local hemodynamic changes by remodeling their surrounding ECM in order to counteract or minimize these changes[16,167]. Since remodeling requires changes in adhesive characteristics and/or elaboration of effector molecules into the surrounding milieu, we therefore looked to the syndecans as candidate mediators this response.

Though syndecan-4 was the focus of the adhesion experiments, regulation of syndecan-1 and syndecan-2 have also proven to be of interest for several reasons. One

reason is the functional similarity between syndecan-1 and syndecan-4, as indicated by their similar ability to promote intercellular adhesion in a study of B lymphoid cells[168]. Since the ectodomain primary sequences of these two syndecans are quite dissimilar, it has been suggested that they may resemble each other in conformation, either as monomers or as aggregates[65]. The conclusion was that a secondary or tertiary structural resemblance could be responsible for similar action. A second reason for our interest in other members of the syndecan family is the involvement of syndecan-2 in several cell-ECM interactions, such as FGF-induced fibroblast adhesion[169], and the regulation of actin stress fiber organization in lung carcinoma cells[170]. Lastly, the ability of the HS chains to interact non-specifically with a host of soluble and insoluble ligands, when attached to both cell surface and shed syndecan ectodomains, suggests a role for them in remodeling events.

Our aim was therefore to characterize the gene expression of syndecan-4 under series of well defined strain protocols, particularly as it relates to the expression of syndecan-1 and syndecan-2. Strain protocols were chosen such that they mimicked specific *in vivo* situations known to occur under different physiologic and pathologic circumstances, enabling us to gain insight into the consequences of certain disease states or clinical interventions on vascular wall cell biology.

3.2 Materials and Methods

3.2.1 Cell Culture

Clonetics normal human aortic smooth muscle cells (SMC), culture medium, and supplements were obtained from Cambrex Bio Science (Walkersville, MD), and the cells

were sub-cultured using standard techniques. Smooth Muscle Cell Growth Medium-2 (SmGM-2) was prepared according to the supplier's recommendations (Smooth Muscle Basal Medium (SmBM), supplemented with 5% fetal bovine serum (FBS), 500 μg/mL human epidermal growth factor (hEGF), 5 μg/mL insulin, 2 mg/mL human fibroblast growth factor (hFGF), 50 μg/mL gentamycin, and 50 mg/mL amphotericin-B. Cells were maintained in tissue culture-treated petri dishes at 37ºC, 5% CO_2, and humidified atmosphere. Growth medium was changed every two days, and the cells were passaged 1:4 when the dishes were 80% confluent, using 0.05% Trypsin / 0.53 mM EDTA (Invitrogen Life Technologies, Carlsbad, CA). Experiments were performed on cells between passages 6 and 10 using Quiescence medium, which consisted of basal medium supplemented with 0.5% FBS, 50 μg/mL gentamycin, and 50 mg/mL amphotericin-B.

3.2.2 Mechanical Strain Application

Strain dishes were assembled in the following manner: the bases of bottomless, custom-made plastic petri dishes were fitted with a silicone membrane (0.005" thickness; 40 Durometer; Specialty Manufacturing, Saginaw, MI). The silicone served as the flexible growth area of the strain dishes. 5 μg/mL of human plasma fibronectin (FN; Sigma) in PBS was pre-adsorbed to the growth area for at least 8 hours at 4ºC, serving as a substrate for cell attachment. The cells were then seeded onto the membranes, cultured to 80% confluence in SmGM-2, and then growth-arrested for 24 hours in Quiescence medium. Depending on the experimental conditions, defined static or cyclic tension was applied to the cells using a StrainMaster apparatus (Z-Development, Inc., Cambridge, MA; Figure 10)[171]. All strain protocols were performed at 1 Hz, in order to mimic the

"normal" adult heart rate of 60-80 beats per minute. As shown in Figure 11, the cells were subjected to different regimens of cyclic or static strain. For a given protocol, the cells were either cyclically strained at 1 Hz or held static, and the RNA was harvested at various time points up to 24 hours. Alternatively, the cells were strained at different magnitudes, under either cyclic or static conditions, after which the cells were harvested simultaneously. Lastly the cells were preconditioned by subjecting them to a physiologic level of 10% cyclic strain[172] for 24 hours, followed by 20% strain thereafter. RNA was harvested at specific time points after the initiation of 20% strain.

3.2.3 Cell Viability

In order to ensure that the different treatments were not cytotoxic, Live/Dead Viability/Cytotoxicity assays were performed in order to assess cell viability/injury. Cells were grown to 80% confluence in SmGM-2 and Quiesced for 24 hours. They were then subjected to one of the experimental conditions. They were then rinsed once with PBS and a solution containing 0.5 μM calcein AM and 1 μM ethidium homodimer in PBS (Molecular Probes, Eugene, OR) was added for 15 minutes at 37ºC. The cells were then observed for the generation of red or green fluorescence, using an inverted microscope with epifluourescent illumination (Olympus, Melville, NY) at 100X magnification.

3.2.4 Human Aortic SMC RNA Analysis

To determine syndecan gene expression in human aortic SMCs, real time quantitative PCR was used. Briefly, total RNA was harvested either by using the TRIzol

reagent (Gibco BRL) or the RNeasy Mini kit with DNase digestion (Qiagen, Valencia, CA). The cells growing in a 100 mm culture dish were removed using a cell scraper, and then transferred to microcentrifuge tubes. The TRIzol-treated cells were extracted with chloroform and isopropanol, followed by rinsing with 75% ethanol. RNA was re-suspended in RNase-free water, and the concentration was determined by measuring OD_{260}. The absence of significant DNA or protein contamination was verified by determining the OD_{260}/OD_{280} ratio. cDNA was generated from the extracted RNA using SuperScript III reverse transcriptase (Invitrogen). 5 μg RNA was used in each reaction. For real time PCR analysis, TaqMan Gene Expression Assays (Applied Biosystems, Foster City, CA) were used. Assay sets contained proprietary forward and reverse DNA primers and 5,(6) carboxyfluorescein (6-FAM)-labeled probes specific to the gene of interest were selected from Applied Biosystems' database of genomic assays (Table 2). Assay ID's Hs00174579_m1 (syndecan-1), Hs00299807_m1 (syndecan-2), and Hs00161617_m1 (syndecan-4) were selected. Additionally, Hs99999901_s1 (18S rRNA) and Hs99999903_m1 (β-actin) were selected for use as endogenous controls. Amplification and detection were performed on an ABI Prism 7000 Sequence Detection System (Applied Biosystems), using AmpliTaq Gold DNA Polymerase (Applied Biosystems) in a 5' nuclease reaction.

Data generated from the target gene amplification was normalized to the simultaneously amplified endogenous controls in order to quantify expression levels that were robust to incidental experimental variation. Gene expression in the treated groups was represented relative to that in the unstrained controls.

Table 2. Real time PCR DNA primer and probe sets obtained from the TaqMan Gene Expression Assays database of Applied Biosystems

Target Gene	Assay ID
Human Syndecan-1	Hs00174579_m1
Human Syndecan-2	Hs00299807_m1
Human Syndecan-4	Hs00161617_m1
Eukaryotic 18S rRNA	Hs99999901_s1
Human β-actin	Hs99999903_m1

3.2.5 Statistics and Data Analysis

Values are reported as mean ± SEM. Statistical analysis was performed using SigmaStat 3.0 software package. ANOVA was employed, using the Holm-Sidak test for multiple pairwise comparisons among the treatments. When applicable, logarithmic transformation of the data was necessary prior to statistical analysis in order to make the error variance independent of the mean. In other cases, the Kruskal-Wallis ANOVA on Ranks non-parametric test was used. A p value < 0.05 was considered statistically significant for all tests.

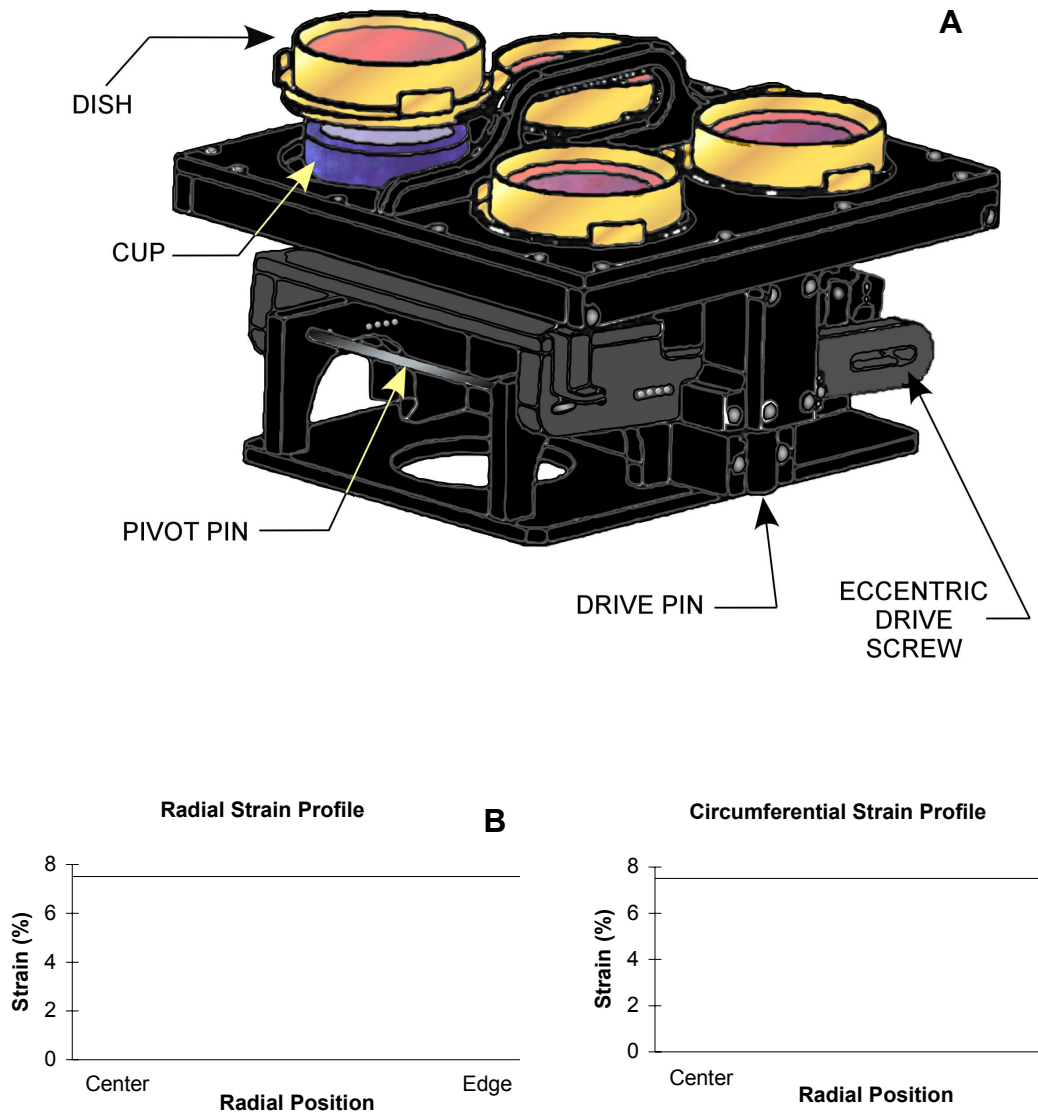

Figure 10. Schematic diagram (A) and strain profiles (B and C) of the StrainMaster apparatus to apply biaxial strain to a monolayer of cells in culture. The dish containing adherent cells is secured onto a docking collar. The circular silicone membrane in each dish is deformed by a cup and platen assembly, as a motor-driven cam displaces the assembly in a sinusoidal manner. Placement of the pivot determines the amplitude of the motion. The theoretically determined radial and circumferential strain profiles demonstrate the ability of this device to apply isotropic and homogeneous strain (Adapted from Schaffer, Chen, and others)[163].

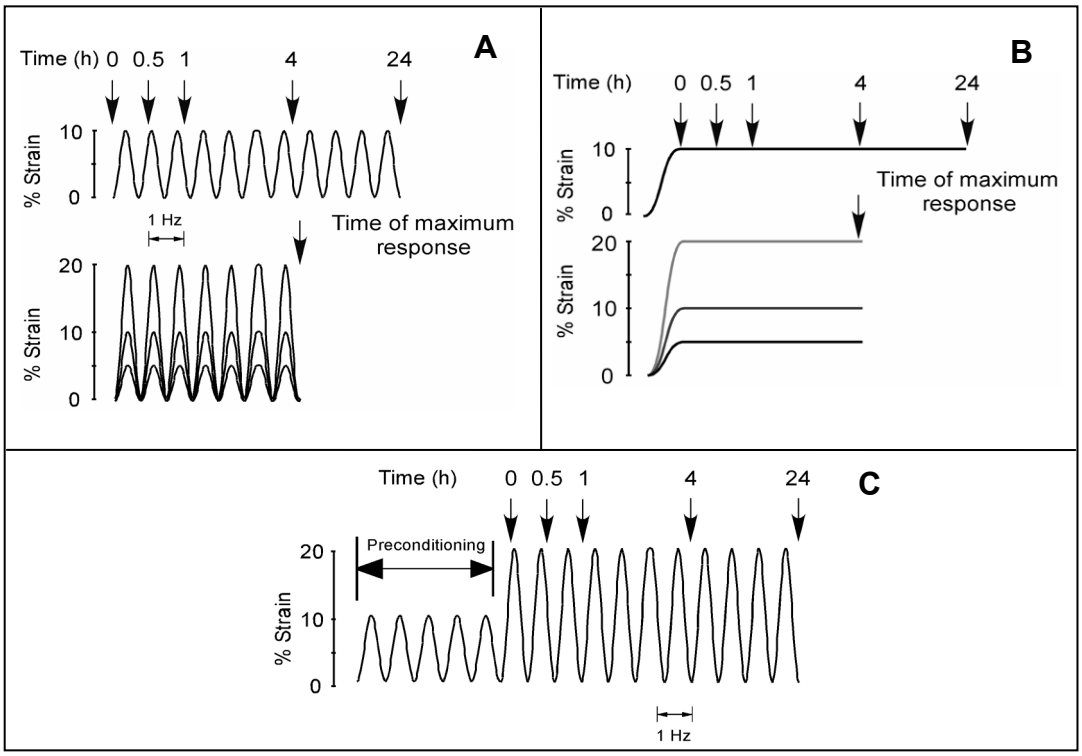

Figure 11. Protocols for the application of mechanical strain. SMCs were subjected to 1 Hz cyclic tension for various time periods and strain magnitudes (A). Alternatively, the cells will be subjected to static tension, and the protocols were repeated (B). Finally, the effect of preconditioning was examined by cyclically stretching the cells at 10% strain for 24 hours, followed by repeating the time-course cyclic tension protocol at 20% strain (C). Arrows indicate sampling points, in which cells were harvested for syndecan gene expression analysis.

3.3 Results

3.3.1 Vascular SMCs Tolerate Mechanical Strain Without Gross Cytotoxicity

As described in the Methods, the cell growth area consisted of a FN pre-adsorbed silicone membrane. Both the membrane and the adherent cells were subjected to various degrees of mechanical strain. The application of cyclic strain was accomplished using the StrainMaster apparatus, which allowed control over the frequency and amplitude of the radial and circumferential strains of the membrane. The details and validation of the mechanical strain device are described elsewhere[162,163,171]. Briefly, unlike fluid displacement[173,174] and vacuum-driven strain devices[155,175-177], the current apparatus was designed with the ability to apply homogeneous (positional invariance of the strain tensor) and biaxially uniform (directional equivalence) strains over the growth area of the membrane. In other words, the radial and circumferential strains were equivalent ($\varepsilon_r = \varepsilon_\theta$).

Cell viability/injury was investigated after each of the periods of mechanical strain. In all cases, viability was assessed using a Live/Dead assay, in which calcein AM and ethidium homodimer were added to the cells. Live cells, containing active esterases, converted the calcein AM to calcein, which produced green fluorescence (~515 nm); conversely, injured/dead cells were permeable to the ethidium homodimer, which produced red fluorescence (~635 nm) when bound to DNA. As Figure 12 demonstrates, most cells stained green, while only a few red-stained ones could be identified, indicating that cells remained viable under all conditions under study. These conditions were representative of those imposed on the cells in the subsequent syndecan gene expression and protein regulation studies.

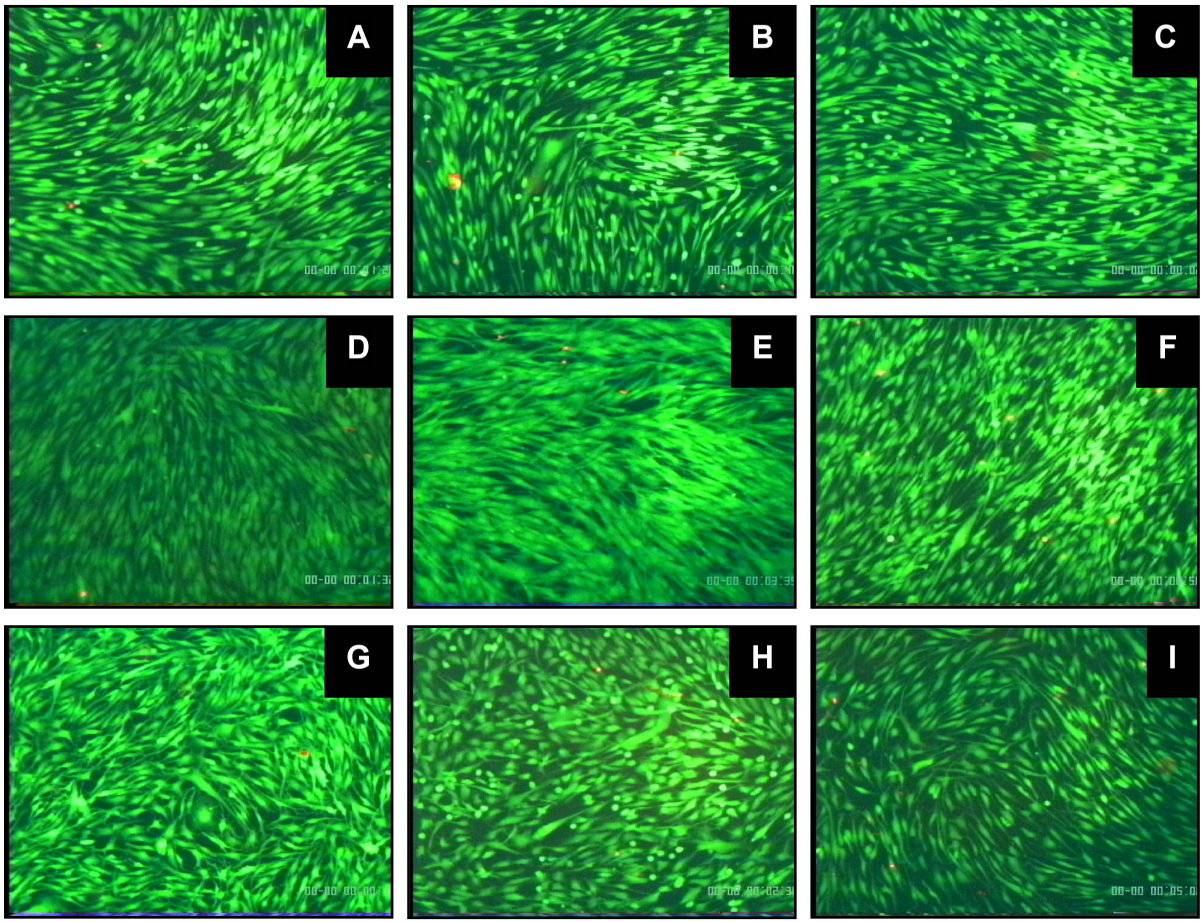

Figure 12. SMC viability after mechanical strain. Cells were grown on elastic membranes, subjected to a representative range of mechanical loading conditions, and assayed for viability by visualizing fluorescence generated after the administration of calcein AM and ethidium homodimer. Cells were visualized at 100X magnification. In (A), cells were not strained. In B-C, the cells were treated with 10% static strain for 1 hour (B) or 24 hours (C). In D-E, cells were treated with 10% cyclic strain for 1 hour (D) or 72 hours (E). In F-G, cells were treated with 20% cyclic strain for 1 hour (F) or 4 hours (G). In H-I, cells were treated with 24 hours of 10% cyclic strain (preconditioning), followed by 1 hour (H) or 4 hours (I) of 20% cyclic strain.

3.3.2 Static Strain Induces Differential Gene Expression Between the Syndecans

Isolated RNA was used for analysis of syndecan-4 gene expression under multiple experimental mechanical strain conditions. For most studies in which the expression pattern of syndecan-4 was analyzed, we also compared the syndecan-4 regulation to that of syndecan-1 and syndecan-2. We first investigated the effect of *in vitro* administration of two levels of static strain on the kinetics of syndecan gene expression over a 24 hour time period. When subjected to 5% static strain, syndecan-4 exhibited a modest rise to 141 ± 40% of unstrained control at 4 hours. Over the remaining 20 hours of the experiment, however, syndecan-4 gene expression fell significantly, when compared to the 4 hour levels, to 79 ± 10% of unstrained control (Figure 13C). When subjected to 10% static strain, the trend was similar to the response to 5% static strain, but the change in magnitude was not significant. At 4 hours, gene expression was only 110 ± 2% of unstrained control, whereas at 24 hours, it was 76 ± 4% (Figure 14C).

When subjected to 5% static strain syndecan-1 exhibited no significant change at any of the time points observed, ranging from 74 ± 13% of unstrained control at 4 hours to 87 ± 20% at 24 hours (Figure 13A). There were significant differences in the syndecan-2 expression, and the pattern was similar to syndecan-4. Like syndecan-4, syndecan-2 expression initially rose slightly to 118 ± 14% of unstrained control (at 1 hour), then levels then fell moderately to 70 ± 8% of unstrained control at 24 hours (Figure 13B), which was a significant reduction from the 1 hour levels.

At the 10% static strain level, there was again no significant change in syndecan-1 gene expression, ranging from 98 ± 45% to 109 ± 20% of unstrained control after 4 and 24 hours, respectively (Figure 14A). On the other hand, syndecan-2 again resembled the

syndecan-4 response; however, the magnitude of the syndecan-2 response was significant. Following the initial 4 hours of strain, in which no significant change occurred, syndecan-2 gene expression fell to 53 ± 12% of unstrained control at 24 hours (Figure 14B).

In addition to the comparisons just described, it was informative to determine if the *magnitude* of static strain influenced syndecan gene expression during any period of our investigation (Figure 15). To determine this, interaction effects between static strain magnitude and duration of the two-way ANOVA data were examined. This analysis identified no significant dependence of gene expression on the magnitude of static strain at any of the time points under investigation. In other words, for each syndecan, gene expression was regulated equivalently for both 5% and 10% strain, within the experimental variability.

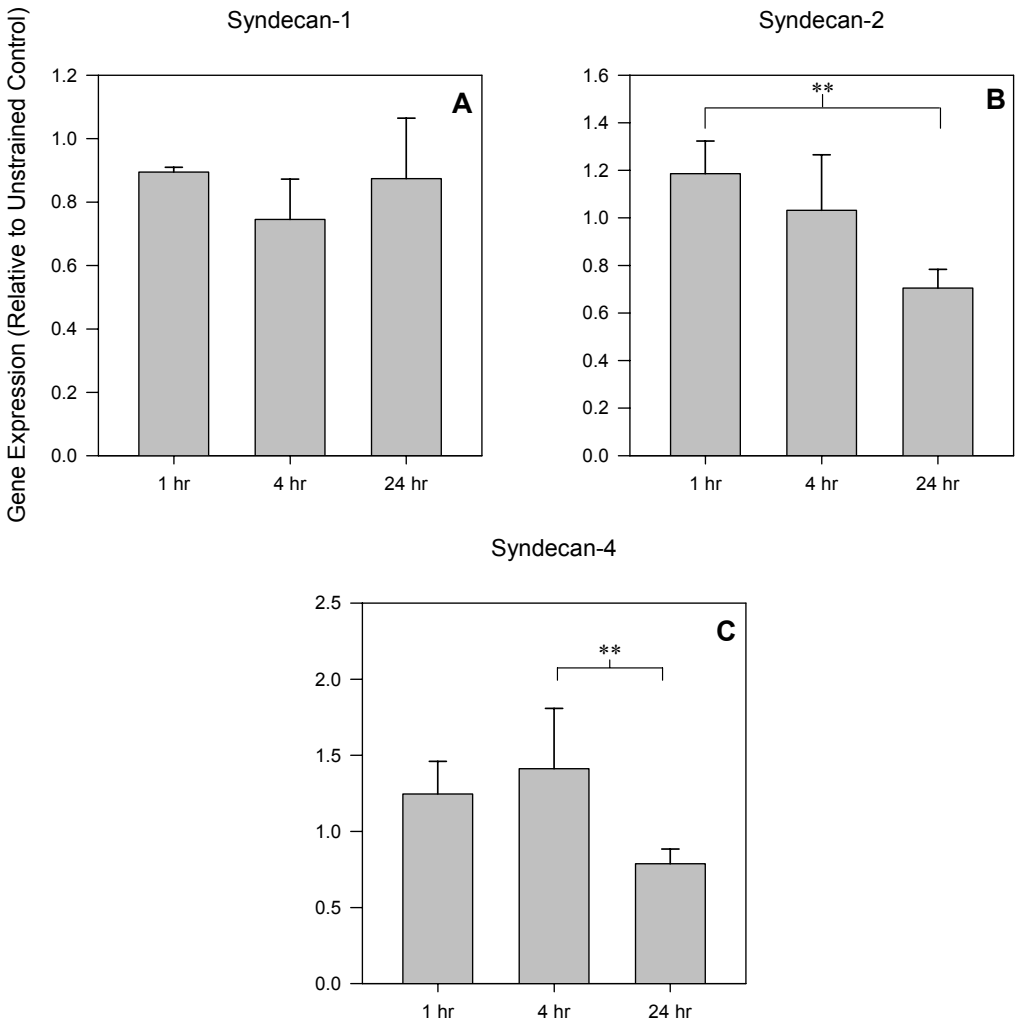

Figure 13. Effect of 5% static strain on syndecan-1 (A), syndecan-2 (B), and syndecan-4 (C) gene expression. Human aortic SMCs were cultured on elastic membranes which were stretched at 1 Hz for the indicated periods of time. The cells were then harvested, and RNA was isolated and analyzed using real-time PCR. All results were internally normalized to 18S rRNA levels, and the syndecan levels are presented relative to unstrained controls. The data represent the means and standard errors of triplicate experiments, and statistical analysis was performed using ANOVA, employing Holm-Sidak's method for multiple pairwise comparisons. (** Indicates a p value < 0.05)

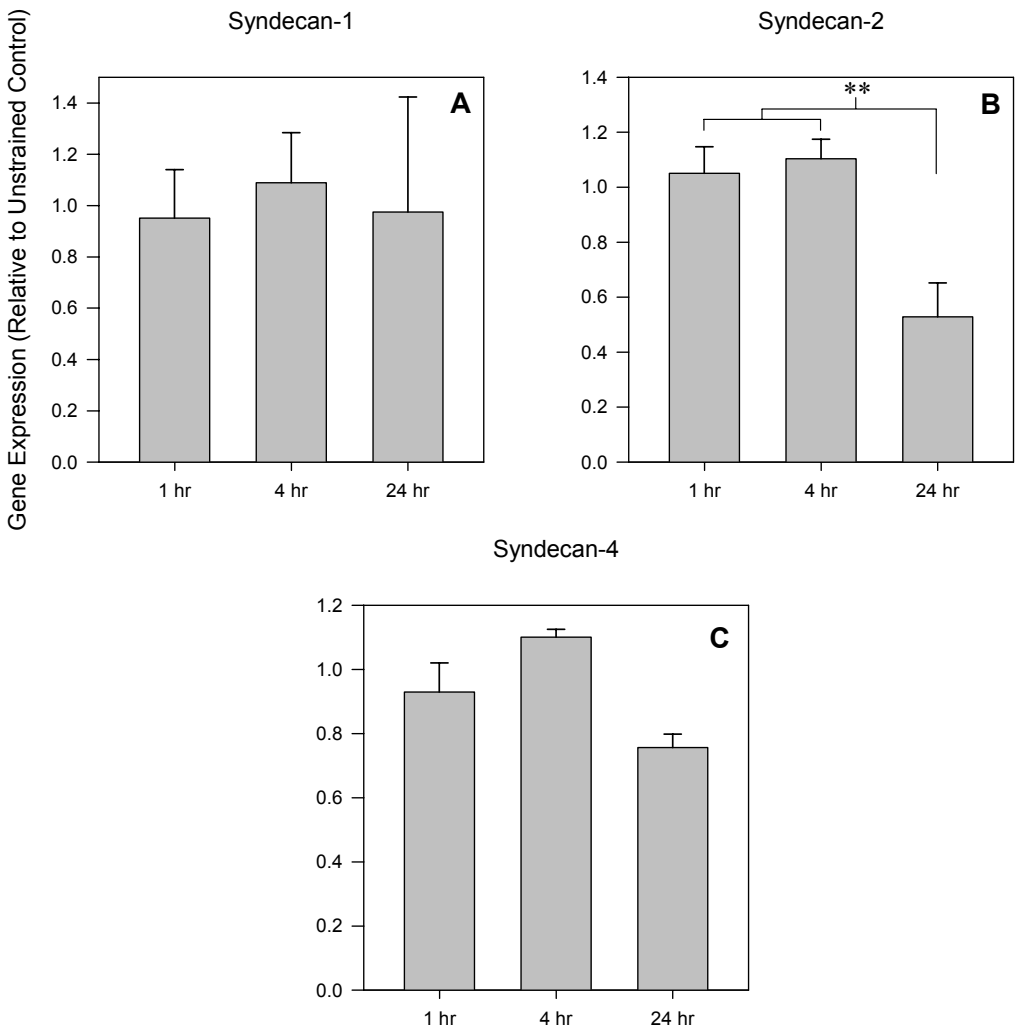

Figure 14. Effect of 10% static strain on syndecan-1 (A), syndecan-2 (B), and syndecan-4 (C) gene expression. Human aortic SMCs were cultured on elastic membranes which were stretched at 1 Hz for the indicated periods of time. The cells were then harvested, and RNA was isolated and analyzed using real-time PCR. All results were internally normalized to 18S rRNA levels, and the syndecan levels are presented relative to unstrained controls. The data represent the means and standard errors of triplicate experiments, and statistical analysis was performed using ANOVA, employing Holm-Sidak's method for multiple pairwise comparisons. (** Indicates a p value < 0.05)

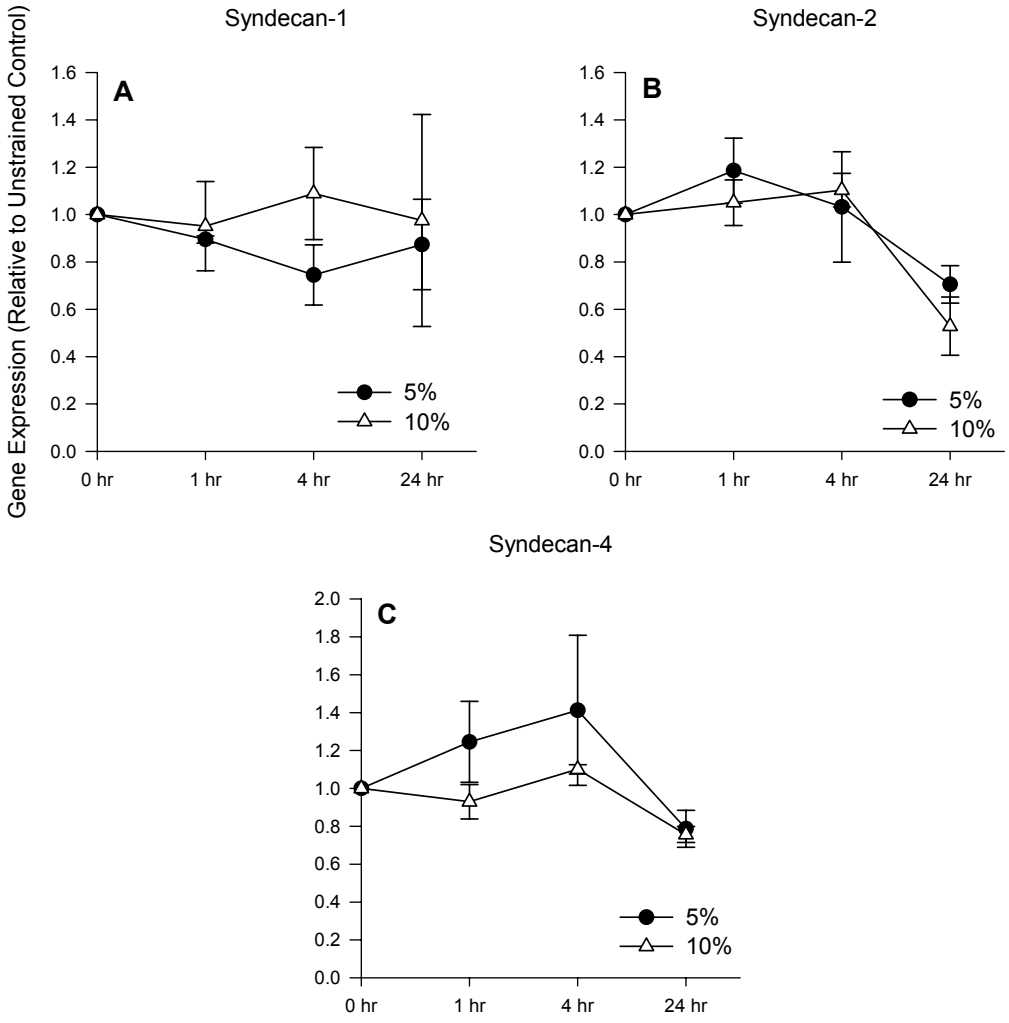

Figure 15. Effect of 5% (●) vs. 10% (△) static strain on syndecan-1 (A), syndecan-2 (B), and syndecan-4 (C) gene expression. Human aortic SMCs were cultured on elastic membranes which were stretched at 1 Hz for the indicated periods of time. The cells were then harvested, and RNA was isolated and analyzed using real-time PCR. All results were normalized to endogenous 18S rRNA, and the syndecan levels are presented relative to unstrained controls. The data represent the means and standard errors of triplicate experiments, and statistical analysis was performed using ANOVA. 2-way interaction analysis resulted in no significant differences.

3.3.3 Cyclic Strain Regulates Syndecan Gene Expression in a Time-Dependent Manner

Given the results from the static strain experiments, it was necessary to evaluate whether the pattern of syndecan expression suggested by the data was purely a stretch-related event, or whether the periodic nature of cyclic strain was important. We investigated whether the *in vitro* administration of cyclic strain influenced the kinetics of syndecan gene expression in vascular SMCs, and we found that the syndecans were again regulated differentially. Under the application of 5% cyclic strain syndecan-4 gene expression exhibited a biphasic response (Figure 16C). It increased significantly from 119 ± 17% of unstrained controls at 1 hour to its peak of 200 ± 34% at 4 hours, and subsequently returned at 24 hours to the level of gene expression seen in the unstrained controls (121 ± 17%).

In contrast to syndecan-4, syndecan-1 and syndecan-2 responded with steady increases in gene expression. Syndecan-1 displayed significant differences between 1 hour and 24 hours and between 4 hours and 24 hours, increasing from 93 ± 6% of unstrained controls at 1 hour to 131 ± 14% at 4 hours to 206 ± 40% at 24 hours. (Figure 16A. Syndecan-2 displayed significant increases between all three time points, increasing from 67 ± 7% of unstrained controls at 1 hour to 117 ± 8% at 4 hours, to 186 ± 17% at 24 hours (Figure 16B).

In order to assess the syndecan gene regulation under more chronic conditions, we chose to evaluate the response to cyclic strain of longer duration for the 10% studies. In addition, the extra data points displayed in Figure 17 (25 and 28 hrs) correspond to the data points used for the subsequent preconditioning experiments. We also chose 10% because of the physiologic relevance of this strain magnitude[166]. Under the application of

10% cyclic strain the results suggested that each syndecan responded in a similar fashion to their response to 5% cyclic strain (Figure 17). Syndecan-4, similar to 5% cyclic strain, significantly increased from 127 ± 19% of unstrained controls at 1 hour to its peak of 182 ± 17% at 4 hours. The subsequent reduction in syndecan-4 gene expression to 99 ± 11% was significant, and was evident at 24 hours. Moreover, the reduced expression levels remained evident at 48 hours (66 ± 12%). Syndecan-1 increased significantly from 107 ± 10% of unstrained controls at 1 hour to 278 ± 33% at 24 hours, and remained elevated at 48 hours (294 ± 31%). Similarly, syndecan-2 significantly increased from 97 ± 14% of unstrained controls at 1 hour to 204 ± 17% at 24 hours, and also remained elevated at 222 ± 43% at 48 hours.

Similar to the analysis of the static data, it was important to determine if the *magnitude* of cyclic strain influenced syndecan gene expression at any time under investigation by examining the interaction effects between cyclic strain duration and magnitude (Figure 18). Our findings in this regard were also similar to those of the static strain protocols; namely, with one exception, there were no significant differences between 5% and 10% cyclic strain for any of the syndecans. The exception was syndecan-1 gene expression at 24 hours (Figure 18A), which exhibited a significant difference between 5% and 10% strain after 24 hours, indicating that the increase in syndecan-1 expression depended on both the magnitude and duration of cyclic strain.

To further investigate the effects of strain magnitude on syndecan gene expression, we chose magnitudes in which vascular injury occurs. Using a dose-response study, we subjected the cells to levels of cyclic strain ranging from 5% up to 20% for 4 hours (Figure 19). The encouraging results from the earlier experiments which demonstrated a

significant syndecan-4 response at this time guided our decision. Unfortunately, the results indicated that cyclic strain of this duration failed to yield significant differences at various levels of strain, even at magnitudes able to cause cell injury. Possible conclusions from this are that (1) 4 hours of strain was not long enough for significant differences in gene expression to become evident, (2) the cells did not sense 20% strain as a condition that was significantly different than 5%, or (3) the increased membrane strain was ineffectively transmitted to the cells. To investigate the possibility that the cellular response to 20% strain required longer than 4 hours, we conducted the experiments described below. As described below, these protocols also included a period of mechanical preconditioning.

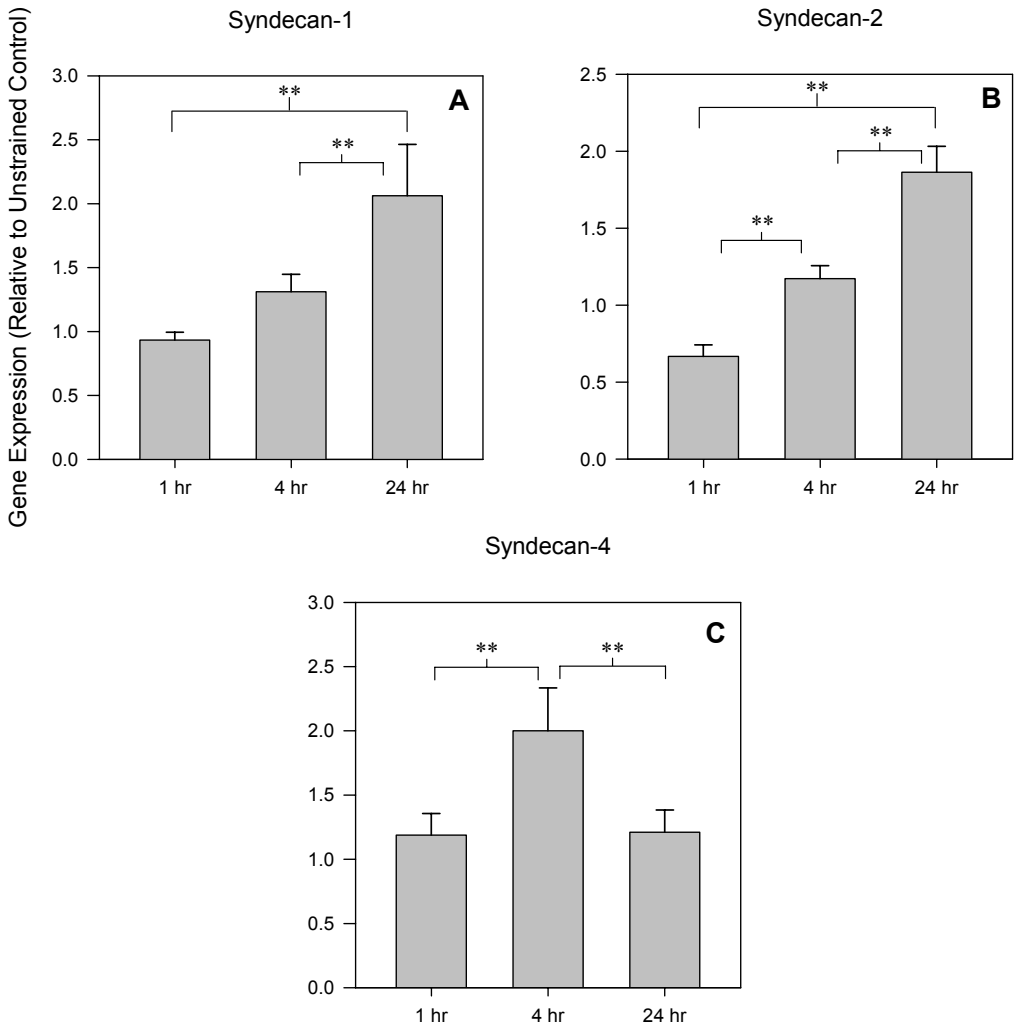

Figure 16. Effect of 5% cyclic strain on syndecan-1 (A), syndecan-2 (B), and syndecan-4 (C) gene expression. Human aortic SMCs were cultured on elastic membranes which were stretched at 1 Hz for the indicated periods of time. The cells were then harvested, and RNA was isolated and analyzed using real-time PCR. All results were internally normalized to 18S rRNA levels, and the syndecan levels are presented relative to unstrained controls. The data represent the means and standard errors of at least triplicate experiments, and when necessary, statistical analysis was performed on the data after logarithmic transformation. ANOVA was then performed, employing Holm-Sidak's method for multiple pairwise comparisons. (** Indicates a p value < 0.05)

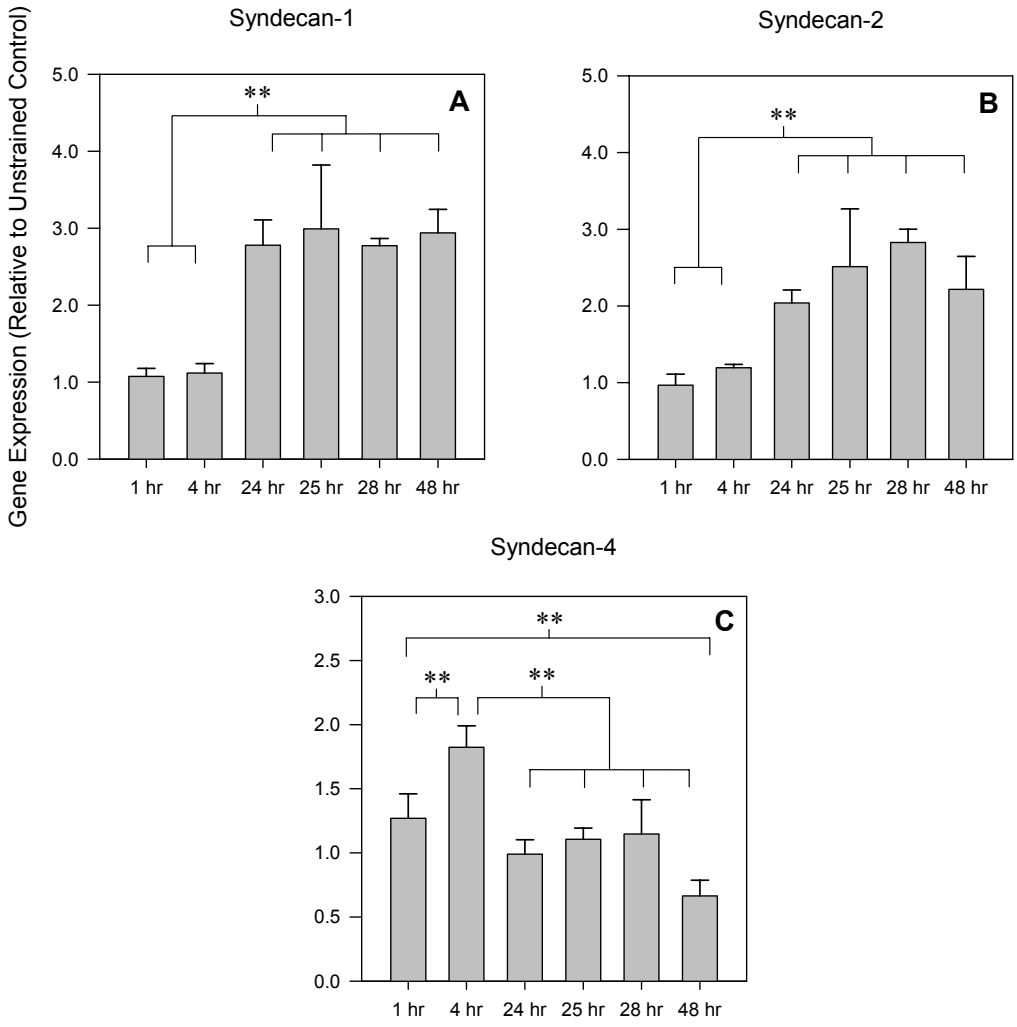

Figure 17. Effect of 10% cyclic strain on syndecan-1 (A), syndecan-2 (B), and syndecan-4 (C) gene expression. Human aortic SMCs were cultured on elastic membranes which were stretched at 1 Hz for the indicated periods of time. The cells were then harvested, and RNA was isolated and analyzed using real time PCR. All results were internally normalized to 18S rRNA levels, and the syndecan levels are presented relative to unstrained controls. The data represent the means and standard errors of at least triplicate experiments, and when necessary, statistical analysis was performed on the data after logarithmic transformation. ANOVA was then performed, employing Holm-Sidak's method for multiple pairwise comparisons. (** Indicates a p value < 0.05)

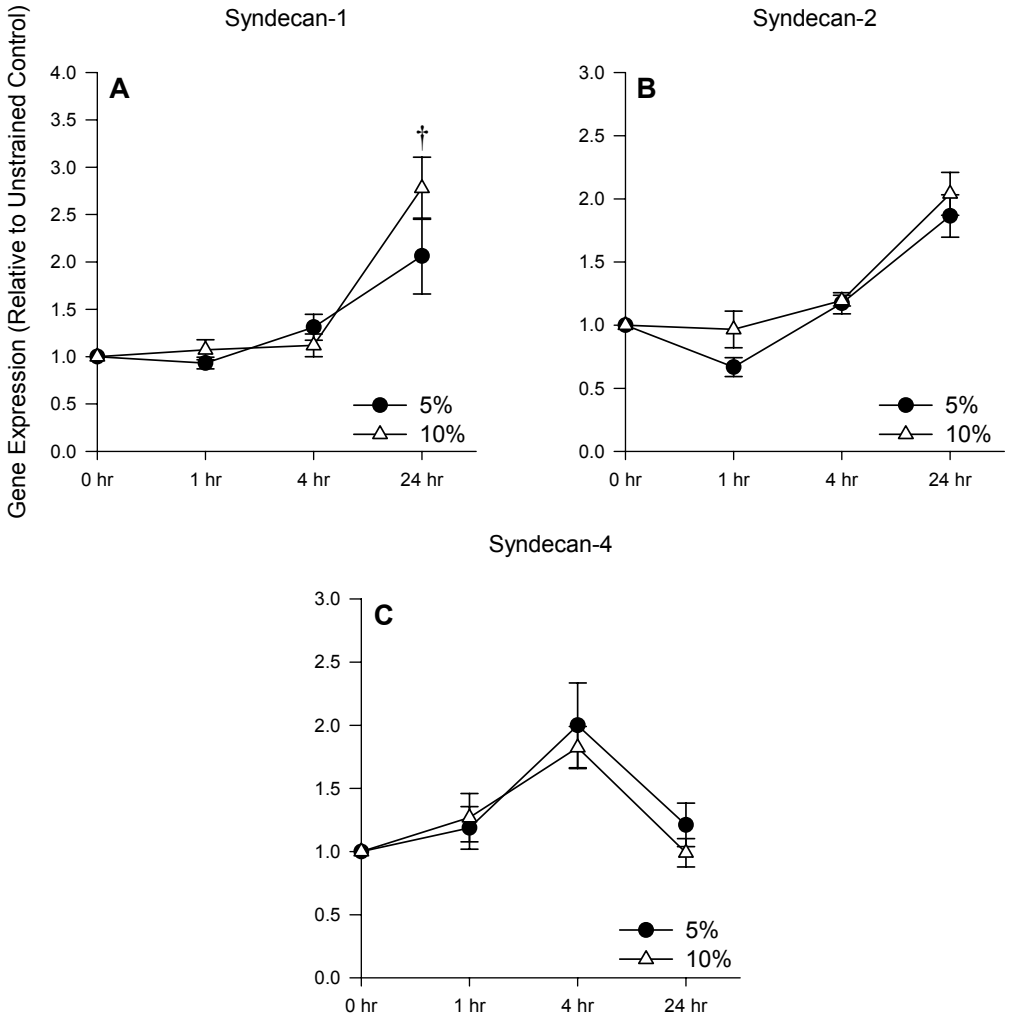

Figure 18. Effect of 5% (●) vs. 10% (△) cyclic strain on syndecan-1 (A), syndecan-2 (B), and syndecan-4 (C) gene expression. Human aortic SMCs were cultured on elastic membranes which were stretched at 1 Hz for the indicated periods of time. The cells were then harvested, and RNA was isolated and analyzed using real-time PCR. All results were normalized to endogenous 18S rRNA, and the syndecan levels are presented relative to unstrained controls. The data represent the means and standard errors of at least triplicate experiments, and statistical analysis was performed using ANOVA, employing Holm-Sidak's method for multiple pairwise comparisons. († Indicates a p value < 0.05 for comparisons between treatment groups at the indicated time point)

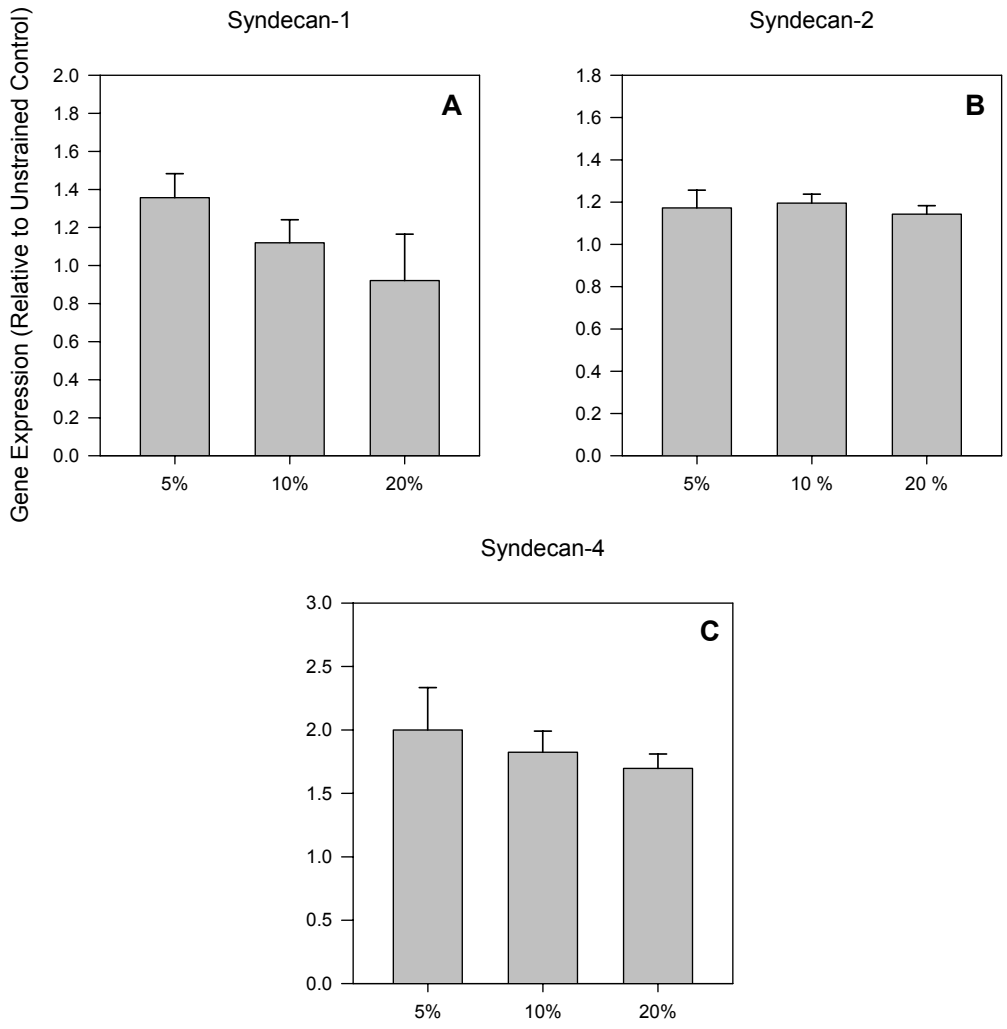

Figure 19. Dose response of cyclic strain on syndecan-1 (A), syndecan-2 (B), and syndecan-4 (C) gene expression. Human aortic SMCs were cultured on elastic membranes which were stretched at 1 Hz for 4 hours at the indicated maximum strain amplitudes. The cells were then harvested, and RNA was isolated and analyzed using real-time PCR. All results were internally normalized to 18S rRNA levels, and the syndecan levels are presented relative to unstrained controls. Data represent the means and standard errors of at least triplicate experiments, and statistical analysis was performed using ANOVA.

3.3.4 Preconditioning Exhibits Syndecan-Specific Gene Regulation

Given the apparently greater dependence of syndecan gene expression on the duration, rather than magnitude, of cyclic strain, our investigations took two approaches. We examined (1) whether these responses were stable or transient, and (2) whether, after an adjustment or preconditioning period, strain magnitude would reveal itself as a significant factor in syndecan gene expression. In other words, we sought to investigate if any possible effects of strain magnitude in the previous experiments were masked by the temporal nature of the responses to mechanical stimuli. To accomplish these aims, we used a final set of strain protocols, in which the cells were subjected to cyclic strain preconditioning, followed by a 10% or 20% cyclic strain time-course evaluation. The reason for this protocol was that SMCs *in vivo* exist in a mechanically dynamic oscillatory environment. It would therefore follow that this type of environment, rather than static culture, should serve as the baseline for experimentation. Our preconditioning experiments consisted of 24 hours of cyclic strain at a total magnitude of 10% strain, and this was followed by the presence or absence of a step increase of an additional 10% strain (20% total) for the indicated periods of time up to 24 hours.

Figure 20 outlines the results of this study, comparing the gene expression of cells strained for various times following the preconditioning period. The filled circles represent cells in which the step increase did <u>not</u> occur, while the open triangles represent cells in which the 10% step increase did occur. For syndecan-4, the response in gene expression in the 1, 4, and 24 hours following the preconditioning period (Figure 20C) was similar to what was observed during the initial onset of cyclic strain (both 5% and 10%; Figure 18C). Namely, a significant initial increase in gene expression from 99 ±

11% of unstrained controls just after preconditioning to 181 ± 1% at 4 hours of 20% cyclic strain occurred, followed by a significant decrease to 78 ± 2% at 24 hours of 20% cyclic strain. Meanwhile, there were no significant changes in syndecan-4 gene expression in the cells kept at 10% cyclic strain following the preconditioning period. It was also noteworthy that after 4 hours of strain beyond the preconditioning period, the difference in syndecan-4 gene expression between cells remaining at 10% strain and those stepped up to 20% strain following the preconditioning period was significant.

Like syndecan-4, the syndecan-1 gene response responded to the step increase in cyclic strain much like it did to the initial onset of cyclic strain (Figure 20A and Figure 18A). Upon increasing the strain magnitude to 20%, syndecan-1 gene expression during the 24 hours following the preconditioning period included a monotonic increase in gene expression over time. Syndecan-1 levels significantly increased from 278 ± 18% of unstrained controls at end of the preconditioning period to 516 ± 55% after 24 hours of the 20% cyclic strain period. During this same period of time, the syndecan-1 gene expression of cells kept at 10% cyclic strain remained constant, ranging from 277 ± 9% of unstrained controls to 299 ± 33%. In fact, at 24 hours of strain beyond the preconditioning period, the difference between cells subjected to 10% vs. 20% strain following the preconditioning period was significant.

Unlike the other syndecans, the gene expression of syndecan-2 was not significantly affected by a 10% step increase in strain magnitude following preconditioning (Figure 20B). Whether the strain was maintained at 10% or stepped up to 20% cyclic strain following the preconditioning period, syndecan-2 gene expression varied only slightly. Syndecan-2 expression in cells maintained at 10% cyclic strain

ranged from 204 ± 17% of unstrained controls to a maximum of 283 ± 17%. In cells treated with a step increase of 10% additional strain, syndecan-2 gene expression likewise increased to only 254 ± 28% of unstrained controls.

Taken together, the preconditioning results suggest that the cyclic strain-induced gene regulation of all three syndecans under investigation stabilized during the preconditioning period. However, unlike syndecan-2, syndecan-1 and syndecan-4 retained their ability to respond to a step increase in strain magnitude – each with its own characteristic response. Syndecan-4, whose gene expression had returned to baseline by the end of the preconditioning period, showed an immediate response to the step increase in strain magnitude. Syndecan-1, whose gene expression had reached an elevated plateau by the end of the preconditioning period, showed that it retained the capacity for a continued increase in gene expression.

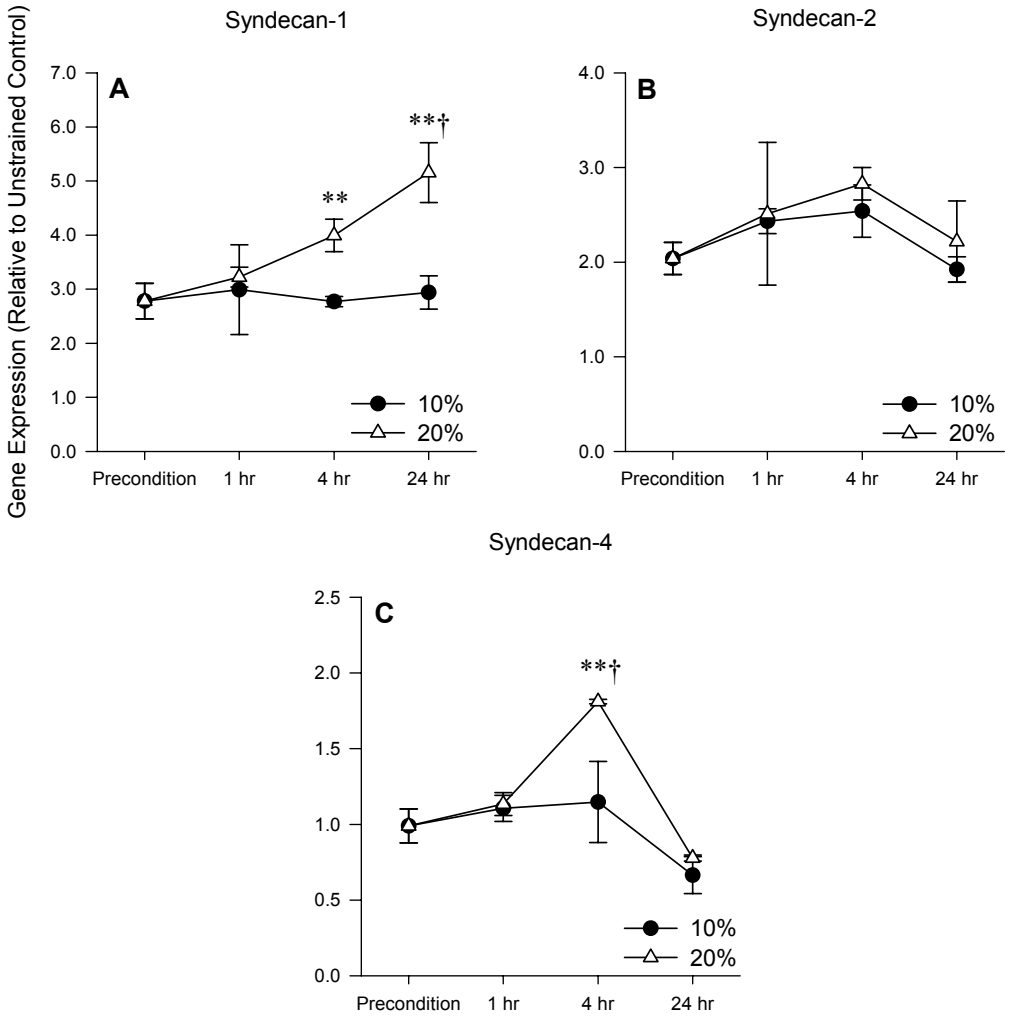

Figure 20. Effect of 24 hour preconditioning at 10% cyclic strain, followed by 10% (●) vs. 20% (△) cyclic strain on syndecan-1 (A), syndecan-2 (B), and syndecan-4 (C) gene expression. Human aortic SMCs were cultured on elastic membranes which were stretched at 1 Hz at 10% cyclic strain for 24 hours, followed by 20% cyclic strain for the indicated periods of time. The cells were then harvested, and RNA was isolated and analyzed using real-time PCR. All results were internally normalized to 18S rRNA, and the syndecan levels are presented relative to unstrained controls. The data represent the means and standard errors of at least triplicate experiments, and when necessary, statistical analysis was performed on the data after logarithmic transformation. ANOVA was then performed, employing Holm-Sidak's method for multiple pairwise comparisons. (** Indicates a p value < 0.05 for comparisons with preconditioned cells. † Indicates a p value < 0.05 for comparisons between treatment groups at the indicated time point.)

3.4 Discussion

3.4.1 Perspective on the 2-Deminsional Strain Device

As principal components of the mechanically dynamic vascular wall, SMCs *in vivo* are subject to forces which are poorly recapitulated in conventional cell culture. Unfortunately, the mechanical properties of three dimensional organ culture models of blood vessels are not well characterized, and the interactions of the different cell types confound potential results. For this reason, we chose to employ the StrainMaster apparatus for our experiments. Leung et al. and Meikle et al. were some of the first to quantitatively study the effect of tension on cells in vitro[178,179], while Hasegawa et al. were the first to use a deformable circular substrate[180]. Despite some limitations, this system has been well characterized by others, and was useful for examining the regulation of syndecan gene expression by specific mechanical stimuli. The strain protocols in our experiments were chosen as *in vitro* approximations of physiologic conditions, and as such, the first requirement was that the cells remained viable for the duration of any given protocol. We demonstrated that this requirement was met using a Live/Dead viability assay, in which negligible cell death occurred.

3.4.2 Strain Assay Limitations

One concern regarding the strain device used in our experiments, as described by Brown et al., was the presence of reactive fluid stress, which was induced by motion of the overlying nutrient medium[181]. The components of this stress appeared in the form of normal (due to hydrostatic pressure and fluid vertical acceleration) and shear (due to fluid velocity gradients) stresses. Although a potential limitation of our experiments was that

the biological significance of these stresses were not taken into account, Brown et al.'s analysis suggests that the effects were minimal for the particular strain device we used. Using finite element modeling, the authors found that for the StrainMaster apparatus, the reactive *normal stress* remained essentially constant during cyclic stretch. On the other hand, for the Flexercell Unit, this stress varied throughout the duty cycle depending on the radial position. Moreover, while the reactive *shear stress* for the Flexercell Unit was described as irregular, the StrainMaster apparatus displayed significant shear stress only at the circular lip region.

Another potential limitation of the strain device was the heat generated by the friction of the membrane and platen sliding past each other, despite the use of lubricants. Though not likely to be a significant consideration in our current experiments, this phenomenon may become so in future experiments where strain magnitudes, and thus sliding distance, are increased.

Admittedly, the robustness of any conclusions regarding the effects of strain magnitude required that any temporal effects be stabilized. In other words, the experiments required that syndecan gene expression levels were at steady-state at the time in which any change in magnitude took place. It was reasonable to assume that this requirement was met for the experiments in which this change in magnitude took place only at the start of the experiment. However, in the preconditioning experiments, it was necessary to validate that the strained cells had reached a new steady-state by the end of the preconditioning period. This was accomplished by examining syndecan gene expression in cells from parallel experiments – which were kept at the preconditioned magnitude for the duration of the experiment.

Conversely, conclusions regarding the effects of duration of strain required that the magnitude be held constant. The strain device we chose to use was well suited to meet this requirement as far as membrane strain was concerned. It has been validated to reproducibly impart a wide range of homogeneous and equibiaxial strains to an overlying membrane[162,163]. Moreover, the silicone elastomer substrate exhibited stable elastic properties over the duration and range of temperatures used in our experiments. Plastic deformation, fatigue, and viscoelastic properties such as stress relaxation and time dependence are potential considerations which were not significant attributes of the chosen system.

Unfortunately, the requirement for constant strain magnitude was not necessarily maintained by the SMC monolayer, and our analysis did not take into consideration the biophysical mechanisms underlying the transmission of stresses between the silicone substrate and SMC membrane. A potential limitation of our experimental system was that the silicone substrate strain was assumed to be equivalent to the cellular strain; however, the validity of this assumption required that at least two critical conditions be met. The first condition was that the *cells formed rigid and stable adhesive contacts* with the underlying membrane. The second was that the *cells had negligible stiffness* of their own. As outlined below, neither of these conditions was necessarily true.

3.4.3 Cellular Mechanics Considerations

As discussed previously, cell adhesion is a complex process that occurs due to the interaction of various molecules, including syndecan[63,64] and integrin receptors[182,183]. *Adhesive contacts*, or focal adhesions, that form between cells and the ECM undergo

dynamic assembly and disassembly. Thus, they are neither stable nor completely rigid. They are widely regarded as receptor nodes that connect the cytoskeleton to the membrane and cytoplasm, and key aspects of their biological importance have been well characterized. On the intracellular side, focal adhesions are linked to the cytoskeleton, which assembles and disassembles to varying degrees based on cell locomotion and division. On the extracellular side, focal adhesions adhere to ECM glycoproteins, such as FN and vitronectin, which are often secreted by the cells themselves. This multi-domain provisional matrix allows lateral mobility of the "cell anchors" based in part on the presence of rigid structural proteins, such as collagens. Therefore, in our model system, the rigidity of the ECM, which is sandwiched between the silicone and cell membranes, itself contributes to mobility of the cell anchors. In addition to these examples of receptor mobility, focal adhesions can be also endocytosed by the cell and recycled, eliminating the anchor altogether.

The presence of dynamic and quantifiable *cell stiffness* makes the second condition fail as well. In cellular mechanics, a full description of the stress on a cell incorporates the contributions from the ECM, focal adhesion complexes, the cytoskeleton, in addition to the area of the cell membrane in direct contact with an applied force. Though the actual physical deformations of adherent cells are difficult to theoretically characterize, several models attempting to describe the cell mechanical properties have been proposed, and one in particular has gained considerable support – tensegrity, or tensional integrity.

3.4.4 Tensegrity and the Effect Cell Prestress on Membrane Strain

The idea of tensegrity was made popular by R. Buckminster Fuller[184] as an architectural design principle, and has recently been championed in reference to cell biomechanics by Ingber[185-194]. The theory suggests, among other things, that an externally-applied stress is transmitted by discrete molecular networks that extend through the cytoplasm, and this transmission depends on interactions between all three cytoskeletal filament systems – actin, intermediate, and microtubules. It places an emphasis on hierarchical, rather than isolated systems, to explain cell behavior, and models the cytoskeleton as a prestressed framework composed of molecular struts, ropes, and cables. This is in contrast to half-space models[195-197] and theories which suggest that the stress is borne exclusively by the submembranous cortical actin layer[198] of individual cells. Internal tensile load/prestress, a fundamental feature of tensegrity, is believed to help stabilize cell shape, and this principle is useful in explaining what strains the cells in our experiments might actually experience. The theory suggests that cell stiffness is a linear function of cell prestress[199,200]; the result of this increased stiffness in our experiments may have been decreased local cellular strain, leading to decreased stimulus for cellular responses. Conversely, strain hardening is thought to mediate transduction of mechanical signals across the plasma membrane through the cytoskeleton[201].

Tensegrity is a useful tool for explaining various cellular processes. For example, it has been shown in SMCs that tension on integrins leads to intracellular decompression of microtubules, resulting in compensatory polymerization[202,203], and that cyclic strain results in increased stress fiber formation[204,205]. In addition, others have shown that the cytoskeleton of adherent cells develops mechanical stresses that oppose distortions in cell shape[15,187,193], that disruption of any of the three major cytoskeletal filament systems

results in a decrease in cell stiffness[191], and that this stiffening is an active process, requiring both actin polymerization and myosin activation[206]. Also, forces applied to integrins produce an increase in focal adhesion assembly in various cell types. In fact, stress-activated signals transmitted by integrins are distinct from those due integrin receptor clustering alone. The results of Xu have made this description more complex by demonstrating that the cytoskeleton can strain harden and strain soften, depending on the characteristics of the applied strain[201]. He reconciled these findings by comparing the cytoskeleton with weakly-crosslinked polymer networks, which can easily slide past one another when strained slowly, but whose stiffness increases dramatically with increasing strain rate.

The tensegrity theory also implicates a mechanism for the activation of mechanosensitive receptors and channels located in areas not in direct apposition with the underlying substrate. Since information is often distributed among numerous pathways, potentially leading to many different responses, mechanosensors may be located on the apical surface or even the nuclear membrane. In fact, both cell motility and cell cycle progression can be inhibited by either disruption of the actin cytoskeleton or inhibition of cytoskeletal tension generation. Since the cells generate their own internal prestress in the actin cytoskeleton, balanced by internal microtubule struts and ECM adhesions, such mechanosensors could respond to signals from inside the cell, through their molecular linkages to the cytoskeleton.

Together, when coupled with adhesive contacts with a flexible substrate, the processes that result in an increase in the cell's internal prestress and resistance to global structural rearrangements are manifested as increased cell traction. Overall, cell traction

results in relative compression of the silicone substrate underneath the cells and tension in the substrate elsewhere, leading to an effective compliance mismatch at different areas along the surface. When the substrate is therefore subjected to a certain level of external strain, that strain is not transmitted uniformly over the entire surface, and since the cells have a higher elastic modulus than the silicone, the area not directly under the cells will need to deform to a greater extent in order for the substrate as a whole to achieve a given total strain.

An added consequence of the non-uniform, position-dependent variations in substrate strain is that the compliance mismatch leads to local elevated strain, and therefore shear stress, gradients at the cell-substrate attachment points. In part, this means that receptors at the cell periphery experience the maximum shear stress, while those closer to the centers of the cells experience much less. These elevated shear forces are more likely to overcome the cell adhesive forces, ultimately resulting in sliding of the membrane relative to the cells. In fact, these phenomena occur at the multicellular level as well as the single cell level. As the SMC monolayer forms, and the cells create adhesive contacts with other cells as well as the substrate, cells at the periphery effectively shield those in the interior from the applied strain. If the shear forces experienced by these cells overcome the cell adhesive forces, the result will be a redistribution of the forces over a smaller effective cell adhesion contact area.

3.4.5 Syndecan Gene Expression Dependence on Strain Protocols

Despite the failure to meet the two criteria mentioned above, we can draw important conclusions from the results obtained using the present strain device. In the

studies described in this chapter, we characterized the regulation of syndecan-4 gene expression in vascular SMCs by various mechanical strain protocols. In addition, we examined the similarities between syndecan-4 and two other syndecans expressed by our cell system – syndecan-1 and syndecan-2. Analysis of syndecan expression in response to static strain served as a useful beginning for the study of the strain-induced gene regulation. We found that this mechanical environment regulated syndecan-4 and syndecan-2 similarly. Both genes displayed reduced expression at longer durations of static strain, while syndecan-1 seemed to be altogether unresponsive to static strain. The static protocol was limited in that it modeled a small subset of the mechanical environments to which vascular SMCs are subjected. Nonetheless, this strain regime was useful for modeling vascular mechanics during cardiopulmonary bypass[153], and to a lesser extent PTCA and initial stent placement; however, modeling normal and pathologic hemodynamics required a cyclic model.

When subjected to cyclic strain, the gene expression of all three syndecans was regulated in slightly different ways. Syndecan-4 exhibited a bimodal response, increasing rapidly by 4 hours and then returning to or below baseline. This response was conserved at various levels of strain magnitude. Syndecan-1 and syndecan-2, on the other hand increased steadily over a 24 hour period, but then remained constant for the duration of the experiments. It is noteworthy that syndecan-1 gene expression appeared to be responsive to both strain magnitude and duration. As Figure 18A shows, 24 hour syndecan-1 gene expression was sensitive to the magnitude of cyclic strain, unlike the other syndecans. This behavior of syndecan-1 gene expression correlated with the preconditioning data, in which syndecan-1 gene expression remained responsive to a step

increase in strain magnitude. Combined, these data suggest that regulation of syndecan-1 may be a critical component of the cellular response to chronic injury.

The preconditioning results for both syndecan-4 and syndecan-1 were interesting because they demonstrated responsiveness to changes beyond the initial perturbation. Assuming that the 24 hour preconditioning period was of sufficient duration to allow the cells to reach steady-state, the baseline syndecan-4 gene expression seemed to be at the level of unstrained cells. At the onset of a change in the mechanical environment, syndecan-4 gene expression quickly increased, but then rapidly returned to that baseline. Recent work in our lab has demonstrated that syndecan-4 RNA was regulated in a similar fashion by cyclic strain in a balloon angioplasty model[164], and we have also previously shown evidence to suggest that syndecan-4 is an immediate early gene[82]. Our current results further support the previous work and suggest either the presence of a strong negative feedback mechanism and/or a rapid exhaustion of a key component of this early response. In other words, the mechanism by which the cells sensed the mechanical stimulus was rapidly activated, but then rapidly switched off and reset.

Syndecan-1 gene expression, on the other hand, never returned to the unstrained baseline, within the time frame of our experiments. As long as the mechanical stimulus was present, gene expression remained elevated. Yet upon the step increase in strain magnitude, syndecan-1 gene expression increased above the newly-established preconditioned baseline, and did not return during the length of the experiment. These findings seem to implicate a weak or nonexistent feedback mechanism and/or a large syndecan-1 genetic reserve. In other words, syndecan-1 gene expression retained the capacity to be regulated beyond what was initially observed in the assay. Under the

influence of an additional mechanical stimulus, additional syndecan-1 gene expression was available. In light of the kinetics of the syndecan-1 response, one strain protocol that could help to clarify syndecan-1 regulation would be a dose response study of 5%, 10%, and 20% strain evaluated at 24 hours rather than 4 hours.

The above findings underscore the importance of understanding syndecan gene regulation in vascular biology. Syndecans, through their roles in cell-ECM adhesion, growth factor binding, protease activity, wound healing, and embryonic morphogenesis, serve as important transducers of mechanical stimuli. In particular, by using defined cyclic and static strain protocols, we were able to gain a better appreciation of the characteristics of this gene regulation in the mechanically dynamic vessel wall. The logical and necessary next step in our understanding of the regulation of syndecans will be the analysis of protein expression and ectodomain shedding in response to many of the above strain protocols. Since the regulatory mechanisms that govern gene vs. protein expression are distinct, future experiments should be aimed at identifying and manipulating them. The goals of such experiments would be to both alter and to understand the importance of syndecan protein expression in mechanically strained cells. The experiments described in the next chapter represent examples of such experiments, in which intracellular MAP kinase signaling pathways were targeted for their potential role in mediating syndecan-4 responsiveness to cyclic mechanical strain.

CHAPTER 4

CYCLIC STRAIN – INDUCED REGULATION OF SYNDECAN-4 PROTEIN IS INFLUENCED BY MAP KINASE ACTIVITY

Given the results from the gene expression studies, we focused our interest on syndecan-4 protein regulation. For various reasons the gene and protein expression patterns of a given protein often don't correlate, and we became interested in one of these potential reasons in particular – MAP kinase signaling. In fact, a body of evidence has accumulated linking certain intracellular signaling pathways to the regulation of both cell surface and the shed ectodomains of HSPGs. Additionally, numerous reports have demonstrated that MAP kinase pathways are activated by mechanical stress[149,207-209]. Our aim was to assess the influence of MAP kinase signaling on syndecan-4 expression and ectodomain shedding[‡]. We postulated that, through the regulation of these key intracellular signaling events, mechanical strain modulates cell surface syndecan-4 levels, and therefore plays a pivotal role in vascular remodeling.

4.1 Background and Significance

4.1.1 Importance of MAP Kinase Signaling

MAP kinases are a family of serine/threonine kinases intricately involved in the conduction and amplification of critical cellular signaling pathways. The family includes ERK1/2, p38 MAP kinase, and c-Jun NH_2-terminal kinase/stress-activated protein kinase (JNK/SAPK). As a group, they are well-known to be activated in response to a variety of

[‡] See Appendix B for supplemental syndecan-1 and syndecan-2 data

extracellular stimuli, and are commonly employed by cells to transmit extracellular signals into cellular responses, including proliferation, differentiation, apoptosis, and adaptation to external stress. When initially discovered, these pathways were thought to be activated by distinct stimuli. For example, ERK1/2 (also known as p44/42 MAP kinase) are a pair of 44 and 42 kD protein kinases that were classically thought to be involved with cellular responses to growth and neurotrophic factors[210]. p38 MAP kinase is a 38 kD protein kinase that was thought to be involved in the cellular response to inflammatory cytokines and a variety of cellular stresses[211]. JNK/SAPK, first described as UV-activated kinase, was initially shown to be involved in cellular responses similar to p38 MAP kinase, but it also appears to offer protection against apoptosis[212,213]. More recently, ERK1/2 has been shown to be involved in the regulation of transcriptional and translational activation of a variety of proteins. In addition, ERK1/2 signaling also occurs due to cellular stresses, such as heat shock, hyperosmolarity, oxidative stress, radiation, and ultraviolet (UV) light. Cellular response to these stresses were initially thought to be mediated through JNK/SAPK and p38 MAP kinase signaling. As a group, the MAP kinases represent key molecules in separate, but highly interconnected, phosphorylation cascades.

We have previously determined that the ERK1/2 signaling pathway is involved in the up-regulation and shedding of syndecan-4 in response to oxidative stress[214]. In addition, Fitzgerald et al. have demonstrated that metalloproteinase-dependent syndecan-1 and syndecan-4 shedding involves selective MAP kinase activity[215]. Specifically, ERK1/2 activity was found to be required for shedding induced by EGF and thrombin receptor activation, while p38 MAP kinase activity was not involved. These authors also

demonstrated that cellular stress induced by hyperosmolarity or ceramide treatment trigger shedding via PKC-dependent pathways that are likely upstream of JNK/SAPK activation. We therefore postulated that cyclic mechanical stress-induced activation of ERK1/2 and/or other MAP kinase signaling mechanisms results in the up-regulation of syndecan-4 expression and shedding.

4.1.2 Syndecan Ectodomain Shedding

Ectodomain shedding is common to many membrane-bound proteins, including cytokines, growth factors, and adhesion proteins[216]. It has been shown to play an important role in various diseases, including rheumatoid arthritis (tumor necrosis factor alpha (TNFα) receptor), Alzheimer's disease (β-APP), and some types of cancer (EGF receptor)[217,218]. It is a means of releasing functionally intact effector molecules into the surrounding medium. For example, shedding of syndecan-1 and syndecan-4 ectodomains has been shown to localize the KC chemokine to alveolar fluid, resulting in transepithelial neutrophil migration and eventual inflammation[219]. Shedding of syndecan-1 and syndecan-4 ectodomains can also be enhanced by growth factors[71], by cellular stress[215], and by microbial virulence factors[220], and by conditioned media from mechanically-strained cells. Though the mechanism of syndecan-4 shedding is not yet fully understood, several proposed mechanisms exist[71,219,220]. The aim of this study was to determine, through selective inhibition, if MAP kinase signaling is involved in syndecan-4 protein expression and shedding under the influence of mechanical strain.

4.2 Materials and Methods

4.2.1 Cell Culture

Clonetics normal human aortic SMCs, culture medium and supplements were obtained from Cambrex Bio Science, and the cells were sub-cultured using standard techniques. SmGM-2 was prepared according to the supplier's recommendations (SmBM, supplemented with 5% FBS, 500 µg/mL hEGF, 5 µg/mL insulin, 2 mg/mL hFGF, 50 µg/mL gentamycin, and 50 mg/mL amphotericin-B. Cells were maintained in tissue culture-treated petri dishes at 37ºC, 5% CO_2, and humidified atmosphere. Growth medium was changed every two days, and the cells were passaged 1:4 when the dishes were 80% confluent, using 0.05% Trypsin / 0.53 mM EDTA. Experiments were performed on cells between passages 6 and 10 using Quiescence medium, which consisted of SmBM supplemented with 0.5% FBS, 50 µg/mL gentamycin, and 50 mg/mL amphotericin-B.

4.2.2 Mechanical Strain Application

Strain dishes were assembled in the following manner: the bases of bottomless, custom-made plastic petri dishes were fitted with silicone membrane (0.5 inch thickness; 40 Durometer). The silicone served as a flexible growth area of the strain dishes. For all experiments, 5 µg/mL human plasma FN in PBS was pre-adsorbed to the growth area for at least 8 hours at 4ºC, serving as a substrate for cell attachment. The cells were then seeded onto the membranes, cultured to 80% confluence in SmGM-2, and then growth-arrested for 24 hours in Quiescence medium.

Depending on the experimental conditions, defined static or cyclic tension was applied to the cells using a StrainMaster apparatus. Contacting surfaces of the membrane and strain device were lubricated with Dawn concentrated dishwashing liquid. Static and

cyclic tensions were applied using a StrainMaster apparatus that allowed control over the frequency and amplitude of the radial and circumferential strains of the membrane and, and enabled the application of homogeneous and biaxially uniform strains over the entire growth area of the membrane.

The protocol for the application of mechanical strain for subsequent protein analysis was slightly different than for the RNA analysis. Following MAP kinase inhibitor pre-treatment (when appropriate), stretching (1 Hz, 10% cyclic strain) of the various samples commenced in a staggered fashion, based upon the total duration that each was to be strained (Figure 21). Since all samples were harvested simultaneously, stretching of the 24 hour strain samples commenced immediately, whereas stretching of the 4 and 1 hour strain samples were commenced at t = 20 hours and 23 hours, respectively. The reason for this protocol was so that, upon harvesting the cells, we could collect 24 hour shed protein from samples, whether or not the cells were stretched. The only difference between the samples was the fraction of the 24 hour period in which the cells were stretched. Unstrained controls were performed concurrently for all experiments.

4.2.3 MAP Kinase Activation

For the analysis of MAP kinase activation, cells were grown to 80% confluence in SmGM-2 and Quiesced for 24 hours. They were then strained for the indicated time points and lysed using Laemmli sample buffer with 5% β-mercaptoethanol (Sigma-Aldrich, St. Louis, MO). Lysates were sonicated for 20 seconds to shear DNA and reduce viscosity, and then were boiled for 5 min, followed by centrifugation at 16,000 x *g*

for 5 min. Proteins in the supernatants were resolved by sodium dodecyl sulfate polyacrylamide gel electrophoresis (SDS-PAGE) and transferred to 0.45 μm supported nitrocellulose (Bio-Rad). The immunoblots were blocked for 1 hour at room temperature with 5% nonfat dry milk in 0.1% Tween-TBS (20 mM Tris-HCl, 137-150 mM NaCl) pH 7.6, washed with 0.1% Tween-TBS, and labeled overnight at 4ºC with one of the anti-MAP kinase or anti-phospho-MAP kinase primary antibodies (Cell Signaling Technology, Beverly, MA), diluted 1:1000 in 5% bovine serum albumin (BSA) in 0.1% Tween-TBS. This was followed by incubation with horseradish peroxidase anti-rabbit IgG (Cell Signaling Technology), diluted 1:2000 in blocking buffer for 1 hour at room temperature. The immunoblot was then developed using enhanced chemiluminescence, and the labeled proteins were detected using BioMax MR autoradiography film. Levels of protein were quantified by densitometry using ONE-Dscan image analysis software.

4.2.4 MAP Kinase Inhibition

U0126 (Cell Signaling Technology), SB203580 (EMD Biosciences, San Diego, CA), and (L)-JNK Inhibitor 1 (EMD Biosciences) were used to inhibit the phosphorylation cascades of the MAP kinase family (Table 3). U0126 is a selective inhibitor of MAP kinase kinase (MEK) 1 and 2 activation, which are upstream activators of ERK1 and ERK2. SB203580 and (L)-JNKI1, on the other hand, act by directly inhibiting the activity of p38 MAP kinase and JNK/SAPK, respectively. U0126 and SB203580 were reconstituted in dimethyl sulfoxide (DMSO; Sigma-Aldrich), and administered to the cells at a final concentration of 20 μM. An equal volume of sterile DMSO was used as a vehicle control for the untreated cells. (L)-JNKI1 was reconstituted

in H_2O and administered to the cells at a final concentration of 2 μM. An equal volume of sterile H_2O was added to the untreated controls. The inhibitors were added to the cells at the indicated concentrations for 30 minutes prior to the onset of the 24 hour experimental period (Figure 21). This resulted in all samples receiving the inhibitor or control treatment for the same length of time, regardless of when the straining of the particular sample actually commenced. Though possibly unnecessary, after 20 hours, an additional dose of each inhibitor at an empiric concentration equal to half the initial dose was administered to the cells. This was done in order to account for degradation and/or metabolism of the initially applied dose. The reasons that additional dose was equal to only half the initial dose were (1) that only 4 hours remained in the experiments, and (2) to avoid cytotoxic concentrations of the inhibitors that may not have undergone degradation.

Table 3. Mitogen-activated protein kinases of interest and chemical inhibitors.

MAP Kinase	Inhibitor	Concentration
ERK1/2 MAP kinase	U0126	20 μM
p38 MAP kinase	SB203580	20 μM
JNK/SAPK	(L)-JNK Inhibitor 1	2 μM

4.2.5 Shed Proteoglycan Isolation and Quantification

The following protocols were adapted from Reiland et al.[221] and Rioux et al.[222]. After the cells were treated with one of the strain protocols, the conditioned medium was passed through a 0.2 μM membrane filter (Millipore, Billerica, MA) in order to remove detached cells and debris. For shed syndecan-4 purification urea was added to bring the

final concentration to 4 M. The media (15 mL) was first concentrated to 400 µL using a 10,000 MWCO Amicon Ultra-15 Centrifugal Filter Unit. The retentate was bound to a Vivapure Mini Diethylamine weak anion exchange column (Vivascience, Edgewood, NY) using an equilibration buffer (20 mM NaOAc pH 5, 4 M urea, 0.5% Triton X-100, 1 mM EDTA, 1 mM Na_2SO_4, 200 mM NaCl). Proteoglycans were then eluted using 100 µL of the same buffer containing 1 M NaCl. Using Bio-Spin 6 (Bio-Rad, Hercules, CA) gel filtration columns for buffer exchange, the samples were transferred to a reaction buffer containing 3 mM $Ca(OAc)_2$, 10 mM EDTA, 10 mM HEPES pH 7.0, 0.1% Triton X-100, 10 mM NEM (Sigma-Aldrich), and protease inhibitors (200 µM 4-(2-aminoethyl)benzenesulfonylfluoride (AEBSF), 160 nM aprotinin, 10 µM bestatin, 3 µM E-64, 4 µM leupeptin, and 2 µM pepstatin A)(EMD Biosciences). Total protein was quantified using the BCA method. GAG chains were digested by combining 30 µL of each sample with 2 mU heparitinase and 8 mU chondroitinase ABC (*P. vulgaris*, EC 4.2.2.4, Seikagaku America). The samples were incubated for 4 hours at 37ºC, after which the samples were placed on ice and ready for analysis.

For shed syndecan-4 detection, a Bio-Dot SF slot blot apparatus (Bio-Rad) was assembled by stacking two sheets of 0.45 µm Immobilon-P PVDF membrane (Millipore) on top of three sheets of Bio-Dot SF filter paper (Bio-Rad). Conditioned media was diluted 1:10 in heparitinase buffer containing no Triton X-100, and was then applied directly to the membrane using vacuum filtration. The membrane was blocked for 1 hour at room temperature in 5% nonfat dry milk in 0.04% Tween-TBS pH 7.4. The immunoblot was then labeled overnight at 4ºC with anti-syndecan-4 mAb (antibody 8G3; provided by Dr. Guido David, K. U. Leuven, Belgium) diluted 1:2000 in 1% nonfat dry

milk in 0.04% Tween-TBS pH 7.4. It was then washed in 0.04% Tween-TBS pH 7.4, followed by incubation with horseradish peroxidase anti-mouse IgG, diluted 1:5000 in blocking buffer for 1 hour. The immunoblot was then developed using enhanced chemiluminescence, and the labeled protein was detected using BioMax MR autoradiography film. Levels of protein were quantified by densitometry using ONE-Dscan image analysis software.

4.2.6 Cell-Associated Proteoglycan Isolation and Quantification

For cell-associated syndecan-4 purification, the cells were washed twice with cold PBS, and then 500 µL of lysis buffer was added to them, containing 20 mM Tris-HCl pH 7.4, 150 mM NaCl, 10 mM EDTA, 1% Triton X-100, and protease inhibitors. Following a 15 minute incubation on ice, the cells were scraped from the plates and homogenized by passing several times through a 26G needle. The cell lysates were centrifuged at 16,000 x *g* for 15 min at 4ºC. Urea was added to 350 µL of the resulting supernatants up to a final concentration of 4 M, and the lysate was bound to a Vivapure Mini Diethylamine weak anion exchange column using the same equilibration buffer as for the conditioned medium. Proteoglycans were then eluted using 100 µL of the same buffer containing 1 M NaCl. Using Bio-Spin 6 gel filtration columns for buffer exchange, the samples were transferred to the same heparitinase reaction buffer, and the total protein was quantified using the BCA method. GAG chains were digested by combining 30 µL of each sample with 2 mU heparitinase and 8 mU chondroitinase ABC. The samples were incubated for 4 hours at 37ºC, after which an equal volume of Laemmli sample buffer containing 5% β-mercaptoethanol was added. The samples were resolved by SDS-PAGE, and then were

transferred to a 0.45 μm Immobilon-P PVDF membrane. The membrane was blocked and probed, and syndecan-4 was detected in the same manner as for shed syndecan-4.

4.2.7 Statistics and Data Analysis

Values are given as mean ± SEM. Statistical analysis was performed using SigmaStat 3.0 software package. ANOVA was employed, using the Holm-Sidak or Tukey tests for multiple pairwise comparisons among the treatments. When applicable, logarithmic transformation of the data was necessary prior to statistical analysis in order for it to conform to the ANOVA assumptions. A p value < 0.05 was considered statistically significant for all tests.

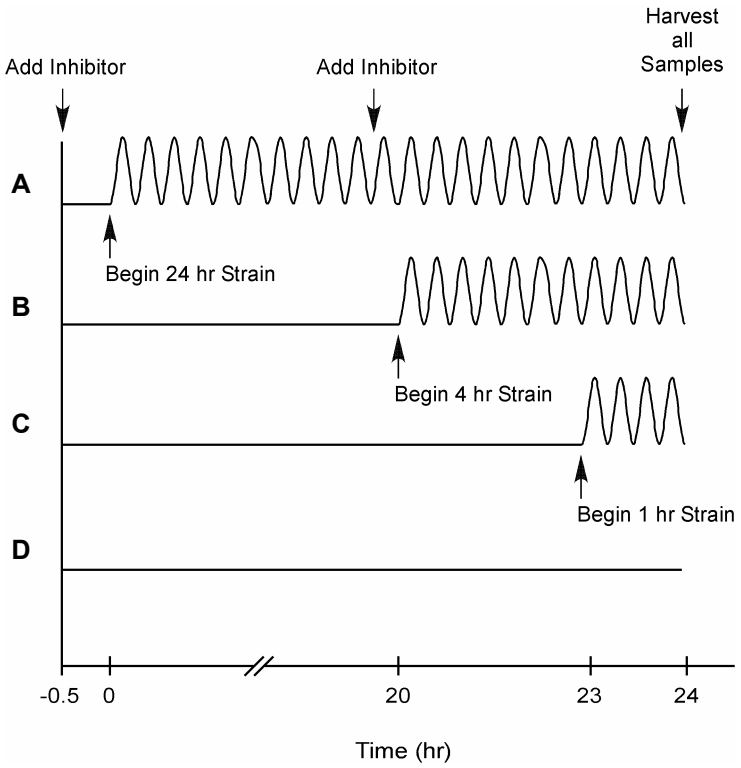

Figure 21. Protocols for the application of mechanical strain for subsequent protein analysis. For MAP kinase inhibitor studies, the cells were pre-treated for 30 minutes, and again at t = 19.5 hours for any given experiment. Beginning at t = 0, stretching (1 Hz, 10% cyclic strain) of the various samples commenced in a staggered fashion, based upon the total duration that each was to be strained. Since all samples were harvested simultaneously, stretching of the 24 hour strain samples commenced immediately (A), whereas stretching of the 4 hour (B) and 1 hour (C) strain samples were commenced at t = 20 hours and 23 hours, respectively. Unstrained controls (D) were performed concurrently for all experiments.

4.3 Results

4.3.1 Cyclic Strain Regulates Shed and Cell-Associated Syndecan Protein

The StrainMaster device was again used to mechanically strain cells in order to gain insight into the influence of cyclic strain on syndecan-4 regulation. For these experiments, the strain protocol we chose to employ was 10% cyclic strain, 1 Hz, for various periods of time. This choice of strain protocol was based on work by others demonstrating the physiologic relevance of 10% cyclic strain on aortic SMCs[158-161] and from the results from the previous chapter, in which we demonstrated that this level of strain was sufficient to observe significant changes in syndecan-4 gene expression. This magnitude of strain was therefore an appropriate initial set-point for analysis of syndecan-4 protein regulation.

Since HSPGs can be released from the membrane via ectodomain shedding, quantification required an analysis of two separate protein sub-populations – cell-associated and shed. Therefore, in our analysis of syndecan-4 protein expression, we measured the sub-populations independently. The syndecan-4 gene expression data suggested that strain-induced regulation occurred within the initial 4 hours of strain. In the current experiments, shed protein was observed by slot blotting of non-heparitinase-digested samples (Figure 22). The specificity of the antibody and its ability to detect a single band by Western blotting permitted this application of the antigen directly to the membrane without introducing error into the densitometry analysis. The results demonstrated that shed protein levels increased significantly throughout the duration of stretch, ranging from 237 ± 57% of unstrained controls at 1 hour to 537 ± 109% at 24 hours. On the other hand, cell-associated syndecan-4 levels initially decreased to 38 ±

11% of controls at 1 hour, increased significantly to 181 ± 22% at 4 hours, and then significantly dropped again to 70 ± 6% at 24 hours. Thus, the kinetics of the cell-associated syndecan-4 response closely mimicked the gene expression data, suggesting that the immediate loss of total cell-associated syndecan-4, via shedding from the cell surface, was initially recovered by newly-synthesized syndecan-4 from existing RNA. The combination of increased gene expression and continued protein synthesis during the first 4 hours of strain likely resulted in the eventual elevation of syndecan-4 cell-associated protein levels. After that, gene expression dropped off, leading to the return of protein expression to basal levels.

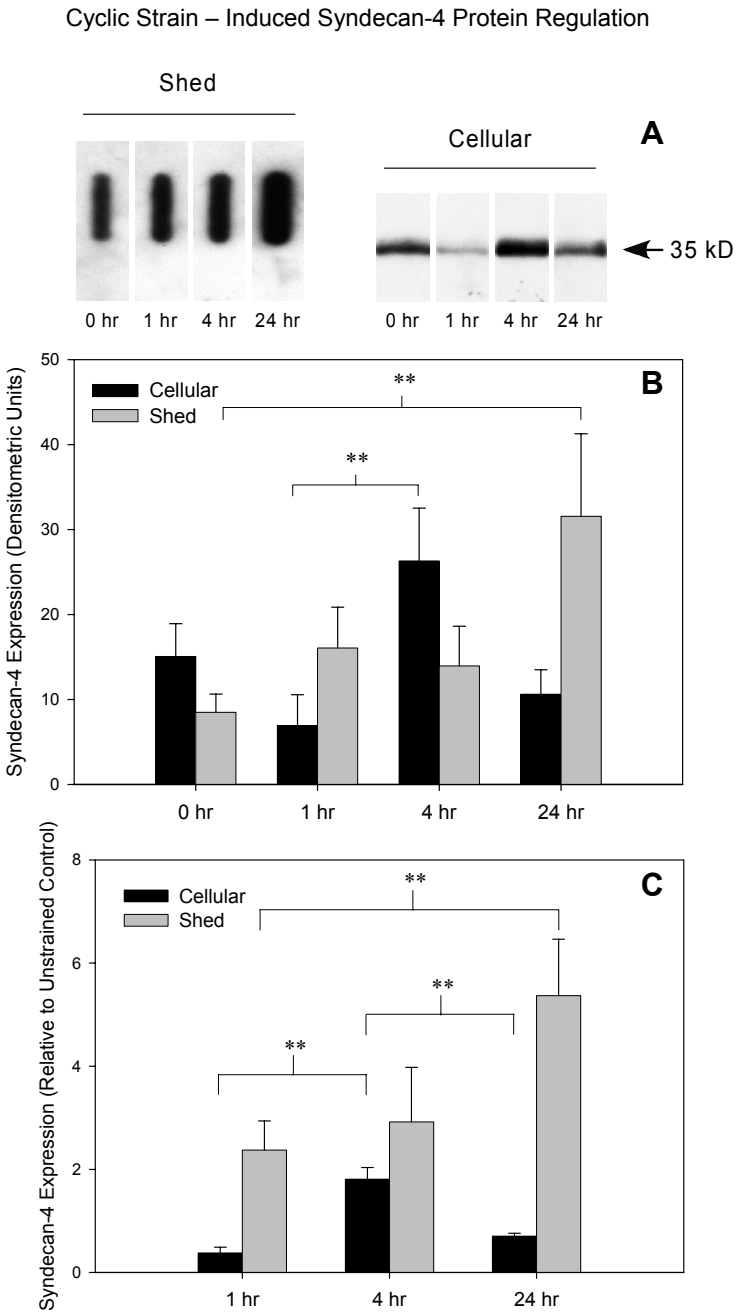

Figure 22. Immunoblot (A) and densitometry (B and C) analyses demonstrating syndecan-4 protein expression and shedding in response to cyclic mechanical strain. Human aortic SMCs were cultured on elastic membranes and stretched for the indicated periods of time. Cell-associated (■) or shed (■) protein was isolated and analyzed by Western or slot blot, respectively. All syndecan protein levels are presented as raw densitometric data (B) or relative to unstrained controls (C). Data represent the mean and standard errors from at least three independent experiments. ANOVA was performed using Tukey's (B) or Holm-Sidak's (C) method of multiple pairwise comparisons. (** Indicates a p value < 0.05)

4.3.2 Cyclic Strain Activates MAP Kinases

With the observation that the syndecan-4 was regulated by cyclic mechanical strain, we investigated the signaling pathways involved in this process. As stated earlier, the total pool of syndecan-4 consists of cell-associated and shed protein, and regulation of these sub-populations most likely occur via distinct mechanisms. The intracellular events which take place as the cells regulate this protein under the influence of this mechanical strain have not been well described.

We first examined, through Western immunoblotting of the total and phosphorylated kinases, whether the initiation of cyclic strain activated these signaling pathways. In the presence of 10% cyclic strain, we found that all three MAP kinases were activated. While the total ERK1/2 remained constant, the ratio of phosphorylated/total ERK1/2 increased to from 107% prior to strain to 246% at 30 minutes, and remained elevated at 60 minutes (Figure 23). Similarly, p38 MAP kinase was activated by cyclic strain. The ratio of phosphorylated/total p38 increased from 8% prior to strain to 284% at 15 minutes. Following this, phospho-p38 levels dropped, reaching 49% at 60 minutes (Figure 24). Finally, JNK/SAPK was also activated by cyclic strain. The ratio of phosphorylated/total JNK/SAPK increased from 6% prior to strain to 183% at 60 minutes, while the total JNK/SAPK levels remained constant (Figure 25). Given these results, we then tested the hypothesis that MAP kinase signaling influences syndecan-4 regulation. We accomplished this by utilizing chemical inhibitors of specific steps in these signal transduction cascades.

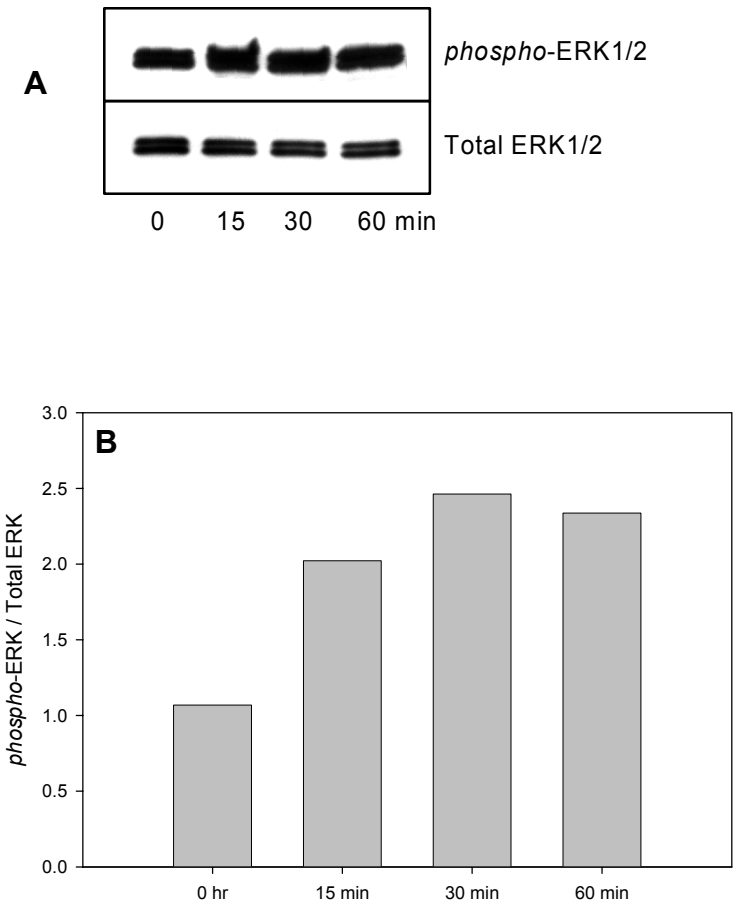

Figure 23. Phosphorylation of ERK1/2 MAP kinase in response to cyclic mechanical strain. Representative Western immunoblotting (A) and densitometry analysis (B) demonstrate time-dependent activation of ERK1/2 activation. Human aortic SMCs were cultured on elastic membranes and subjected to cyclic mechanical strain for the indicated periods of time. Cells were then lysed and proteins were resolved by SDS-PAGE and transferred a nitrocellulose membrane. Detection was performed using antibodies to total and phospho-ERK1/2, followed by chemiluminescence and visualization on autoradiography film. Levels of protein were quantified using image analysis software, and the data are presented as the ratio of the phosphorylated to the total cellular ERK1/2 MAP kinase levels.

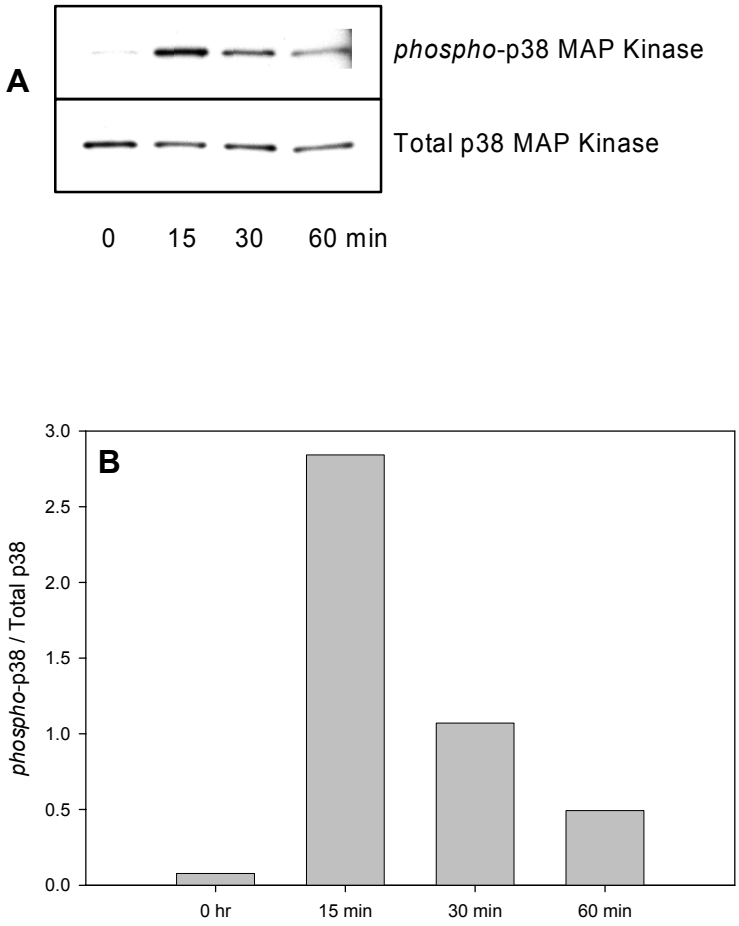

Figure 24. Phosphorylation of p38 MAP kinase in response to cyclic mechanical strain. Representative Western immunoblotting (A) and densitometry analysis (B) demonstrating time-dependent activation of p38 MAP kinase activation are shown. Human aortic SMCs were cultured on elastic membranes and subjected to cyclic mechanical strain for the indicated periods of time. Cells were then lysed and proteins were resolved by SDS-PAGE and transferred to a nitrocellulose membrane. Detection was performed using antibodies to total and phospho-p38, followed by chemiluminescence and visualization on autoradiography film. Levels of protein were quantified using image analysis software, and the data are presented as the ratio of the phosphorylated to the total cellular p38 MAP kinase levels.

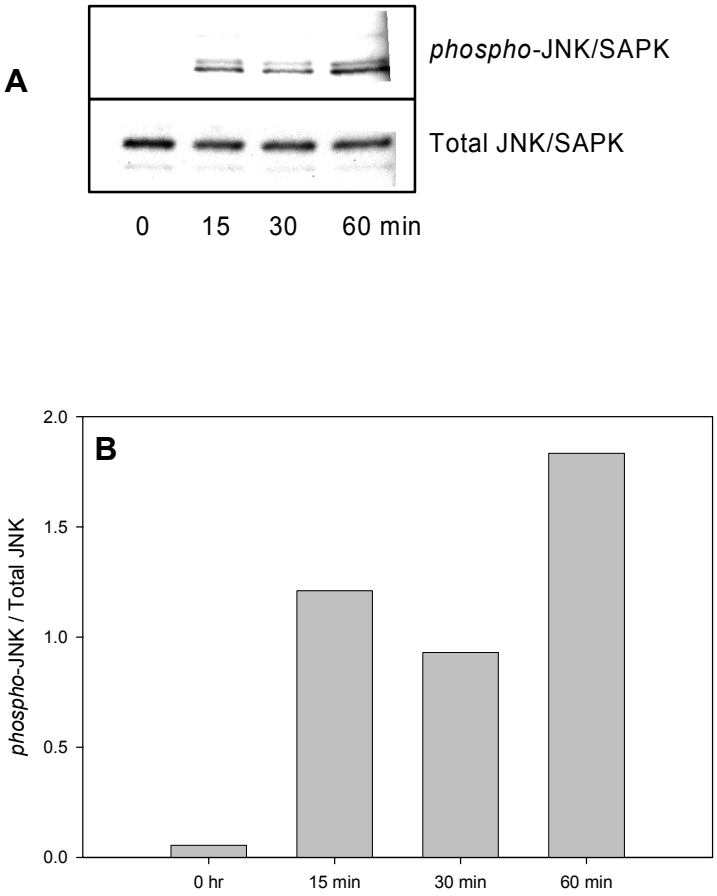

Figure 25. Phosphorylation of JNK/SAPK in response to cyclic mechanical strain. Representative Western immunoblotting (A) and densitometry analysis (B) demonstrating time-dependent activation of JNK/SAPK activation are shown. Human aortic SMCs were cultured on elastic membranes and subjected to cyclic mechanical strain for the indicated periods of time. Cells were then lysed and proteins were resolved by SDS-PAGE and transferred to a nitrocellulose membrane. Detection was performed using antibodies to total and phospho-JNK/SAPK, followed by chemiluminescence and visualization on autoradiography film. Levels of protein were quantified using image analysis software, and the data are presented as the ratio of the phosphorylated to the total cellular JNK/SAPK levels.

4.3.3 MAP Kinase Inhibition Alters the Response of Cell-Associated Syndecan-4 to Cyclic Strain

We first examined the strain-mediated regulation of total cell-associated syndecan-4, which consisted of both the intracellular and membrane-bound protein. Shed syndecan-4 was separated from this fraction, by removal of the conditioned media and washing of the cell monolayer prior to cell lysis, and then saved for later analysis. In order to examine if activation of the various MAP kinases influenced the regulation of cell-associated syndecan-4 protein, our strategy involved pre-treating the cells for 30 minutes with 20 μM U0126 as an inhibitor of ERK1/2, 20 μM SB203580 as an inhibitor of p38 MAP kinase, or 2 μM JNKI1 as an inhibitor of JNK/SAPK[‡]. The inhibitors U0126[223] and SB203580[224] have become well established tools for specifically inhibiting critical steps in their respective MAP kinase pathway. The inhibitor JNKI1, on the other hand, has not been studied as widely; nevertheless, it has also been shown to have specific bioactivity[212,213]. As an example, cells pre-treated with U0126 prior to stimulation with 15 or 30 minutes of 10% cyclic strain exhibited a decrease in the levels of phospho-ERK1/2, compared with untreated controls (Figure 26). We therefore sought to examine the consequence of this loss of activation on syndecan-4 protein regulation.

We first validated that the inhibitors were not cytotoxic at the concentrations used in our investigations, using a Live/Dead assay to assess cell viability/injury (Figure 27). The results demonstrate that no significant cell death occurred under the conditions used. We then measured the cell-associated syndecan-4 protein levels of cyclically strained

---

[‡] For the MAP kinase studies the term 'treatment' refers to the administration of one of the MAP kinase inhibitors for 30 minutes prior to the onset of cyclic strain. Control cells were strained without any inhibitor.

cells treated with or without one of the MAP kinase inhibitors. All data presented have been normalized to the unstrained, untreated controls. For the various comparisons, interaction effects between inhibitor treatment and duration of cyclic strain of the two-way ANOVA data were examined. This analysis enabled us to identify treatment effects that were dependent upon the duration of strain.

In cells pre-treated with U0126, we found a significant difference in cell-associated syndecan-4 expression between treated and control cells at 24 hours (Figure 28). While cell-associated syndecan-4 levels in the untreated cells had fallen to 30 ± 9% of unstrained controls, the cells strained in the presence of U0126 only fell to 62 ± 16%. At the other time points, the regulation of cell-associated syndecan-4 was independent of U0126 treatment, and thus, ERK1/2 activity: in the unstrained controls and those strained for 4 hours, ERK1/2 inhibition caused a slight but insignificant decrease in cell-associated syndecan-4. Results were similar for cells pre-treated with SB203580 (Figure 29). In the unstrained controls and those strained for 4 hours, p38 inhibition actually caused a slight but insignificant increase in cell-associated syndecan-4, and while cell-associated syndecan-4 levels in the untreated cells again fell to 30 ± 9% of unstrained controls, the presence of SB203580 resulted in a sustained level of cell-associated syndecan-4 protein at 24 hours (82 ± 23% of unstrained controls).

Pre-treatment with JNKI1 uniquely affected cell-associated syndecan-4 regulation in two ways (Figure 30). First, it resulted in a significant difference in cell-associated syndecan-4 expression between treated and control cells that was opposite of what was observed in the U0126 and SB203580 studies. Second, its effects were observed at 4 hours, considerably earlier than in the other studies. Specifically, while cell-associated

syndecan-4 levels in the untreated cells rose to 165 ± 24% of unstrained controls, the cells treated with JNKI1 fell to 77 ± 15%. In fact, in the presence of JNKI1, cell-associated syndecan-4 expression was suppressed at all time points.

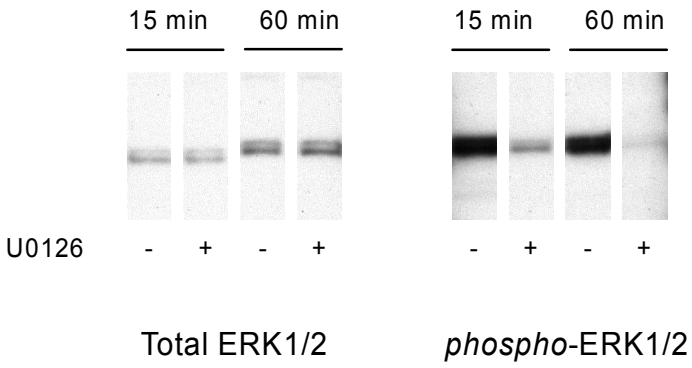

Figure 26. Immunoblots demonstrating the inhibition of ERK1/2 MAP kinase activation in the presence of U0126. Human aortic SMCs were cultured on elastic membranes and subjected to cyclic mechanical strain for the 15 or 60 minutes in the presence or absence of 20 μM U0126 in DMSO. Cells were then lysed and proteins were resolved by SDS-PAGE and transferred to a nitrocellulose membrane. Detection was performed using antibodies to total and phospho-ERK1/2, followed by chemiluminescence and visualization on autoradiography film.

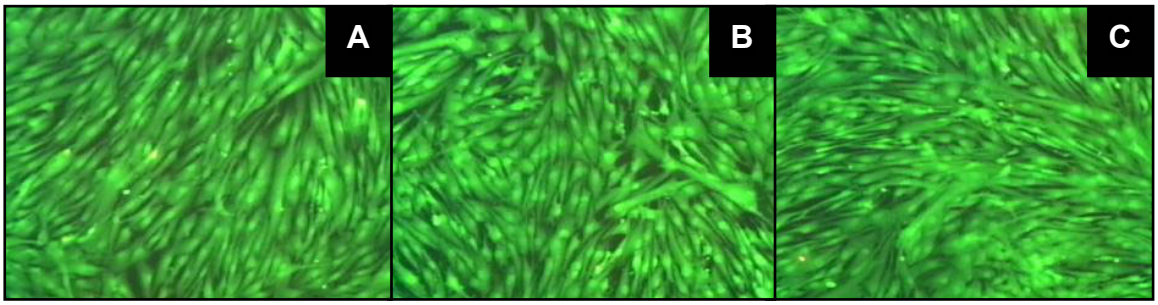

Figure 27. SMC viability when exposed to MAP Kinase inhibitors. Cell viability was determined after a 24 hour exposure to (A) 20 μM U0126, (B) 20 μM SB203580, or (C) 2 μM (L)-JNKI1 by visualizing fluorescence generated after the administration of calcein AM and ethidium homodimer. Visualization of cells was at 100X magnification.

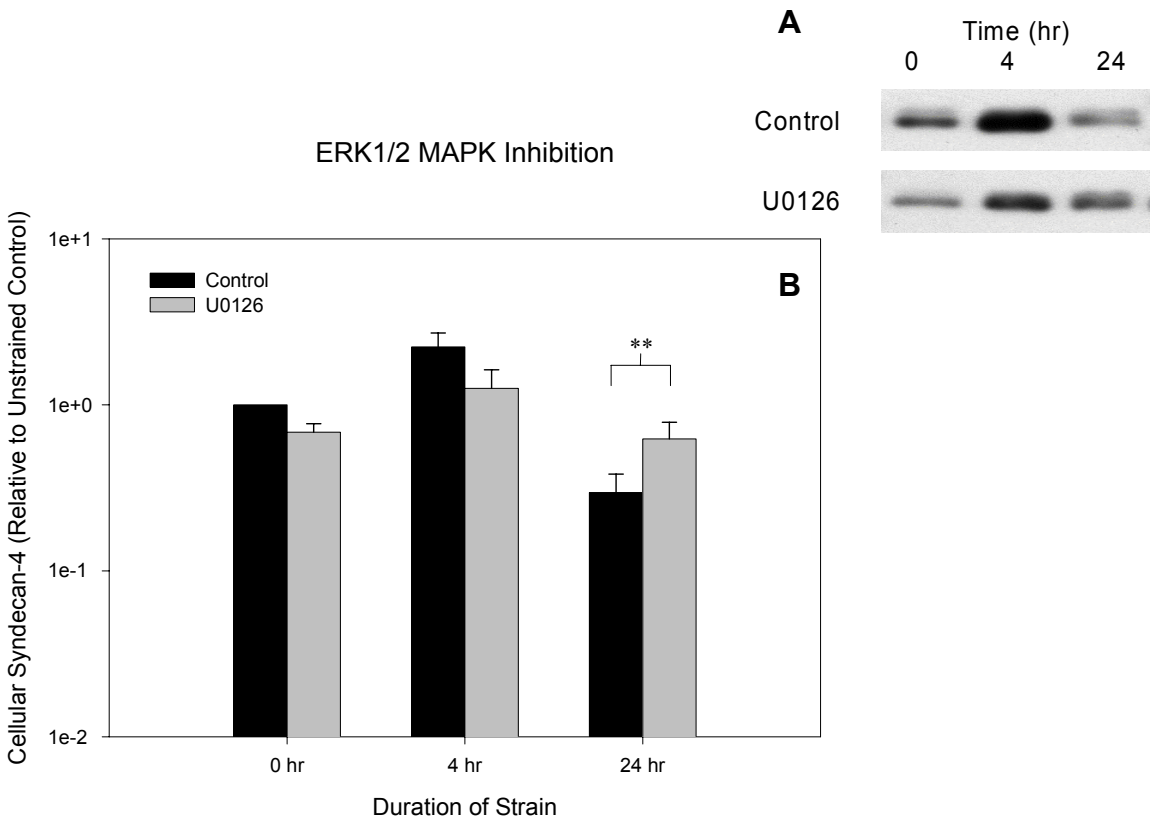

Figure 28. Effect of ERK1/2 MAP kinase inhibition on the 24 hour accumulation of cell-associated syndecan-4 protein due to cyclic mechanical strain. ERK1/2 inhibition was obtained by treatment with 20 μM U0126 (■) in DMSO for 30 minutes. Control cells (■) were treated with the same volume of DMSO vehicle. Cells were subjected to 1 Hz cyclic strain for 0 to 24 hours. As described in Methods, the initiation of cyclic strain was staggered so that all dishes were harvested simultaneously. The cell-associated fractions were lysed and then bound to a diethylamine anion exchange column; proteoglycans were eluted and GAG chains were digested with heparitinase and chondroitinase. (A) Proteins were resolved by SDS-PAGE and electrophoretically transferred to a PVDF membrane. Detection was performed using anti-syndecan-4 primary and HRP-conjugated secondary antibodies, followed by enhanced chemiluminescence and visualization on autoradiography film. Levels of protein were quantified by densitometry using image analysis software. (B) Concentrations were normalized to the syndecan-4 expression of unstrained, untreated control cells. Data represent the mean and standard errors from at least three independent experiments. After logarithmic transformation of the data in order to make the error variances independent of the means, statistical analysis was performed using ANOVA, employing Holm-Sidak's method for multiple pairwise comparisons. (** Indicates a p value < 0.05)

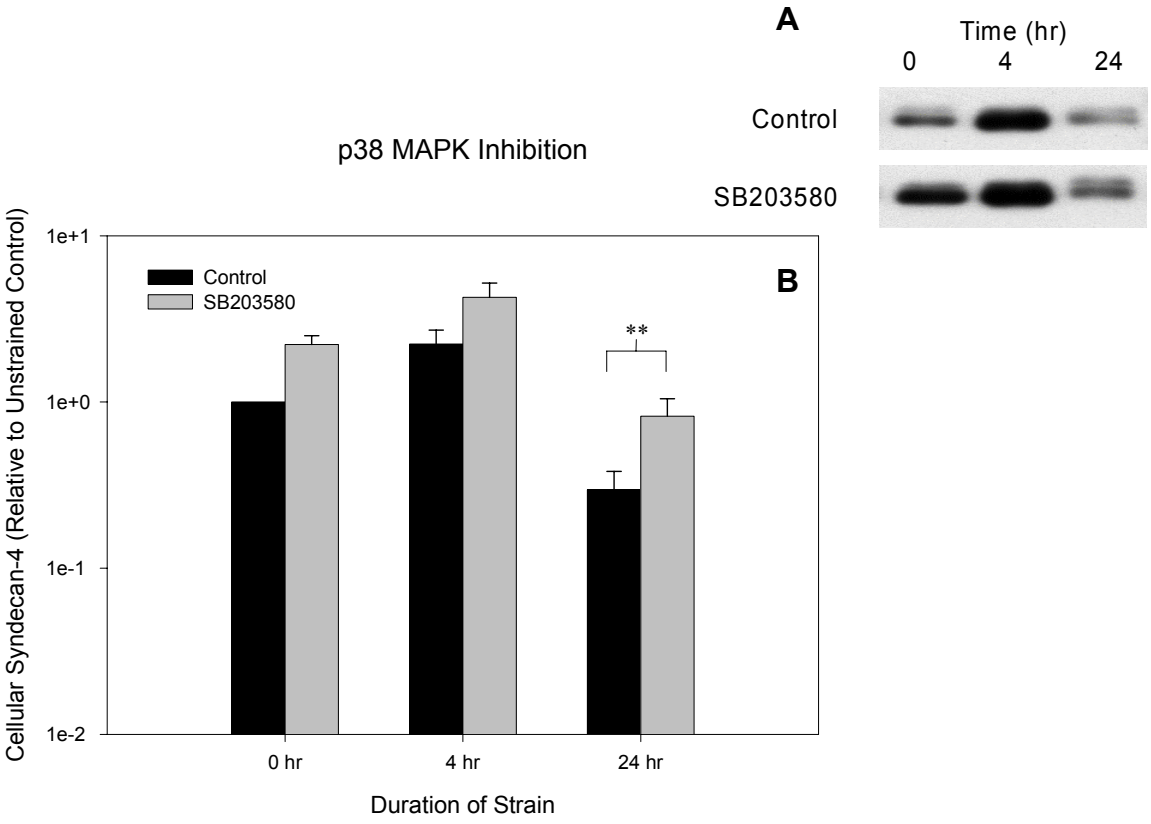

Figure 29. Effect of p38 MAP kinase inhibition on the 24 hour accumulation of cell-associated syndecan-4 protein due to cyclic mechanical strain. p38 MAP kinase inhibition was obtained by treatment with 20 μM SB203580 (■) in DMSO for 30 minutes. Control cells (■) were treated with the same volume of DMSO vehicle. Cells were subjected to 1 Hz cyclic strain for 0 to 24 hours. As described in Methods, the initiation of cyclic strain was staggered so that all dishes were harvested simultaneously. The cell-associated fractions were lysed and then bound to a diethylamine anion exchange column; proteoglycans were eluted and GAG chains were digested with heparitinase and chondroitinase. (A) Proteins were resolved by SDS-PAGE and electrophoretically transferred to a PVDF membrane. Detection was performed using anti-syndecan-4 primary and HRP-conjugated secondary antibodies, followed by enhanced chemiluminescence and visualization on autoradiography film. Levels of protein were quantified by densitometry using image analysis software. (B) Concentrations were normalized to the syndecan-4 expression of unstrained, untreated control cells. Data represent the mean and standard errors from at least three independent experiments. After logarithmic transformation of the data in order to make the error variances independent of the means, statistical analysis was performed using ANOVA, employing Holm-Sidak's method for multiple pairwise comparisons. (** Indicates a p value < 0.05)

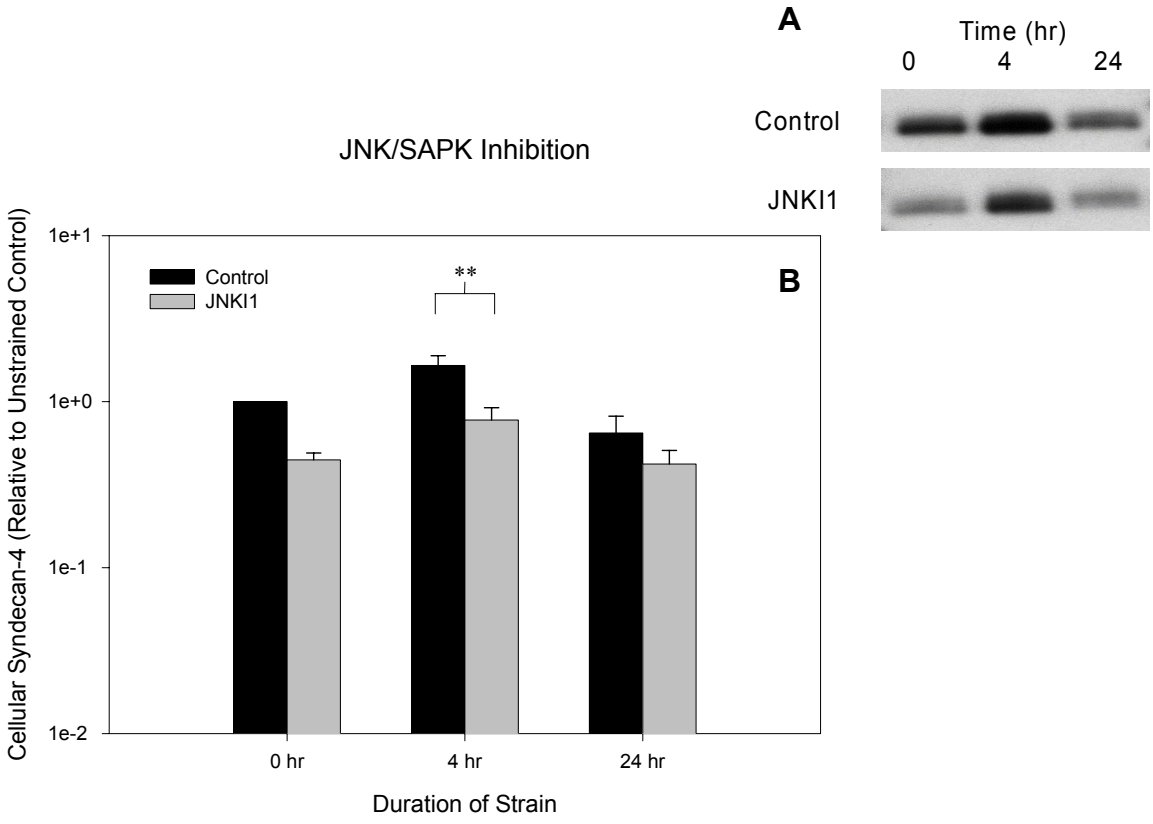

Figure 30. Effect of JNK/SAPK inhibition on the 24 hour accumulation of cell-associated syndecan-4 protein due to cyclic mechanical strain. JNK/SAPK inhibition was obtained by treatment with 2 μM (L)-JNKI1 (■) for 30 minutes. Control cells (■) were treated with the same volume of H_2O vehicle. Cells were subjected to 1 Hz cyclic strain for 0 to 24 hours. As described in Methods, the initiation of cyclic strain was staggered so that all dishes were harvested simultaneously. The cell-associated fractions were lysed and then bound to a diethylamine anion exchange column; proteoglycans were eluted and GAG chains were digested with heparitinase and chondroitinase. (A) Proteins were resolved by SDS-PAGE and electrophoretically transferred to a PVDF membrane. Detection was performed using anti-syndecan-4 primary and HRP-conjugated secondary antibodies, followed by enhanced chemiluminescence and visualization on autoradiography film. Levels of protein were quantified by densitometry using image analysis software. (B) Concentrations were normalized to the syndecan-4 expression of unstrained, untreated control cells. Data represent the mean and standard errors from at least three independent experiments. After logarithmic transformation of the data in order to make the error variances independent of the means, statistical analysis was performed using ANOVA, employing Holm-Sidak's method for multiple pairwise comparisons. (** Indicates a p value < 0.05)

4.3.4 MAP Kinase Inhibition Alters the Cyclic Strain Induced Shedding of Syndecan-4

The regulation of protein shedding is distinct from total protein expression, and although they are interrelated, they have distinct regulatory mechanisms[217]. Our objective was to determine to what degree MAP kinase activation regulated strain-induced syndecan-4 shedding. Similar to the cell-associated syndecan-4 studies, our experimental strategy for MAP kinase inhibition was through the use of pharmacological inhibitors. The analysis involved determining the 24 hour cumulative shedding of syndecan-4, during which the cells were strained for all, part, or none of the time. For example, the experimental sample designated as 0 hour strain consisted of conditioned media collected after a 24 hour period during which cells were not subjected to cyclic strain. Consequently, the sample consisted of constitutively-shed protein only. All values were first normalized to the untreated, constitutive shedding controls, and interaction effects from the two-way ANOVA were examined as before. At each time point, values for the treated samples were expressed as the percent change from the untreated controls. In cells pre-treated with U0126, we found significant suppression of syndecan-4 shedding at both 4 and 24 hours (Figure 31). After 4 hours of cyclic strain, shed levels were reduced to 12 ± 4% of unstrained controls by the presence of U0126, compared to 227% ± 42% in the untreated controls. After 24 hours, the level shed syndecan-4 from the treated cells had increased to only 209 ± 66% of unstrained controls, significantly different than the 1,110 ± 376% increase observed in the untreated controls. It was also notable that the presence of U0126 also suppressed the levels of constitutively-shed syndecan-4.

In contrast to the U0126 data, cells pre-treated with SB203580 demonstrated a

strain-induced increase in shed syndecan-4 that was not significantly affected by the inhibition of p38 (Figure 32). Although there were marginal decreases at each time point in the study, it is only noteworthy that, similar to U0126 pre-treatment, the cells exhibited a slight decrease in constitutively-shed syndecan-4 in the presence of SB203580. At 4 hours, the shed levels had increased to 177 ± 68% of unstrained controls, while at 24 hours, the levels had increased to 679 ± 263%. Finally, pre-treatment with JNKI1 reduced the shedding of syndecan-4 in a manner similar to U0126. At 4 hours, shed levels were significantly reduced from 97 ± 28% of unstrained controls to 7 ± 3%, while at 24 hours, shed syndecan-4 was significantly reduced from 230 ± 49% of unstrained controls to 67 ± 23%. Also similar to U0126, the presence of JNKI1 suppressed the levels of constitutively-shed syndecan-4.

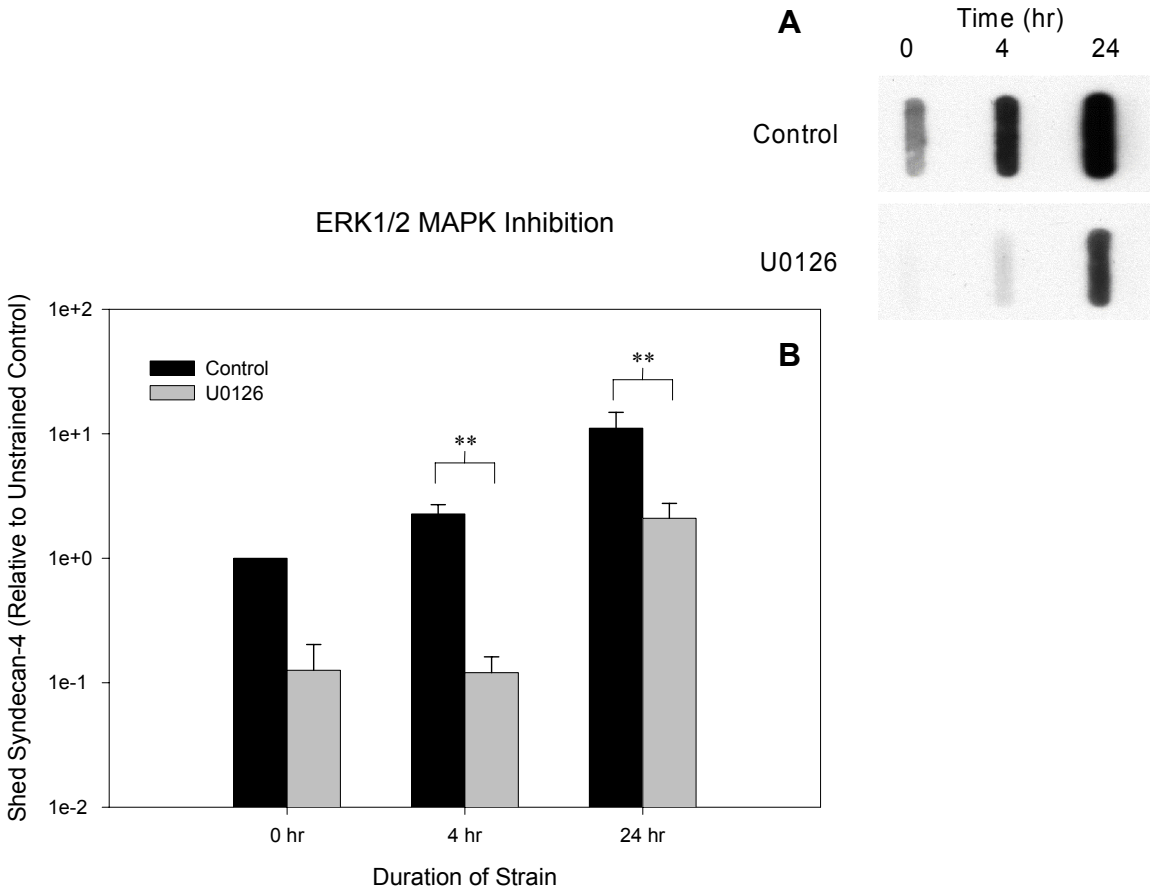

Figure 31. Effect of ERK1/2 MAP kinase inhibition on the 24 hour accumulation of shed syndecan-4 protein due to cyclic mechanical strain. ERK1/2 inhibition was obtained by treatment with 20 μM U0126 (■) in DMSO for 30 minutes. Control cells (■) were treated with the same volume of DMSO vehicle. Cells were subjected to 1 Hz cyclic strain for 0 to 24 hours. As described in Methods, the initiation of cyclic strain was staggered so that all dishes were harvested simultaneously. The cell-free conditioned media were concentrated 30X and then bound to a diethylamine anion exchange column; proteoglycans were eluted, and the samples were applied directly to a PVDF membrane using a slot blot apparatus. (A) Detection was performed using anti-syndecan-4 primary and HRP-conjugated secondary antibodies, followed by enhanced chemiluminescence and visualization on autoradiography film. Levels of protein were quantified by densitometry using image analysis software. (B) Concentrations were normalized to the syndecan-4 expression of unstrained, untreated control cells. Data represent the mean and standard errors from at least three independent experiments. After logarithmic transformation of the data in order to make the error variances independent of the means, statistical analysis was performed using ANOVA, employing Holm-Sidak's method for multiple pairwise comparisons. (** Indicates a p value < 0.05)

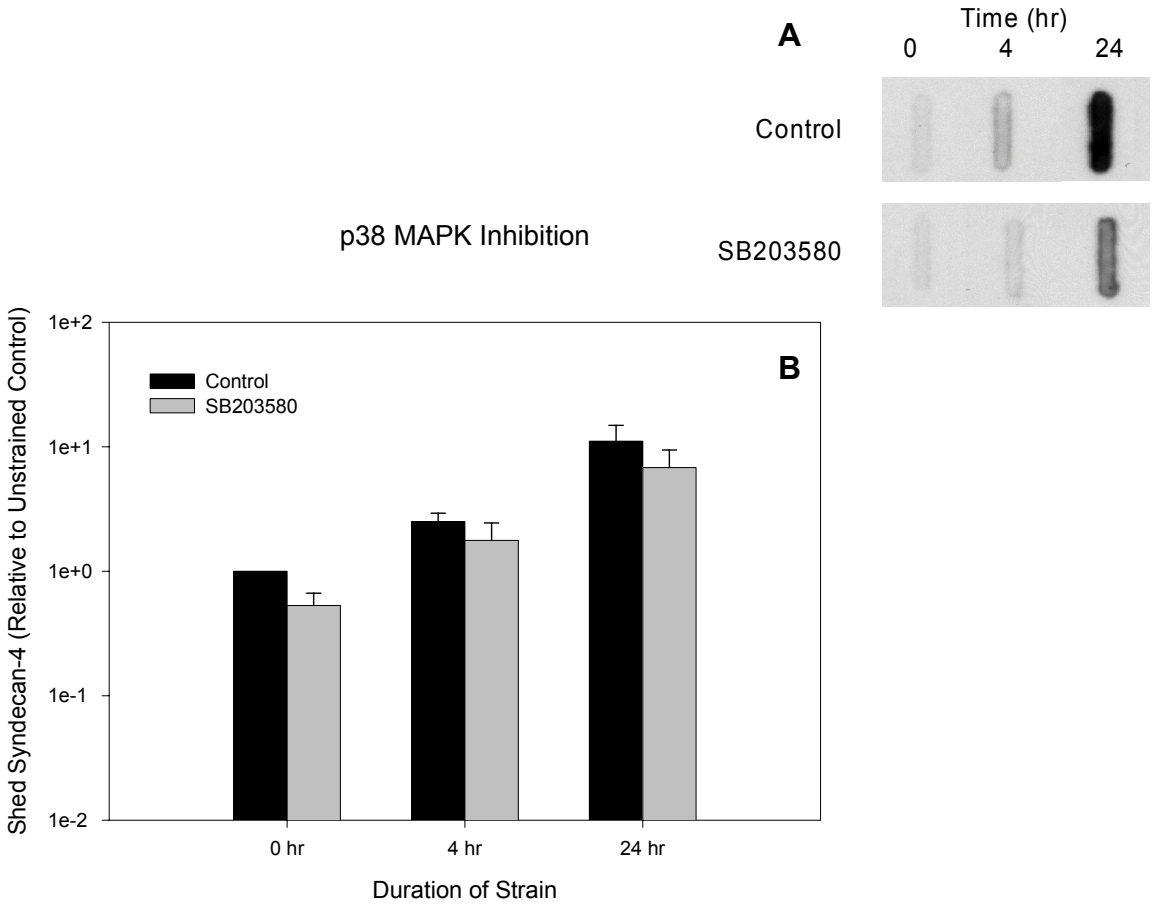

Figure 32. Effect of p38 MAP kinase inhibition on the 24 hour accumulation of shed syndecan-4 protein due to cyclic mechanical strain. p38 MAP kinase inhibition was obtained by treatment with 20 μM SB203580 (■) in DMSO for 30 minutes. Control cells (■) were treated with the same volume of DMSO vehicle. Cells were subjected to 1 Hz cyclic strain for 0 to 24 hours. As described in Methods, the initiation of cyclic strain was staggered so that all dishes were harvested simultaneously. The cell-free conditioned media were concentrated 30X and then bound to a diethylamine anion exchange column; proteoglycans were eluted, and the samples were applied directly to a PVDF membrane using a slot blot apparatus. (A) Detection was performed using anti-syndecan-4 primary and HRP-conjugated secondary antibodies, followed by enhanced chemiluminescence and visualization on autoradiography film. Levels of protein were quantified by densitometry using image analysis software. (B) Concentrations were normalized to the syndecan-4 expression of unstrained, untreated control cells. Data represent the mean and standard errors from at least three independent experiments. After logarithmic transformation of the data in order to make the error variances independent of the means, statistical analysis was performed using ANOVA, employing Holm-Sidak's method for multiple pairwise comparisons. (** Indicates a p value < 0.05)

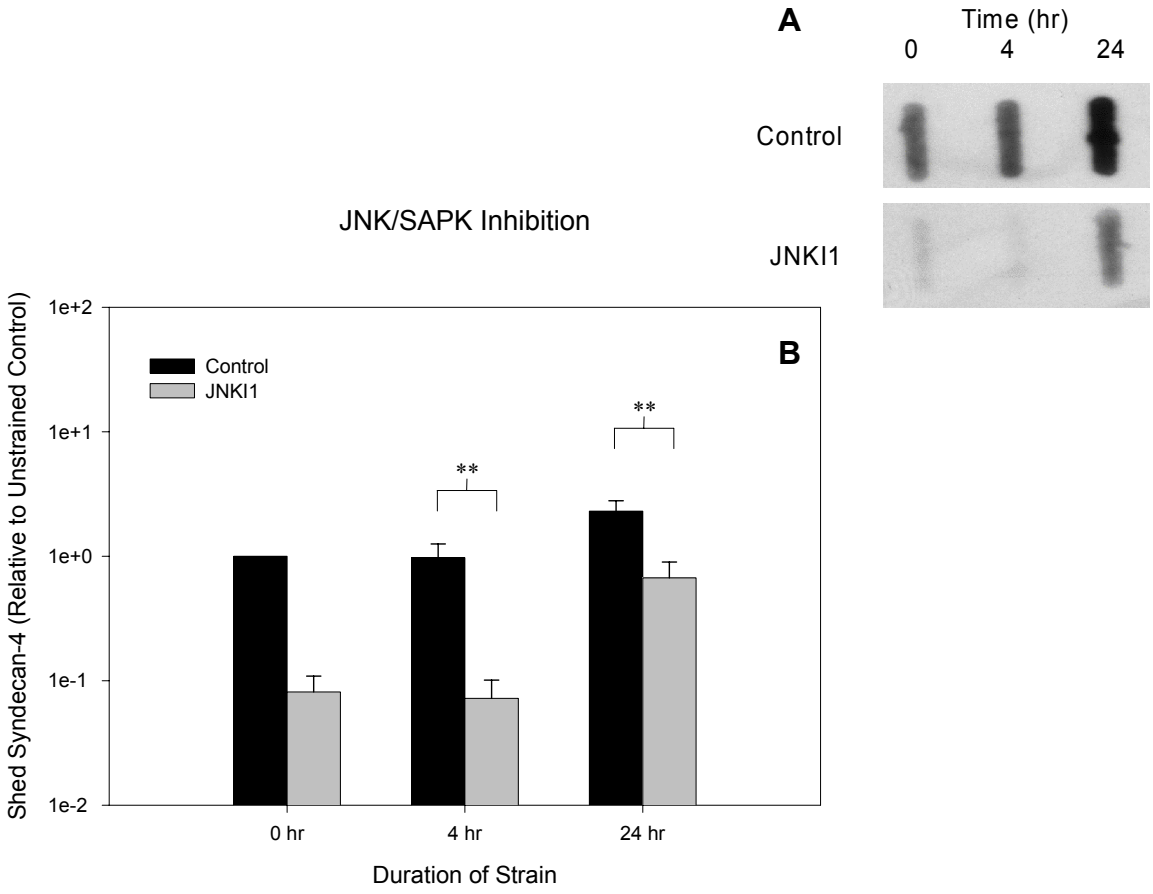

Figure 33. Effect of JNK/SAPK inhibition on the 24 hour accumulation of shed syndecan-4 protein due to cyclic mechanical strain. JNK/SAPK inhibition was obtained by treatment with 2 μM (L)-JNKI1 (■) for 30 minutes. Control cells (■) were treated with the same volume of H_2O vehicle. Cells were subjected to 1 Hz cyclic strain for 0 to 24 hours. As described in Methods, the initiation of cyclic strain was staggered so that all dishes were harvested simultaneously. The cell-free conditioned media were concentrated 30X and then bound to a diethylamine anion exchange column; proteoglycans were eluted, and the samples were applied directly to a PVDF membrane using a slot blot apparatus. (A) Detection was performed using anti-syndecan-4 primary and HRP-conjugated secondary antibodies, followed by enhanced chemiluminescence and visualization on autoradiography film. Levels of protein were quantified by densitometry using image analysis software. (B) Concentrations were normalized to the syndecan-4 expression of unstrained, untreated control cells. Data represent the mean and standard errors from at least three independent experiments. After logarithmic transformation of the data in order to make the error variances independent of the means, statistical analysis was performed using ANOVA, employing Holm-Sidak's method for multiple pairwise comparisons. (** indicates a p value < 0.05)

4.4 Discussion

4.4.1 Potential Mechanisms of Cell-Associated vs. Shed Syndecan Regulation

Cells regulate expression and shedding of syndecans via complex mechanisms that are not completely understood, including gene expression, post-translational modification, and protein trafficking [215,225,226]. Because increased protein synthesis does not necessarily result in increased protein shedding, and vice versa, we elected to separately characterize the kinetics of both cell-associated and shed syndecan-4 protein expression in response of cyclic mechanical strain, and to examine the effect of MAP kinase signaling on these processes.

Our studies demonstrated that 10% cyclic strain activated MAP kinase signaling. Through inhibition of specific enzymes in these signaling pathways, our results suggest that MAP kinase signaling played an important role in cyclic strain-induced syndecan-4 regulation. Specifically, all three MAP kinase pathways were involved in the strain-induced regulation of cell-associated syndecan-4. In particular, JNK/SAPK inhibition reduced the observed increase in cell-associated syndecan-4 that was typically seen after 4 hours of cyclic strain. Therefore, signaling via the JNK/SAPK pathway appeared to be required for the acute and transient increase in cell-associated syndecan-4. Conversely, ERK1/2 and p38 MAP kinase inhibition reduced the observed decrease in cell associated syndecan that occurred after 24 hours of cyclic strain. Therefore, ERK1/2 and p38 MAP kinase signaling pathways appeared to be responsible for the decrease in cell-associated syndecan-4 that was observed after prolonged periods of cyclic strain.

On the other hand, ERK1/2 and JNK/SAPK inhibition reduced constitutive syndecan shedding and also appeared to limit accelerated shedding that occurred after

initiation of acute cyclic strain. Signaling via the p38 MAP kinase pathway did not appear to be involved. It is noteworthy that shedding in response to cyclic strain was not completely eliminated by U0126 and JNKI1, as evidenced by the increased shed syndecan-4 levels at 24 hours. This may have been due to either the action of cellular compensatory mechanisms or to the loss of activity of the inhibitors.

While the cyclic strain-induced cell-associated syndecan-4 protein levels followed a pattern similar to the gene expression, shed levels continued to increase for the duration of the study. There are several possible explanations for this. As mentioned previously, the most direct correlation with syndecan-4 gene expression is with the regulation of the cell-associated fraction. The levels of this fraction are governed by translation from newly synthesized and existing syndecan-4 RNA, syndecan-4 proteolysis, ectodomain shedding, as well as any positive and/or negative feedback controls due to accumulation or deprivation of products along the way. All of these processes must be taken into consideration when attempting to fully characterize how cell-associated syndecan-4 is regulated. Shed syndecan-4, on the other hand, is regulated by the newly synthesized and existing protein levels, trafficking to and deposition in the cell membrane, proteolytic cleavage of the ectodomains into the surrounding medium, as well as any feedback mechanisms.

Given both the overlap and independence of the regulatory mechanisms, it was therefore difficult to conclude with certainty the causes of the differential effects of the MAP kinase inhibitors. Despite this, our data most likely suggest that inhibition of ERK1/2 and JNK/SAPK had the primary effect of reducing syndecan-4 ectodomain *shedding* – both constitutive and cyclic strain-mediated, and we would speculate that this

effect was most likely through post-translational activation of a membrane protease. This can explain why the shed syndecan-4 levels in the U0126 and JNKI1 pre-treated cells were significantly less than controls both constitutively and after 4 hours of cyclic strain. It could also explain why syndecan-4 levels in the U0126 pre-treated cells remained elevated at 24 hours; however, the reduced cellular levels in the JNKI1 pre-treated cells at 24 hours suggests that an additional and/or separate mechanism took place for this MAP kinase. Additionally, the persistent elevation of cell-associated syndecan-4 by p38 MAP kinase inhibition, in the absence of an appreciable effect on shed levels, suggests that p38 MAP kinase signaling was involved in the reduction of cell-associated syndecan-4 under chronic cyclic strain. It would appear that this was due to a reduction in syndecan-4 protein synthesis, rather than due to an effect on shedding. In other words, the chronic stress-induced reduction in syndecan-4 occurred at least in part via a p38 MAP kinase-dependent mechanism.

Candidate targets for MAP kinase-dependent regulation of syndecan-4 shedding include the zinc-dependent, hydroxamate-sensitive metalloproteinases (MMPs). In particular, the soluble, membrane-type MMP (MT-MMP) and ADAM families of cell-associated proteases/secretases have been shown to have diverse biological activity, including important roles in ectodomain shedding, cell adhesion, tumor metastasis, wound healing, and atherogenesis[216,218,227-235]. MT-MMPs are a subset of MMPs that are anchored to the cell membrane via either a transmembrane domain or a GPI anchor, while the typical multifunctional ADAM contains discrete pro-, metalloprotease, disintegrin-like, cysteine-rich, epidermal growth factor-like repeat, transmembrane, and cytoplasmic tail domains. While MMPs and MT-MMPs act strictly as proteases, the

various domains confer on ADAMs the ability both to promote cell-cell / cell-ECM adhesion and to induce ectodomain shedding of several important bioactive molecules[107,236]. Some of these shed molecules include syndecans, L-selectin, intercellular adhesion molecule-1 (ICAM-1), vascular cell adhesion molecule-1 (VCAM-1), TGFα, β-amyloid precursor protein (APP), angiotensin converting enzyme (ACE), and they have been shown to be controlled by MAP kinase-dependent and independent mechanisms[215,237-241]. Prior reports from our lab and others have demonstrated that syndecan shedding is regulated by a variety of stimuli, including extracellular ligands[71,225], bacterial virulence factors[220,242], and stress[214,219]. However, only a select subset of these stimuli have been shown to act via MAP kinase signaling. In particular, ERK1/2 and PKC signaling have been shown to be required for RANTES-induced shedding of syndecan-1 and syndecan-4 in HeLa cells[241] and for EGF and thrombin receptor-induced shedding in mouse epithelial cells[215]. Most other reports on the mechanism of syndecan shedding have focused on the involvement of intracellular tyrosine kinase[243] and MMP[219,226,229] activity on this process. Furthermore, work by Sumpio and others investigating the role of cyclic strain-induced intracellular signaling activity on various vascular cell processes[244,245], including SMC alignment and proliferation[155,157,165], has not addressed the circumstances surrounding ectodomain shedding. However, given the body of published evidence, as well as our current data, it is likely that the mechanism of cyclic strain-induced shedding contains some of the same mediators as agonist-induced shedding. In particular, it is also likely that MAP kinases are regulators of metalloproteinase activity. Overall, this field is lacking a comprehensive description of the multi-step process of cyclic mechanical strain detection,

intracellular signaling, and subsequent syndecan shedding regulation. For this reason, our results serve as an important contribution to this area, and it will be exciting to uncover the methods in which this modulation of cell-associated and shed syndecan-4 levels affects the ability of the cells to adapt to cyclic strain.

4.4.2 Limitations of Pharmacological Blockade of MAP Kinase Signaling

Part of the uncertainty in the above conclusions stems from the target assay system. Though extensively studied[246-248], the MAP kinase pathways are highly regulated and interconnected, which has made experimental design difficult and hindered the development of solid conclusions. Each cascade involves sequential activation of at least five levels of protein kinases, and each is usually initiated by transmission of signals from growth factor or tyrosine kinase receptors via members of the Rho family of small GTP-binding proteins. The ERK1/2 pathway, classically associated with transmitting signals leading to cell proliferation and differentiation, is typically initiated by activation of receptor tyrosine kinases (RTKs), such as EGF receptor, by binding one of its ligands. This leads to activation of the small G-protein Ras, then membrane translocation and activation of Raf, dual phosphorylation of MEK1/2, and then threonine and tyrosine phosphorylation of ERK1/2. ERK1/2 can then phosphorylate cytosolic targets such as MAP kinase-activated kinase (MAPKAPK), phospholipase A_2 and RSK or can translocate to the nucleus to activate transcription factors such as Elk-1 and c-Myc. These transcription factors ultimately bind to the promoter sequences of specific genes to regulate gene expression. Many of these same steps occur also when this pathway is activated by calcium influx or integrin activation. It is noteworthy that, due to its

involvement in cell proliferation, the activity of this pathway has been associated with oncogenic transformation.

The p38 MAP kinase and JNK/SAPK pathways, collectively known as the SAPK pathways[249], each share some similarities to the canonical ERK1/2 model. For example, each of the three pathways involves the sequential phosphorylation of kinases that are structurally and functionally similar to corresponding kinases in the other two pathways. In fact, similar to ERK1 and ERK2, the chief kinases of these two pathways also exist in several isoforms – JNK1/2 and p38α, β, and γ[250]. In addition, the p38 MAP kinase and JNK/SAPK pathways can be initiated by RTK activation. However, each of the SAPK pathways is activated in response to a unique but overlapping set of stimuli. For p38 MAP kinase, this set consists of inflammatory cytokines (such as TNFα) and Fas ligand binding to the TNFα receptor, oxidative stress, and UV irradiation. Conversely, the JNK/SAPK pathway has been shown to be activated by growth factor binding, UV and γ irradiation, mechanical and oxidative stress, chemotherapeutic agents, activation of G-protein-associated receptors, as well as inflammatory cytokine and Fas ligand binding to the TNFα receptor. Activation of the p38 MAP kinase pathway, and subsequent activation of MAPKAPKs or phosphorylation of various transcription factors, including ATF-2 and Sap-1a, leads to cellular responses that include cytokine production and apoptosis. Similarly, activation of the JNK pathway, and subsequent activation of transcription factors c-Jun, ATF-2, Elk-1, and p53, leads to growth, differentiation, adaptation, and apoptosis. Indeed, the cellular response ultimately depends on the context and associated factors in which these pathways proceed.

Despite the complexity of these pathways, the inhibitors used in this study were

useful tools; however, when investigating such a group of closely-related mechanisms, the studies were limited by the specificity of the given target. In other words, the inhibitor of a specific enzyme in a given MAP kinase pathway was only useful to the extent that it didn't interact with similar enzymes of a different pathway. Unfortunately, this loss of specificity has been shown by others to occur in a dose-dependent manner. Additionally, a potential weakness of these studies is the considerable overlap of the pathways. Since many of the key molecular targets are activated as part of multiple pathways, they allow for the existence of accessory paths toward the activation of a given end target. It is possible that, due to this redundancy, the inhibitors used were not as specific as required for detailed analysis. Lastly, the compounds used for pharmacologic inhibition offer experimental challenges. For example, they often suffer from limited stability in culture. Another problem is that some only offer competitive inhibition. Additionally, due to the particular solubility profile, control experiments require the use of potentially cell-stimulatory or cytotoxic solvents. For example, U0126 and SB203580 required the use dimethyl sulfoxide, while JNKI1 was soluble in water. This may be an explanation for the different trends seen in the shed syndecan-4 levels when no inhibitor was present. Some alternatives to the use of pharmacological inhibitors include dominant negative mutants and antisense constructs[207,251,252] in order to compete with or inhibit the native bioactive molecule. In addition, the collective analysis of singular and multifactorial approaches, in which several targets are blocked at once, is required for a more comprehensive description.

4.4.3 Functional Consequences of Altered Syndecan Expression

In summary, the cyclic strain-induced alteration of both the cell-associated and shed syndecan-4 is likely the result of the interaction of several mechanisms, of which only a small sampling was investigated in these studies. Furthermore, the true behavior of vascular SMCs in the native artery is unique to the structural environment of the surrounding tissue. Nevertheless, the functional consequences of altered syndecan-4 expression involve those related to the quantity present on the cell membrane and the levels present as soluble effector molecules in the surrounding interstitium. Since the shed ectodomains are released intact from the cell membrane, they can compete with remaining cell surface syndecans for ligand binding. This involves interactions with the vast array of heparin-binding proteins, including ECM proteins, growth factors, cytokines, proteases/protease inhibitors, and adhesion molecules. Depending on the normal cellular response to the interaction with the specific ligand, the presence of the newly shed, competing HS-containing ligands will abrogate that response. Alternatively, heparin-binding proteins whose activity is altered by their interaction with heparin and HSPGs will be able to attain this activity level without needing to be in proximity to cells. Wound fluids are examples of such cell-depleted environments. Another consequence results from the sequestration of growth factors and cytokines, leading to cell chemotaxis toward a specific area, which may be necessary for the effective resolution of tissue damage.

Alterations in the cell-associated syndecan-4 expression will also have a variety of consequences. Due to its involvement in the development of focal adhesions and stress fibers along with β_1 or β_3 integrins, an up-regulation of cell-associated (and assuming membrane-bound) syndecan-4 will likely lead to the formation of a higher

density of, and thus stronger in aggregate, adhesions to the appropriate substrate. Up-regulation and aggregation of intact, membrane-bound syndecan-4 molecules will also result in increased cytoskeletal organization via intracellular adaptor proteins, such as vinculin, talin, paxillin, and others. In addition, the syndecan-4-mediated increase in PKCα and possibly RhoA activity, as well as mechanotransduction via FAK signaling, will all lead to increased downstream cellular activity. Revisiting the tensegrity theory from the previous chapter, the increased cytoskeletal organization in particular will likely lead to increased cell stiffness and cell traction when the cells are stretched. Of course, the consequence over time would be negative feedback due to the apparent reduction in the cellular strain and therefore a decreased stimulus for continued syndecan-4 gene and protein synthesis.

As an example, the response of SMCs to both hypertension-induced arteriosclerosis and angioplasty-induced restenosis involves cell proliferation, migration, and MAP kinase activation[253]. It is likely that the initial response to the increased mechanical stress involves syndecan-4 proteolytic ectodomain shedding from the cell surface. The subsequent liberation from adhesions allows the cells to proliferate, migrate, and secrete ECM components (in addition to the shed ectodomains) in such a way as to increase the thickness of and ultimately restore the initial stress in the vascular wall. Over time, recovery of the cell-surface syndecan-4 levels, focal adhesions, and cytoskeletal assembly will allow the cells to re-stabilize in a manner better suited to endure the stress of their new mechanical environment.

CHAPTER 5

CONCLUSIONS AND FUTURE DIRECTIONS

The studies described in this dissertation provide a framework for exploring more fully the role of syndecans in vascular biology and the pathogenesis of diseases precipitated by mechanical insult. Like any framework, the interconnectedness of the structure as a whole is what makes it attractive and creates room for further exploration. In addition, many gaps require filling before the structure can be considered complete, and its strength ultimately relies on the foundation upon which its anchors place the greatest deal of weight. To that effect, the experiments described here were motivated by recent work of others describing the fundamental biology of syndecans and their various roles in cellular function, and the elucidation of various regulatory steps and signaling mechanisms has fueled the current interest. Additionally, the appreciation of and ability to manipulate the local cellular mechanical environment using engineering approaches have provided valuable insight into syndecan function.

In the present study, we employed a device capable of exerting equibiaxial strain to an elastic membrane, and have reported that the application of mechanical strain regulates the gene expression of syndecan-1, syndecan-2, and syndecan-4 in a time-dependent manner. In light of the kinetics of the syndecan-1 gene response, one strain protocol that could help to clarify syndecan-1 regulation would be a dose response study of 5%, 10%, and 20% strain evaluated at 24 hours or longer. The 4 hour time point was chosen because of the preliminary syndecan-4 data; however, the syndecan-1 data now suggest that longer times may yield important findings as well. While earlier evidence

has indicated that syndecan-4 is an early response gene in vascular injury[164,254], we have demonstrated that SMCs also regulate expression of these syndecans differentially based on whether the strain is static or cyclic. In future experiments, various design considerations could be explored. For example, it would be useful to apply strain in a defined, but anisotropic manner. Given the tendency of vascular SMC to orient themselves based on the direction of strain, we would expect cell orientation, and possibly function, to depend on the characteristics of the strain field. In addition, independent variations in frequency, duty cycle, and strain rate would provide additional stimuli. Frequency manipulation would allow for the modeling of certain arrhythmias due to anemia or hormones. On the other hand, strain rate manipulation would allow for the administration of a more physiologic (rather than sinusoidal) waveform to the cells.

Future experiments could also explore the relationship between membrane and cellular strain. In reference to the earlier discussion, the existence of cell prestress and strain hardening make methods of determining strain-induced cell stiffness important. A reasonable method would be to microscopically visualize (using fluorescent probes for example) and compare the magnitude of strain at different points on the elastic membrane before and after cells have adhered, and at certain time points during a given cyclic strain protocol. This would identify regions of non-homogeneity, and the analysis would provide a description and location of strain gradients. These areas might ultimately prove to be foci of characteristic cellular activity. For example, others have demonstrated a role for α-actinin-dependent crosslinking of F-actin networks, integrin binding and aggregation in strain hardening phenomena *in vitro* and *in vivo*[199,201,255].

The duration of cyclic strain is another potential area of investigation.

Experiments in which SMCs have been strained for more than a week have identified increased actin filament organization, focal adhesion formation, and cell stiffness[204,205]. Along with those employing an increased duration of cyclic strain, experiments could be performed in which markers of cell injury, such as lactate dehydrogenase or DNA leakage assays, are analyzed.

We also investigated the strain-mediated expression of cell-associated and shed syndecan-4, and some of the intracellular signaling mechanisms involved in this process. These studies were inspired by the work of various others, who have studied signal transduction pathways in response to cyclic strain, and who provided persuasive evidence that cyclic strain rapidly activates MAP kinases. Their work suggested that MAP kinases were important transducers of mechanical stress-induced responses of multiple cell types, including SMCs. In our experiments, we targeted the signaling pathways of ERK1/2, a pair of 44 and 42 kD protein kinases involved with cellular response to growth factors[210], p38 MAP kinase, a 38 kD protein kinase involved in the cellular response to inflammatory cytokines and endotoxins[211], and JNK/SAPK, a pair of 54 and 46 kD protein kinases involved in cellular responses to UV radiation and heat shock[212,213]. We found that MAP kinase signaling is required for the normal response to mechanical strain. In particular, ectodomain shedding was diminished in the absence of intact ERK1/2 and JNK/SAPK pathways.

In addition to examining the cell-associated and shed protein levels of the other syndecans in response to the previously described conditions, the use of genetic knockout models of the various syndecans could serve as useful tools for comparing the requirement for the various syndecan functions in the response to different stress, such as

hypoxia and septic shock. For example, current work in our lab is aimed at using one such model to characterize the involvement of syndecan-4 in atherogenesis. Using these models, in combination with selective re-introduction of certain syndecan functions, such as stress fiber formation, PKCα signaling, and growth factor and other ligand sequestration, could provide significant insight into syndecan function under certain pathophysiologic conditions.

Since the mechanism of syndecan shedding is unknown, this represents an area with great potential for additional experiments. Some could include the use of potential alternative mediators of shedding, or inhibitors of known sheddases, in order determine if the same or similar cellular responses occur. Alternatively, the use of other inhibitors of the MAP kinase pathway, such as retinoids and certain steroid hormones[256,257], or even certain phosphatases could aid in clarifying the steps involved. Protein kinase inhibitors such as genistein and tyrphostin are additional tools that could be used to further characterize strain-mediated syndecan shedding.

Since vascular remodeling requires the coordinated interaction between cell surface adhesion molecules and the ECM, important adaptive cellular changes take place in response to a variety of external signals, including mechanical stress. One critical event induced by a change in mechanical environment is altered cell locomotion with a presumed change in cell-matrix interactions, including cell-substrate adhesive forces. Since syndecan-4 has been implicated in cell-ECM adhesive interactions, we postulated that mechanical forces could mediate remodeling-related cell behavior through an effect on syndecan-4 expression. The glass microsphere adhesion assay described in these studies proved to be a sensitive and effective means of quantifying cell-matrix

interactions of well spread cells. Due to the importance of cell adhesion to engineered surfaces in tissue engineered vascular graft development, our studies allowed us to examine the effect of syndecan-4 regulation on a critical functional characteristic of SMCs. In future endeavors, this assay offers the advantage of simplicity and adaptability, due to the range of forces and substrates that can be evaluated with different cell types and under various experimental conditions. A future step could be to quantify the changes in adhesive strength of cells after subjecting them to cyclic mechanical strain; however, since the adhesion assay requires a rigid support substrate, it is unfortunately incompatible with the current cyclic strain set-up.

The studies describes here also utilized an adenoviral vector system as a means of genetically modifying the cells of interest. Despite its advantages over a number of other gene targeting methods, viral transduction systems such as this are labor intensive and suffer from some degree of variability. As promising, more novel, technologies become established in our lab, such as RNA Interference (RNAi), which utilizes short interfering RNA (siRNA), as a means of specifically silencing gene transcripts, we may have the ability to circumvent some of the problems inherent in the current transfection and knockout strategies.

Further experimentation could be also aimed at targeting syndecan-4 protein levels and characterizing its role in adhesion formation. It is very likely that regulation of expression, trafficking, post-translational modification such as sulfation and acetylation, and ectodomain shedding may influence adhesion in a manner distinct from the effects of gene regulation. Since cell adhesion involves a coordinated cascade of biochemical and biophysical events, modulation of both its magnitude and kinetics is likely to involve

several overlapping processes. Furthermore, when relating cell-associated syndecan-4 regulation with its functional consequences on cell adhesion, the *cell surface* syndecan-4 levels (determined by FACS analysis or enzyme-linked immunosorbent assay (ELISA)), is likely to correlate better.

Armed with an understanding of the role of syndecan-4 in these and other reparative vascular events, the goal of our investigations was to contribute to the foundational knowledge that will facilitate the development of rational treatment options for adhesion-dependent pathologic processes, including fibroproliferative disorders and cancer metastasis, as well as post-injury restenosis in blood vessels. We are confident that a more detailed understanding of strain-induced molecular events, and the ability of cells to interact through mechanochemical signals via the syndecan family of HSPG receptors, will allow us to gain a greater insight into the mechanisms underlying cellular attachment and the extent of matrix remodeling. The results from these studies offer methods of enhancing matrix stability in situations such as engineering cardiovascular tissue equivalents and enhancing atherosclerotic plaque stability. The negative impact that cardiovascular disease has on health in the United States is enormous, and treatment options may eventually include cell cycle regulation of SMCs, syndecan-specific pharmacologic blockade, or manipulation of downstream signaling events. These efforts would seek to inhibit cellular recognition and/or response to such events as the mechanical strain inflicted by balloon angioplasty or stent implantation. In addition, enhancement of matrix stability by augmenting the cellular responses to mechanical stimuli, in conjunction with preconditioning, is a promising method in which to construct durable vascular grafts. Thus, the rationale for future experimentation is that mechanical

strain is an impetus for, and HSPGs are critical mediators of, matrix-driven cell adhesive, migratory, and remodeling phenomena.

APPENDIX A

MODELING THE MODIFIED CENTRIFUGATION ASSAY[117]

A.1 Materials and Methods

A.1.1 Cell culture

PAC-1 immortalized rat pulmonary artery SMCs were provided by Dr. Abraham Rothman. Though immortalized, these cells retain expression of important markers of SMC phenotype, including angiotensin II, norepinephrine, and α-thrombin receptors, and also SMC isoforms of α-actin, myosin heavy and regulatory light chains, α-tropomyosin, meta-vinculin, phosphoglucomutase, and calponin[115]. The cells were cultured using standard cell culture techniques. Growth medium consisted of M199 Medium, supplemented with 10% FBS, L-glutamine, 100 U/L penicillin, 100 μg/L streptomycin, and 10 U/L amphotericin B. Quiescence medium consisted of growth medium, supplemented with 0.5% FBS. Cells were incubated at 37ºC, 5% CO_2, in a humidified atmosphere.

A.1.2 Surface Adsorption

The relationship between bulk solution and surface concentrations of heparin-binding peptides was quantified by radiolabeling the peptides with ^{125}I and adsorbing different concentrations to the surfaces of glass beads. The tyrosine-containing peptides were radiolabeled using IODO-Beads Iodination Reagent according to the manufacturer's instructions. Briefly, 1 mCi $Na^{125}I$ per 100 μg target protein was oxidized and incorporated into the protein, using PBS pH 7.2 as the reaction buffer. The reaction was

terminated by removing the beads from the mixture. Unincorporated ^{125}I was removed using a D-Salt Desalting Column (Pierce). The protein was precipitated by incubation in 10% trichloroacetic acid (TCA) for 45 minutes, followed by centrifugation at 16,000 x *g* and washing of the pellet twice with 10% TCA. The amount of radioactivity in the pellet was measured using a γ-counter (LKB-Wallac RiaGamma 1274). The protein concentration was determined using the Bradford method (Bio-Rad), and the specific activity (SA) in cpm/μg was then calculated and used for surface density (SD) determinations.

Cover slips (15 mm diameter) were used to determine adsorption onto glass. The discs were incubated with the ^{125}I-labeled protein, diluted 1:100 in unlabeled protein, and incubated at 4ºC for 24 hours. The discs were then blocked with 1% BSA in PBS at room temperature for 45 minutes, and then washed with PBS. The adsorbed radioactivity of each disc was determined using a γ-counter. The protein concentration vs. SD was determined using the following equation (dilution = 100):

$$SD = \left(\frac{cpm}{SA * Area} \right) * (Dilution) \qquad \text{(A.1)}$$

A.1.3 Glass Microsphere Adhesion Assay

Cell-substrate adhesive strength was determined by employing a modified centrifugation assay. Briefly, human plasma FN was pre-adsorbed onto 30-50 μm (mean diameter = 38.5 μm) glass microspheres (Polysciences, Warrington, PA) by incubating them in 100 μg/mL of the protein at 4ºC for at least 24 hours. The microspheres were

then washed five times with PBS, blocked with 1% BSA in PBS for 45 minutes at room temperature, and washed three more times in PBS. At this point, the microspheres were suspended in serum-free medium (MCDB 104 Medium, Gibco BRL) supplemented with Supplement-X (10 mg/L insulin, 5.5 mg/L transferrin, 6.7 μg/mL sodium-selenite; Gibco BRL), 2 mM L-glutamine (Mediatech), 1 mM $CaCl_2$ and Penicillin/Streptomycin. PAC-1 cells were sub-cultured at an initial density of $3x10^5$ cells/mL into each of the 72 inner wells of a 96-well culture-treated strip plate (Corning) and cultured in growth medium until 80% confluent (approximately 4 days). The cells were then quiesced for 24 hours, rinsed twice with PBS, and 200 μL of the microsphere suspension was placed in each well on top of the cell monolayer. The cells were incubated for 6 to 8 hours at 37ºC, after which the strip wells were detached in sets of two, placed inverted into a 12-well plate, filled with 0.01% BSA in PBS. Each plate was placed in a swing-bucket holder and centrifuged (Thermo EC), at designated speeds ranging from 500-3400 rpm (approximately 50-2500 x *g*) for one minute from the time maximum angular velocity was reached.

In this assay a range of detachment forces was applied to a population of matrix-coated glass microspheres, and the quantity of beads that adhered to the monolayer of cells upon inversion of the culture dish varied in a time-dependent manner. In plotting the percentage of adherent microspheres vs. the relative centrifugal force (*RCF*), the force value at which 50% of the microspheres detached could be determined and was designated as RCF_{50}. For example, the RCF_{50} was approximately 500 ± 100 x *g* for FN-coated glass microspheres that had been deposited and incubated for 6 hours on a monolayer of PAC-1 cells.

Different samples were centrifuged for 1 minute in increments of 500 rpm. Each well was then viewed at 40X magnification using an inverted microscope (Nikon) with ambient visible light illumination. The reflection of the rounded microspheres provided adequate contrast with low background noise, and enabled precise image measurements. Since the area covered by the microspheres was proportional to the total number attached to the cells, the fraction of glass microspheres remaining was determined by measuring the covered area, using IP Lab Spectrum image analysis software (Scanalytics). The results were fit to the following symmetrical logistic model (Equation 2.2), using the Marquardt-Levenberg algorithm, where f is the percent adherent glass microspheres, f_0 is the percent adherent at zero force, b is the decay slope, and RCF was measured in gravitational units, g. The parameters b and RCF_{50} were then calculated:

$$f = \frac{f_0}{1 + \exp[b(RCF - RCF_{50})]} \tag{A.2}$$

A.2 Mathematical Modeling of the Adhesion Assay

To calculate the actual negative pressure, or normal force per unit area, applied to the cells during the bead removal process, several assumptions were made. In order to determine the contact area between the cells and the microspheres, spread cells were modeled as a slab of uniform thickness. Due to the presence of the nucleus and lamellipods, the uniform thickness assumption may not be completely accurate. However, the mean thickness of the spots encountered by the beads should be approximately the mean thickness of the cell. To determine the mean thickness, we assumed that the volume of the cells remain constant whether the cell is detached and

rounded or attached and spread. Further, we used a spherical model for detached and rounded cells in calculating its volume. Digital images of cells that are attached and spread as well those that are detached and rounded were captured using a CCD video camera. The pixel size was calibrated with a stage micrometer and the area of the cells was then calculated using simple image analysis techniques. The mean thickness of the cell slab was calculated by

$$\delta = \frac{\frac{4}{3}\pi r^3}{A} \tag{A.3}$$

where δ is the thickness of the slab, r is the mean radius of the detached cells calculated from the area determined from the image analysis, and A is the mean area of the attached and spread cells.

The surface area of the microsphere in contact with the cells is dependent on how deeply the microsphere sinks into the cell (Figure 34). This depth would range between the two extremes: the maximum depth into which the microsphere may sink, i.e., the mean thickness of the cell δ, and the minimum, or zero. The maximum would occur if the bead sank all the way through the cell and came in contact with the bottom of the well, or, more realistically, if the microsphere came to rest in the valley between two adjacent cells. The minimum contact model is highly unlikely, since it requires that the cells be treated as hard objects with zero deformation, thus modeling the interface between the cell and the microsphere as a point contact. Given the relatively high density of the microspheres, the pliability of the cells, and the size of the beads, we chose to use the maximum depth model in calculating the contact surface area.

The amount of normal force applied to the cell surface by the beads during the

centrifugation process can be calculated by

$$F = V\Delta\rho(RCF) \tag{A.4}$$

where F is the force, V is the volume of the microsphere, $\Delta\rho$ is the difference in density between the media and the glass beads, and RCF is the relative centrifugal force. Substituting in for volume, we have

$$F = (\frac{\pi D^3}{6})\Delta\rho(RCF) \tag{A.5}$$

where D is the mean diameter of the microspheres. The negative pressure applied on the cell by the beads during the centrifugation process is simply the force divided by the contact area, or

$$P = \frac{F}{A} = \frac{\left(\frac{\pi D^3}{6}\right)\Delta\rho(RCF)}{\pi D\delta} \tag{A.6}$$

where P is the pressure pulling away from the cell surface, and δ is the thickness of the cell, as described earlier. This equation simplifies to

$$P = \frac{D^2\Delta\rho}{6\delta}(RCF)\,. \tag{A.7}$$

Substituting in the values for D, $\Delta\rho$, and δ, the equation further simplifies to

$$P = 133 \frac{\mu N}{gcm^2} (RCF) \tag{A.8}$$

where *RCF* is expressed in *g*'s (9.81 m/s^2). In other words, for every gravitational unit of acceleration applied to the system, the cells experience 133 μN/cm^2 of negative pressure pulling the microsphere away.

Minimum Contact Area

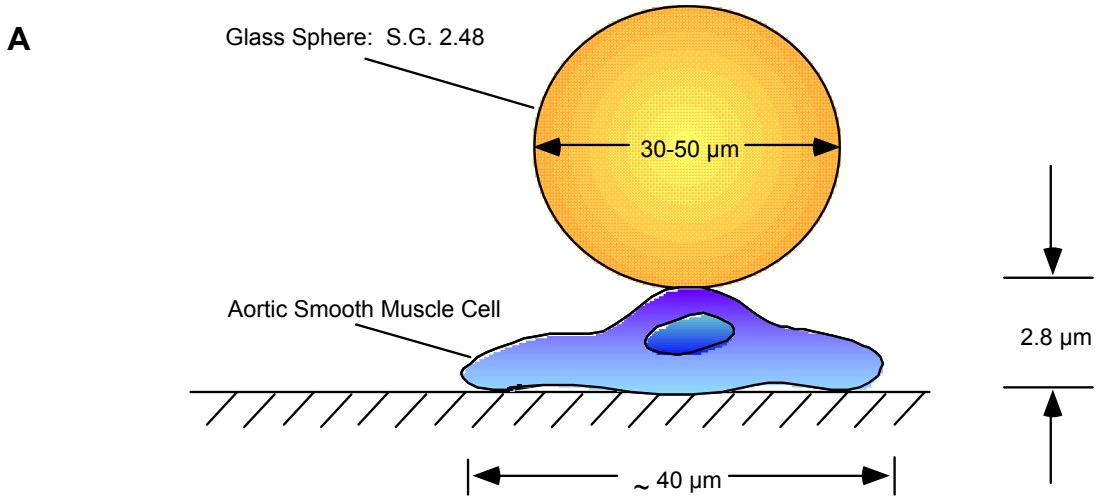

Maximum Contact Area

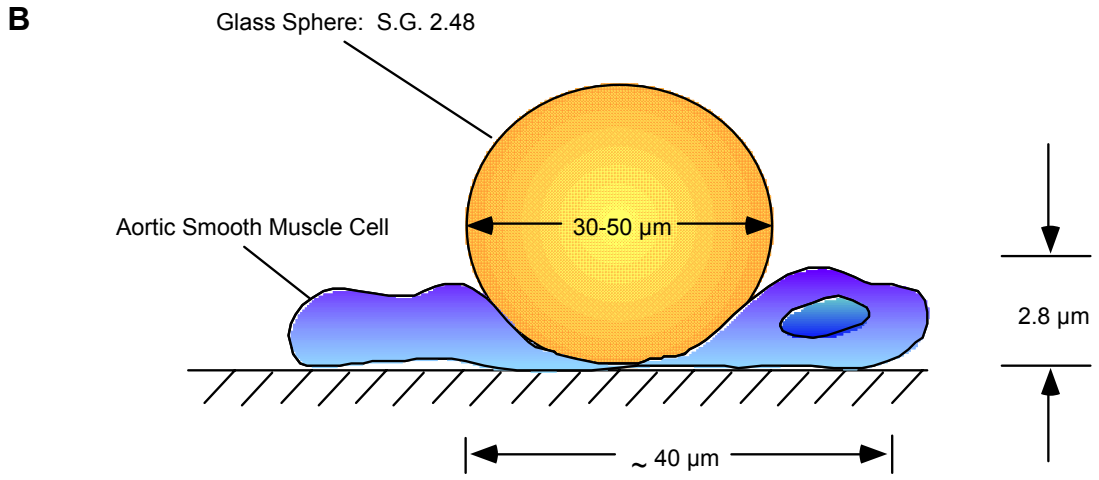

Figure 34. Minimum (A) and maximum (B) contact models of glass microspheres on a confluent layer of vascular smooth muscle cells. The mean thickness of the smooth muscle cells is calculated by dividing the mean volume of the detached cells by the mean area of the spread cells.

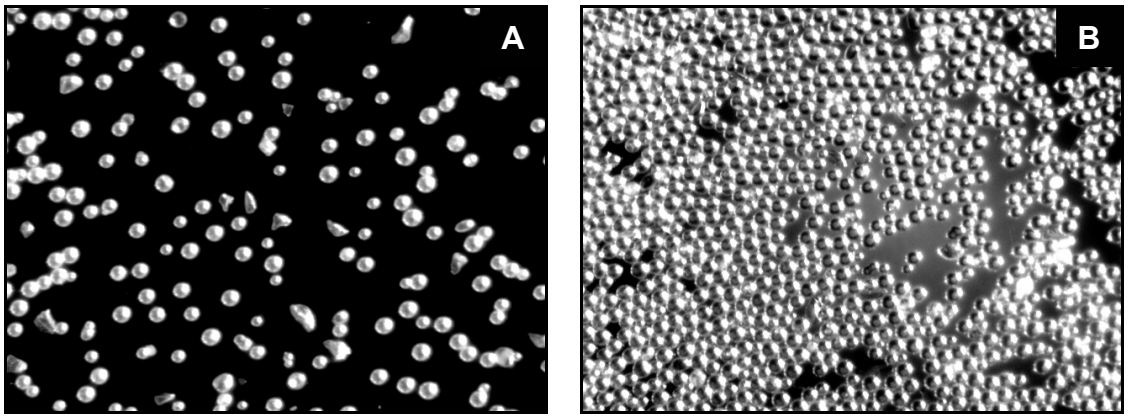

Figure 35. Glass microspheres seeded on PAC1 layer, as visualized at 100X magnification with only ambient light. The microspheres were coated with 100 μg/mL FN overnight and incubated on the cell layer for 1 hour (A) or 8 hours (B) before they were removed by inverting the wells. With a 1 hour incubation, approximately 5% of the microspheres remained adherent, whereas with an 8 hour incubation, nearly 90% remained.

APPENDIX B

SUPPLEMENTAL DATA TO CHAPTER 4

The syndecan-1 and syndecan-2 gene expression data yielded results which focused our interest on the regulation of cell-associated protein and shedding, in comparison with syndecan-4. Preliminary results were obtained, and are presented below.

B.1 Materials and Methods

B.1.1 Cell Culture

Clonetics normal human aortic SMCs, culture medium and supplements were obtained from Cambrex Bio Science, and the cells were sub-cultured using standard techniques. SmGM-2 was prepared according to the supplier's recommendations (SmBM, supplemented with 5% FBS, 500 µg/mL hEGF, 5 µg/mL insulin, 2 mg/mL hFGF, 50 µg/mL gentamycin, and 50 mg/mL amphotericin-B. Cells were maintained in tissue culture-treated petri dishes at 37ºC, 5% CO_2, and humidified atmosphere. Growth medium was changed every two days, and the cells were passaged 1:4 when the dishes were 80% confluent, using 0.05% Trypsin / 0.53 mM EDTA. Experiments were performed on cells between passages 6 and 10 using Quiescence medium, which consisted of SmBM supplemented with 0.5% FBS, 50 µg/mL gentamycin, and 50 mg/mL amphotericin-B.

B.1.2 Mechanical Strain Application

Strain dishes were assembled in the following manner: the bases of bottomless,

custom-made plastic petri dishes were fitted with silicone membrane (0.5 inch thickness; 40 Durometer). The silicone served as a flexible growth area of the strain dishes. For all experiments, 5 μg/mL human plasma FN in PBS was pre-adsorbed to the growth area for at least 8 hours at 4ºC, serving as a substrate for cell attachment. The cells were then seeded onto the membranes, cultured to 80% confluence in SmGM-2, and then growth-arrested for 24 hours in Quiescence medium.

Depending on the experimental conditions, defined static or cyclic tension was applied to the cells using a StrainMaster apparatus. Contacting surfaces of the membrane and strain device were lubricated with Dawn concentrated dishwashing liquid. Static and cyclic tensions were applied using a StrainMaster apparatus that allowed control over the frequency and amplitude of the radial and circumferential strains of the membrane and, and enabled the application of homogeneous and biaxially uniform strains over the entire growth area of the membrane.

The protocol for the application of mechanical strain for subsequent protein analysis was slightly different than for the RNA analysis. Following MAP kinase inhibitor pre-treatment (when appropriate), stretching (1 Hz, 10% cyclic strain) of the various samples commenced in a staggered fashion, based upon the total duration that each was to be strained (Figure 21). Since all samples were harvested simultaneously, stretching of the 24 hour strain samples commenced immediately, whereas stretching of the 4 and 1 hour strain samples were commenced at t = 20 hours and 23 hours, respectively. Non-stretched controls were performed concurrently for all experiments.

B.1.3 Shed Proteoglycan Isolation and Quantification

The following protocols were adapted from Reiland et al.[221] and Rioux et al.[222]. After the cells were treated with one of the strain protocols, the conditioned medium was passed through a 0.2 μM membrane filter (Millipore, Billerica, MA) in order to remove detached cells and debris. For shed syndecan-1 and syndecan-2 purification urea and NaOAc were added to bring the final concentrations to 2 M and 50 mM, respectively. The pH was then adjusted to 4.5 with acetic acid. The conditioned medium was incubated with pre-equilibrated DEAE Sepharose fast flow beads (Sigma-Aldrich) overnight at 4ºC with gentle agitation. Following incubation, the beads were washed three times with PBS and the proteoglycans were eluted with 10 mL of 1 M NaCl in PBS. The medium was concentrated to 1 mL using a 10,000 MWCO Amicon Ultra-15 Centrifugal Filter Unit (Millipore). Total protein was quantified using the BCA method (Pierce Biotechnology, Rockford, IL). GAG chains were digested by adding 250 ng protein to a 70 μL reaction containing 10 mM Tris-HCl pH 7.4, 150 mM NaCl, 4 mM $CaCl_2$, and 5 mU heparitinase (*F. heparinum*, EC 4.2.2.8, Seikagaku America, East Falmouth, MA) for 16 hours at 37ºC, after which an equal volume of Laemmli sample buffer containing 5% β-mercaptoethanol was added to each reaction. The samples were then ready for analysis.

The conditioned medium samples were resolved by SDS-PAGE, and then were transferred to a 0.45 μm Nytran SPC membrane (Schleicher & Schuell, Keene, NH). The membrane was blocked for 1 hour at room temperature in 3% nonfat dry milk / 0.5% BSA in PBS, followed by a 30 minute incubation in the same blocking solution with the addition of 0.3% Tween 20. The immunoblots were labeled overnight at 4ºC with anti-syndecan-1 mAb (Accurate Chemical & Scientific, Westbury, NY) or with anti-

syndecan-2 Ab (Santa Cruz Biotechnology, Santa Cruz, CA), both diluted 1:200 in blocking buffer. They were then washed in 0.5% Igepal CA-630 (Sigma-Aldrich) in TBS pH 7.4, followed by incubation with horseradish peroxidase anti-mouse or rabbit IgG (Bio-Rad) diluted 1:5000 in blocking buffer for 1 hour. The immunoblot was developed using enhanced chemiluminescence (Amersham), and the labeled protein was detected using BioMax MR autoradiography film. Levels of protein were quantified by densitometry using ONE-Dscan image analysis software.

B.1.4 Cell-Associated Proteoglycan Isolation and Quantification

For cell-associated syndecan-1 and syndecan-2 purification, the cells were washed twice with cold PBS, and 500 µL of lysis buffer was added to them, containing 20 mM Tris-HCl pH 7.4, 150 µM NaCl, 10 mM EDTA, 1% Triton X-100, and protease inhibitors. Following a 15 minute incubation on ice, the cells were scraped from the plates and homogenized by passing several times through a 26G needle. The cell lysates were centrifuged at 16,000 x g for 15 min at 4ºC. The supernatants were kept for analysis. As with the conditioned medium, total protein was quantified, but 5 µg of total protein was used in each heparitinase reaction. GAG chains were digested in a 70 µL heparitinase reaction, containing the same components as the conditioned medium, for 16 hours at 37ºC, after which an equal volume of Laemmli sample buffer containing 5% β-mercaptoethanol was added. The samples were then ready for analysis by SDS-PAGE in the same manner as the shed syndecan-1 and syndecan-2 samples.

B.1.5 Statistics and Data Analysis

Values are given as mean ± SEM. Statistical analysis was performed using SigmaStat 3.0 software package. ANOVA was employed, using the Holm-Sidak or Tukey tests for multiple pairwise comparisons among the treatments. When applicable, logarithmic transformation of the data was necessary prior to statistical analysis in order for it to conform to the ANOVA assumptions. A p value < 0.05 was considered statistically significant for all tests.

B.2 Results

B.2.1 Cyclic Strain Regulates Shed and Cell-Associated Syndecan Protein

The StrainMaster device was again used to mechanically strain cells in order to gain insight into the influence of mechanical strain on syndecan regulation. For these experiments, the strain protocol we chose to employ was 10% cyclic strain, 1 Hz, for various periods of time. The promising gene expression data for this strain regime suggested it as an appropriate initial target. The availability of successful experimental conditions for syndecan-4 dictated a more in-depth analysis of that protein's regulation than for syndecan-1 and syndecan-2. However, preliminary studies are represented in Figure 36 and Figure 37. Western immunoblots of conditioned medium from cells strained for 0 and 24 hours, and of lysates from cells strained for 0 and 48 hours revealed a faint 75 kD band corresponding to the heparitinase-digested syndecan-1 core protein (Figure 36A). Shed syndecan-1 from cells strained for 24 hours at 10% cyclic strain was increased to 278% of the unstrained control cells (Figure 36B). In contrast to this, syndecan-1 in the cell lysates of cells strained for 48 hours was reduced to 38%. Syndecan-2 was more readily detected by immunoblotting than syndecan-1, and revealed

a 45-50 kD band in both the shed and cell-associated fractions, corresponding to the heparitinase-digested syndecan-2 core protein (Figure 37A). Similar to the regulation of syndecan-1, shed syndecan-2 from cells subjected to 10% cyclic strain increased to 113% of unstrained controls at 48 hours, while the cell-associated syndecan-2 decreased to 39% at 24 hours.

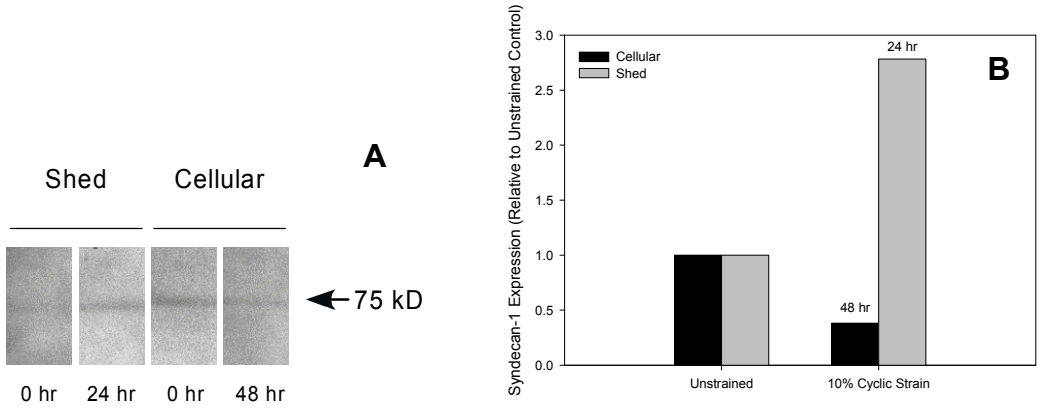

Figure 36. Immunoblot (A) and densitometry (B) analysis demonstrating syndecan-1 protein expression in response to cyclic mechanical strain. Human aortic SMCs were cultured on elastic membranes and stretched for the indicated periods of time. Cell-associated (■) or shed (■) protein was isolated and analyzed by Western blotting. Syndecan-1 protein levels are presented relative to unstrained controls.

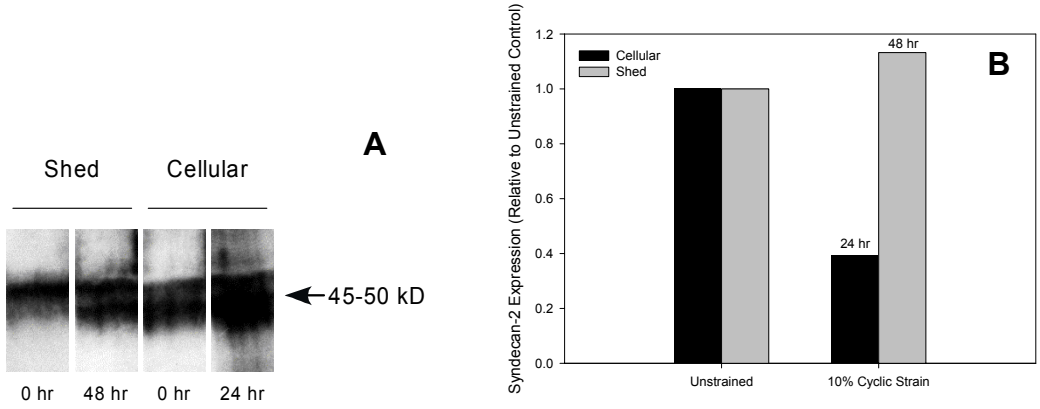

Figure 37. Immunoblot (A) and densitometry (B) analysis demonstrating syndecan-2 protein expression and shedding in response to cyclic mechanical strain. Human aortic SMCs were cultured on elastic membranes and stretched for the indicated periods of time. Cell-associated (■) or shed (■) protein was isolated and analyzed by Western blotting. Syndecan-1 protein levels are presented relative to unstrained controls.

REFERENCES

1. Bernfield M, et al. Functions of cell surface heparan sulfate proteoglycans. *Annual Review of Biochemistry* 1999; **68**: 729-77.

2. Woods A. Syndecans: transmembrane modulators of adhesion and matrix assembly. *Journal of Clinical Investigation* 2001; **107**(8): 935-41.

3. Longley RL, et al. Control of morphology, cytoskeleton and migration by syndecan-4. *Journal of Cell Science* 1999; **112**(Pt 20): 3421-31.

4. Rosenberg RD, Shworak NW, Liu J, Schwartz JJ, and Zhang L. Perspectives series: cell adhesion in vascular biology. *Journal of Clinical Investigation* 1997; **99**(9): 2062-70.

5. American Heart Association. *Heart Disease and Stroke Statistics - 2004 Update*. Dallas, Texas: American Heart Association; 2003.

6. National Center for Health Statistics. *Ambulatory and inpatient procedures in the United States, 1996*: National Center for Health Statistics; 1998.

7. American Heart Association. *Heart Disease and Stroke Statistics - 2003 Update*. Dallas, Texas: American Heart Association; 2002.

8. Scott J. Pathophysiology and biochemistry of cardiovascular disease. *Current Opinion in Genetics and Development* 2004; **14**(3): 271.

9. Bots ML, Dijk JM, Oren A, and Grobbee DE. Carotid intima-media thickness, arterial stiffness and risk of cardiovascular disease: current evidence. *journal of Hypertension* 2002; **20**(12): 2317-25.

10. Seliktar D, Nerem RM, and Galis ZS. The role of matrix metalloproteinase-2 in the remodeling of cell-seeded vascular constructs subjected to cyclic strain. *Annals of Biomedical Engineering* 2001; **29**(11): 923-34.

11. Seliktar D, Black RA, Vito RP, and Nerem RM. Dynamic mechanical conditioning of collagen-gel blood vessel constructs induces remodeling in vitro. *Annals of Biomedical Engineering* 2000; **28**(4): 351-62.

12. Kim BS, Nikolovski J, Bonadio J, and Mooney DJ. Cyclic mechanical strain regulates the development of engineered smooth muscle tissue. *Nature Biotechnology* 1999; **17**(10): 979-83.

13. L'Heureux N, et al. A human tissue-engineered vascular media: a new model for pharmacological studies of contractile responses. *FASEB Journal* 2001; **15**(2): 515-24.

14. L'Heureux N, Paquet S, Labbe R, Germain L, and Auger FA. A completely biological tissue-engineered human blood vessel. *FASEB Journal* 1998; **12**(1): 47-56.

15. Kanda K and Matsuda T. Mechanical stress-induced orientation and ultrastructural change of smooth muscle cells cultured in three-dimensional collagen lattices. *Cell Transplantation* 1994; **3**(6): 481-92.

16. Wootton DM and Ku DN. Fluid mechanics of vascular systems, diseases, and thrombosis. *Annual Review of Biomedical Engineering* 1999; **1**: 299-329.

17. Traub O and Berk BC. Laminar shear stress: mechanisms by which endothelial cells transduce an atheroprotective force. *Arteriosclerosis, Thrombosis & Vascular Biology* 1998; **18**(5): 677-85.

18. Humphrey JD. Mechanics of the arterial wall: review and directions. *Critical Reviews in Biomedical Engineering* 1995; **23**(1-2): 1-162.

19. Patel DJ and Fry DL. The elastic symmetry of arterial segments in dogs. *Circulation Research* 1969; **24**(1): 1-8.

20. von Maltzahn WW, Besdo D, and Wiemer W. Elastic properties of arteries: a nonlinear two-layer cylindrical model. *Journal of Biomechanics* 1981; **14**(6): 389-97.

21. Demiray H and Vito RP. A layered cylindrical shell model for an aorta. *International Journal of Engineering Science* 1991; **29**: 47-54.

22. Hayashi K. Experimental approaches on measuring the mechanical properties and constitutive laws of arterial walls. *Journal of Biomechanical Engineering* 1993; **115**(4B): 481-8.

23. Yu Q, Zhou J, and Fung YC. Neutral axis location in bending and Young's modulus of different layers of arterial wall. *American Journal of Physiology* 1993; **265**(1 Pt 2): H52-60.

24. Xie J, Zhou J, and Fung YC. Bending of blood vessel wall: stress-strain laws of the intima-media and adventitial layers. *Journal of Biomechanical Engineering* 1995; **117**(1): 136-45.

25. Zarins CK, et al. Arterial disruption and remodeling following balloon dilatation. *Surgery* 1982; **92**(6): 1086-95.

26. Waller BF. "Crackers, breakers, stretchers, drillers, scrapers, shavers, burners, welders and melters"--the future treatment of atherosclerotic coronary artery disease? A clinical-morphologic assessment. *Journal of the American College of Cardiology* 1989; **13**(5): 969-87.

27. Honye J, et al. Morphological effects of coronary balloon angioplasty in vivo assessed by intravascular ultrasound imaging. *Circulation* 1992; **85**(3): 1012-25.

28. Fung YC. Biomechanics: mechanical properties of living tissues 2nd ed. 1993, New York: Springer-Verlag. xviii, 568.

29. Ward MR, Pasterkamp G, Yeung AC, and Borst C. Arterial remodeling: mechanisms and clinical implications. *Circulation* 2000; **102**(10): 1186-91.

30. Mignatti P, Rifkin DB, Welgus HG, and Parks WC, *Proteinases and tissue remodeling*, in The Molecular and Cellular Biology of Wound Repair, Clark RAF, Editor. 1996, Plenum Press: New York. p. 427-74.

31. Coats WD, Jr. and Faxon DP. The role of the extracellular matrix in arterial remodelling. *Seminars in Interventional Cardiology* 1997; **2**(3): 167-76.

32. Wight TN. Versican: a versatile extracellular matrix proteoglycan in cell biology. *Current Opinion in Cell Biology* 2002; **14**(5): 617.

33. Rosso F, Giordano A, Barbarisi M, and Barbarisi A. From cell-ECM interactions to tissue engineering. *Journal of Cellular Physiology* 2004; **199**(2): 174-80.

34. Dzau VJ and Gibbons GH. Vascular remodeling: mechanisms and implications. *Journal of Cardiovascular Pharmacology* 1993; **21**(Suppl 1): S1-5.

35. Faxon DP, Coats W, and Currier J. Remodeling of the coronary artery after vascular injury. *Progress in Cardiovascular Diseases* 1997; **40**(2): 129-40.

36. Galis ZS and Khatri JJ. Matrix metalloproteinases in vascular remodeling and atherogenesis: the good, the bad, and the ugly. *Circulation Research* 2002; **90**(3): 251-62.

37. Seliktar D, Nerem RM, and Galis ZS. Mechanical strain-stimulated remodeling of tissue-engineered blood vessel constructs. *Tissue Engineering* 2003; **9**(4): 657-66.

38. Glagov S, Weisenberg E, Zarins CK, Stankunavicius R, and Kolettis GJ. Compensatory enlargement of human atherosclerotic coronary arteries. *New England Journal of Medicine* 1987; **316**(22): 1371-5.

39. Gibbons GH and Dzau VJ. The emerging concept of vascular remodeling. *New England Journal of Medicine* 1994; **330**(20): 1431-8.

40. Langille BL. Arterial remodeling: relation to hemodynamics. *Canadian Journal of Physiology & Pharmacology* 1996; **74**(7): 834-41.

41. Bayer IM, Adamson SL, and Langille BL. Atrophic remodeling of the artery-cuffed artery. *Arteriosclerosis, Thrombosis & Vascular Biology* 1999; **19**(6): 1499-505.

42. Davies PF, et al. Spatial realtionashipsin early signaling events of flow-mediated endothelial mechanotransduction. *Annual Review of Physiology* 1997; **59**(1): 527-49.

43. Chien S, Li S, and Shyy YJ. Effects of mechanical forces on signal transduction and gene expression in endothelial cells. *Hypertension* 1998; **31**(1 Pt 2): 162-9.

44. Jalali S, et al. Shear stress activates p60src-ras-MAPK signaling pathways in vascular endothelial cells 1998; **18**(2): 227-34.

45. Lee RT, et al. Mechanical strain induces specific changes in the synthesis and organization of proteoglycans by vascular smooth muscle cells. *Journal of Biological Chemistry* 2001; **276**(17): 13847-51.

46. Scott NA, et al. Identification of a potential role for the adventitia in vascular lesion formation after balloon overstretch injury of porcine coronary arteries. *Circulation* 1996; **93**(12): 2178-87.

47. Shi Y, et al. Adventitial myofibroblasts contribute to neointimal formation in injured porcine coronary arteries. *Circulation* 1996; **94**(7): 1655-64.

48. Li G, Chen Y-F, Kelpke SS, Oparil S, and Thompson JA. Estrogen attenuates integrin-β_3-dependent adventitial fibroblast migration after inhibition of osteopontin production in vascular smooth muscle cells. *Circulation* 2000; **101**(25): 2949-55.

49. Christen T, et al. Mechanisms of Neointima Formation and Remodeling in the Porcine Coronary Artery. *Circulation* 2001; **103**(6): 882-88.

50. Birkedal-Hansen H. Proteolytic remodeling of extracellular matrix. *Current Opinion in Cell Biology* 1995; **7**(5): 728-35.

51. Li Z, Froehlich J, Galis ZS, and Lakatta EG. Increased expression of matrix metalloproteinase-2 in the thickened intima of aged rats. *Hypertension* 1999; **33**(1): 116-23.

52. Shi Y, et al. Role of matrix metalloproteinases and their tissue inhibitors in the regulation of coronary cell migration. *Arteriosclerosis, Thrombosis & Vascular Biology* 1999; **19**(5): 1150-55.

53. Raghow R. The role of extracellular matrix in postinflammatory wound healing and fibrosis. *FASEB Journal* 1994; **8**(11): 823-31.

54. Stupack DG, et al. Matrix valency regulates integrin-mediated lymphoid adhesion via Syk kinase. *Journal of Cell Biology* 1999; **144**(4): 777-88.

55. Koyama H, Raines EW, Bornfeldt KE, Roberts JM, and Ross R. Fibrillar collagen inhibits arterial smooth muscle proliferation through regulation of Cdk2 inhibitors. *Cell* 1996; **87**(6): 1069-78.

56. Ichii T, et al. Fibrillar collagen specifically regulates human vascular smooth muscle cell genes involved in cellular responses and the pericellular matrix environment. *Circulation Research* 2001; **88**(5): 460-7.

57. Carey DJ. Syndecans: multifunctional cell-surface co-receptors. *Biochemical Journal* 1997; **327**(Pt 1): 1-16.

58. Sanderson RD and Bernfield M. Molecular polymorphism of a cell surface proteoglycan: distinct structures on simple and stratified epithelia. *Proceedings of the National Academy of Sciences of the United States of America* 1988; **85**(24): 9562-6.

59. Steinfeld R, Van Den Berghe H, and David G. Stimulation of fibroblast growth factor receptor-1 occupancy and signaling by cell surface-associated syndecans and glypican. *Journal of Cell Biology* 1996; **133**(2): 405-16.

60. Lander AD. Proteoglycans: master regulators of molecular encounter? *Matrix Biology* 1998; **17**(7): 465-72.

61. Saunders S, Jalkanen M, O'Farrell S, and Bernfield M. Molecular cloning of syndecan, an integral membrane proteoglycan. *Journal of Cell Biology* 1989; **108**: 1547-56.

62. Hsueh YP, Wang TF, Yang FC, and Sheng M. Nuclear translocation and transcription regulation by the membrane-associated guanylate kinase CASK/LIN-2. *Nature* 2000; **404**(6775): 298-302.

63. Woods A and Couchman JR. Syndecan-4 heparan sulfate proteoglycan is a selectively enriched and widespread focal adhesion component. *Molecular Biology Of The Cell* 1994; **5**(2): 183-92.

64. Rapraeger A, Jalkanen M, and Bernfield M. Cell surface proteoglycan associates with the cytoskeleton at the basolateral cell surface of mouse mammary epithelial cells. *Journal of Cell Biology* 1986; **103**(6 Pt 2): 2683-96.

65. Couchman J. Syndecans: proteoglycan regulators of cell-surface microdomains? *Nature Reviews Molecular Cell Biology* 2003; **4**(12): 926-37.

66. McFall AJ and Rapraeger AC. Identification of an adhesion site within the syndecan-4 extracellular protein domain. *Journal of Biological Chemistry* 1997; **272**(20): 12901-4.

67. McFall AJ and Rapraeger AC. Characterization of the high affinity cell-binding domain in the cell surface proteoglycan syndecan-4. *Journal of Biological Chemistry* 1998; **273**(43): 28270-6.

68. Bernfield M, et al. Biology of the syndecans: a family of transmembrane heparan sulfate proteoglycans. *Annual Review of Cell Biology* 1992; **8**: 365-93.

69. Esko JD and Selleck SB. Order out of chaos: assembly of ligand binding sites in heparan sulfate. *Annual Review of Biochemistry* 2002; **71**(1): 435-71.

70. Kato M, et al. Physiological degradation converts the soluble syndecan-1 ectodomain from an inhibitor to a potent activator of FGF-2. *Nature Medicine* 1998; **4**(6): 691-7.

71. Subramanian SV, Fitzgerald ML, and Bernfield M. Regulated shedding of syndecan-1 and -4 ectodomains by thrombin and growth factor receptor activation. *Journal of Biological Chemistry* 1997; **272**(23): 14713-20.

72. Kainulainen V, Wang H, Schick C, and Bernfield M. Syndecans, heparan sulfate proteoglycans, maintain the proteolytic balance of acute wound fluids. *Journal of Biological Chemistry* 1998; **273**(19): 11563-9.

73. Floris S, van den Born J, van der Pol SM, Dijkstra CD, and De Vries HE. Heparan sulfate proteoglycans modulate monocyte migration across cerebral endothelium. *Journal of Neuropathology & Experimental Neurology* 2003; **62**(7): 780-90.

74. Rapraeger AC. Molecular interactions of syndecans during development. *Seminars in Cell & Developmental Biology* 2001; **12**(2): 107-16.

75. Zimmermann P and David G. The syndecans, tuners of transmembrane signaling. *FASEB Journal* 1999; **13**(Suppl): S91-S100.

76. Woods A, Longley RL, Tumova S, and Couchman JR. Syndecan-4 binding to the high affinity heparin-binding domain of fibronectin drives focal adhesion formation in fibroblasts. *Archives of Biochemistry & Biophysics* 2000; **374**(1): 66-72.

77. Baciu PC and Goetinck PF. Protein kinase C regulates the recruitment of syndecan 4 into focal contacts. *Molecular Biology Of The Cell* 1995; **6**(11): 1503-13.

78. Woods A and Couchman JR. Syndecan-4 and focal adhesion function. *Current Opinion in Cell Biology* 2001; **13**(5): 578-83.

79. Wilcox-Adelman SA, Denhez F, and Goetinck PF. Syndecan-4 modulates focal adhesion kinase phosphorylation. *Journal of Biological Chemistry* 2002; **277**(36): 32970-7.

80. Chon JH and Chaikof EL. Soluble heparin-binding peptides regulate chemokinesis and cell adhesive forces. *American Journal of Physiology - Cell Physiology* 2001; **280**(6): C1394-402.

81. Chon JH and Chaikof EL. A von Willebrand factor-derived heparin-binding peptide regulates cell--substrate adhesive strength and chemokinesis behavior. *Biochimica et Biophysica Acta* 2002; **1542**(1-3): 195-208.

82. Li L and Chaikof EL. Mechanical stress regulates syndecan-4 expression and redistribution in vascular smooth muscle cells. *Arteriosclerosis, Thrombosis & Vascular Biology* 2002; **22**(1): 61-8.

83. Thodeti CK, et al. ADAM12/syndecan-4 signaling promotes β_1 integrin-dependent cell spreading through protein kinase Cα and RhoA. *Journal of Biological Chemistry* 2003; **278**(11): 9576-84.

84. Couchman JR, Chen L, and Woods A. Syndecans and cell adhesion. *International Review of Cytology* 2001; **207**: 113-50.

85. Gao Y, Li M, Chen W, and Simons M. Synectin, syndecan-4 cytoplasmic domain binding PDZ protein, inhibits cell migration. *Journal of Cellular Physiology* 2000; **184**(3): 373-9.

86. Tumova S, Woods A, and Couchman JR. Heparan sulfate proteoglycans on the cell surface: versatile coordinators of cellular functions. *International Journal of Biochemistry & Cell Biology* 2000; **32**(3): 269-88.

87. Couchman JR and Woods A. Syndecan-4 and integrins: combinatorial signaling in cell adhesion. *Journal of Cell Science* 1999; **112**(Pt 20): 3415-20.

88. Horowitz A and Simons M. Phosphorylation of the cytoplasmic tail of syndecan-4 regulates activation of protein kinase Cα. *Journal of Biological Chemistry* 1998; **273**(40): 25548-51.

89. Horowitz A, Murakami M, Gao Y, and Simons M. Phosphatidylinositol-4,5-bisphosphate mediates the interaction of syndecan-4 with protein kinase C. *Biochemistry* 1999; **38**(48): 15871-7.

90. Lee D, Oh ES, Woods A, Couchman JR, and Lee W. Solution structure of a syndecan-4 cytoplasmic domain and its interaction with phosphatidylinositol 4,5-bisphosphate. *Journal of Biological Chemistry* 1998; **273**(21): 13022-9.

91. Oh ES, Woods A, and Couchman JR. Syndecan-4 proteoglycan regulates the distribution and activity of protein kinase C. *Journal of Biological Chemistry* 1997; **272**(13): 8133-6.

92. Oh ES, Woods A, Lim ST, Theibert AW, and Couchman JR. Syndecan-4 proteoglycan cytoplasmic domain and phosphatidylinositol 4,5-bisphosphate

coordinately regulate protein kinase C activity. *Journal of Biological Chemistry* 1998; **273**(17): 10624-9.

93. Volk R, Schwartz JJ, Li J, Rosenberg RD, and Simons M. The role of syndecan cytoplasmic domain in basic fibroblast growth factor-dependent signal transduction. *Journal of Biological Chemistry* 1999; **274**(34): 24417-24.

94. McKeever PE and Gee JB. Methods of study agents affecting pulmonary alveolar macrophage adherence: rinsing and centrifugation. *Journal of the Reticuloendothelial Society* 1975; **18**(4): 221-9.

95. Prechtel K, et al. Dynamic force spectroscopy to probe adhesion strength of living cells. *Physical Review Letters* 2002; **89**(2): 28-101.

96. Reyes CD and Garcia AJ. A centrifugation cell adhesion assay for high-throughput screening of biomaterial surfaces. *Journal of Biomedical Materials Research* 2003; **67A**(1): 328-33.

97. van Kooten TG, Schakenraad JM, Van der Mei HC, and Busscher HJ. Development and use of a parallel-plate flow chamber for studying cellular adhesion to solid surfaces. *Journal of Biomedical Materials Research* 1992; **26**(6): 725-38.

98. Garcia AJ, Ducheyne P, and Boettiger D. Quantification of cell adhesion using a spinning disc device and application to surface-reactive materials. *Biomaterials* 1997; **18**(16): 1091-8.

99. Abercrombie M, Heaysman JE, and Pegrum SM. The locomotion of fibroblasts in culture. IV. Electron microscopy of the leading lamella. *Experimental Cell Research* 1971; **67**(2): 359-67.

100. Izzard CS and Lochner LR. Cell-to-substrate contacts in living fibroblasts: an interference reflexion study with an evaluation of the technique. *Journal of Cell Science* 1976; **21**(1): 129-59.

101. Cavallaro U and Christofori G. Cell adhesion and signaling by cadherens and Ig-CAMs in cancer. *Nature Reviews Cancer* 2004; **4**(2): 118-32.

102. Osterud B and Bjorklid E. Role of monocytes in atherogenesis. *Physiological Reviews* 2003; **83**(4): 1069-112.

103. van der Flier A and Sonnenberg A. Function and interactions of integrins. *Cell & Tissue Research* 2001; **305**(3): 285-98.

104. Palecek SP, Loftus JC, Ginsberg MH, Lauffenburger DA, and Horwitz AF. Integrin-ligand binding properties govern cell migration speed through cell-substratum adhesiveness. *Nature* 1997; **385**(6616): 537-40.

105. Woods A and Couchman JR. Protein kinase C involvement in focal adhesion formation. *Journal of Cell Science* 1992; **101**(Pt 2): 277-90.

106. Ishiguro K, et al. Syndecan-4 deficiency impairs focal adhesion formation only under restricted conditions. *Journal of Biological Chemistry* 2000; **275**(8): 5249-52.

107. Iba K, et al. The cysteine-rich domain of human ADAM 12 supports cell adhesion through syndecans and triggers signaling events that lead to β_1 integrin-dependent cell spreading. *Journal of Cell Biology* 2000; **149**(5): 1143-56.

108. Saoncella S, et al. Syndecan-4 signals cooperatively with integrins in a Rho-dependent manner in the assembly of focal adhesions and actin stress fibers. *Proceedings of the National Academy of Sciences of the United States of America* 1999; **96**(6): 2805-10.

109. Moyano JV, et al. Cooperative role for activated $\alpha_4\beta_1$ integrin and chondroitin sulfate proteoglycans in cell adhesion to the heparin III domain of fibronectin. Identification of a novel heparin and cell binding sequence in repeat III5. *Journal of Biological Chemistry* 1999; **274**(1): 135-42.

110. Mostafavi-Pour Z, Askari JA, Whittard JD, and Humphries MJ. Identification of a novel heparin-binding site in the alternatively spliced IIICS region of fibronectin: roles of integrins and proteoglycans in cell adhesion to fibronectin splice variants. *Matrix Biology* 2001; **20**(1): 63-73.

111. Woods A, Oh ES, and Couchman JR. Syndecan proteoglycans and cell adhesion. *Matrix Biology* 1998; **17**(7): 477-83.

112. Thomas SM and Brugge JS. Cellular functions regulated by Src family kinases. *Annual Review of Cell & Developmental Biology* 1997; **13**: 513-609.

113. Burridge K and Chrzanowska-Wodnicka M. Focal adhesions, contractility, and signaling. *Annual Review of Cell & Developmental Biology* 1996; **12**: 463-518.

114. Ross R. The pathogenesis of atherosclerosis: a perspective for the 1990s. *Nature* 1993; **362**(6423): 801-9.

115. Rothman A, et al. Development and characterization of a cloned rat pulmonary arterial smooth muscle cell line that maintains differentiated properties through multiple subcultures. *Circulation* 1992; **86**(6): 1977-86.

116. He TC, et al. A simplified system for generating recombinant adenoviruses. *Proceedings of the National Academy of Sciences of the United States of America* 1998; **95**(5): 2509-14.

117. Chon JH, Mediation of vascular smooth muscle cell adhesion and migration by cell surface heparan sulfate glycosaminoglycans. *Doctoral Thesis - School of Chemical Engineering* 1999, Georgia Institute of Technology, Atlanta. p. 159.

118. Natke B, Venkataraman G, Nugent MA, and Sasisekharan R. Heparinase treatment of bovine smooth muscle cells inhibits fibroblast growth factor-2 binding to fibroblast growth factor receptor but not FGF-2 mediated cellular proliferation. *Angiogenesis* 1999; **3**(3): 249-57.

119. Schriever C, Breithardt G, and Schmidt A. Undersulfation of proteoheparan sulfate stimulates the expression of basic fibroblast growth factor and protein synthesis but suppresses replication of coronary smooth muscle cells. *Biological Chemistry* 1997; **378**(7): 701-6.

120. Sperinde GV and Nugent MA. Heparan sulfate proteoglycans control intracellular processing of bFGF in vascular smooth muscle cells. *Biochemistry* 1998; **37**(38): 13153-64.

121. Shukla D, et al. A novel role for 3-O-sulfated heparan sulfate in herpes simplex virus 1 entry. *Cell* 1999; **99**(1): 13-22.

122. Couchman JR, Austria R, Woods A, and Hughes RC. Adhesion defective BHK cell mutant has cell surface heparan sulfate proteoglycan of altered properties. *Journal of Cellular Physiology* 1988; **136**(2): 226-36.

123. DiMilla PA, Stone JA, Quinn JA, Albelda SM, and Lauffenburger DA. Maximal migration of human smooth muscle cells on fibronectin and type IV collagen occurs at an intermediate attachment strength. *Journal of Cell Biology* 1993; **122**(3): 729-37.

124. Stepp MA, et al. Defects in keratinocyte activation during wound healing in the syndecan-1-deficient mouse. *Journal of Cell Science* 2002; **115**(Pt 23): 4517-31.

125. Gotte M, et al. Role of syndecan-1 in leukocyte-endothelial interactions in the ocular vasculature. *Investive Ophthalmology and Visual Science* 2002; **43**(4): 1135-41.

126. Echtermeyer F, et al. Delayed wound repair and impaired angiogenesis in mice lacking syndecan-4. *Journal of Clinical Investigation* 2001; **107**: R0-R14.

127. Kato M, Saunders S, Nguyen H, and Bernfield M. Loss of cell surface syndecan-1 causes epithelia to transform into anchorage-independent mesenchyme-like cells. *Molecular Biology of the Cell* 1995; **6**(5): 559-76.

128. McClay DR, Wessel GM, and Marchase RB. Intercellular recognition: quantitation of initial binding events. *Proceedings of the National Academy of Sciences of the United States of America* 1981; **78**(8): 4975-9.

129. Giacomello E, Neumayer J, Colombatti A, and Perris R. Centrifugal assay for fluorescence-based cell adhesion adapted to the analysis of ex vivo cells and capable of determining relative binding strengths. *Biotechniques* 1999; **26**(4): 758-62, 64-6.

130. Keselowsky BG, Collard DM, and Garcia AJ. Surface chemistry modulates fibronectin conformation and directs integrin binding and specificity to control cell adhesion. *Journal of Biomedical Materials Research* 2003; **66A**(2): 247-59.

131. Tozeren A, Sung KL, and Chien S. Theoretical and experimental studies on cross-bridge migration during cell disaggregation. *Biophysical Journal* 1989; **55**(3): 479-87.

132. Evans E, Berk D, and Leung A. Detachment of agglutinin-bonded red blood cells. I. Forces to rupture molecular-point attachments. *Biophysical Journal* 1991; **59**(4): 838-48.

133. Litvinov RI, Shuman H, Bennett JS, and Weisel JW. Binding strength and activation state of single fibrinogen-integrin pairs on living cells. *Proceedings of the National Academy of Sciences of the United States of America* 2002; **99**(11): 7426-31.

134. Doroszewski J, Skierski J, and Przadka L. Interaction of neoplastic cells with glass surface under flow conditions. *Experimental Cell Research* 1977; **104**(2): 335-43.

135. Truskey GA and Pirone JS. The effect of fluid shear stress upon cell adhesion to fibronectin-treated surfaces. *Journal of Biomedical Materials Research* 1990; **24**(10): 1333-53.

136. Horbett TA, Waldburger JJ, Ratner BD, and Hoffman AS. Cell adhesion to a series of hydrophilic-hydrophobic copolymers studied with a spinning disc apparatus. *Journal of Biomedical Materials Research* 1988; **22**(5): 383-404.

137. Garcia AJ, Huber F, and Boettiger D. Force required to break $\alpha_5\beta_1$ integrin-fibronectin bonds in intact adherent cells is sensitive to integrin activation state. *Journal of Biological Chemistry* 1998; **273**(18): 10988-93.

138. Fowler HW and McKay AJ. A method for evaluating the adhesion of cells to surfaces. *Journal of Pharmacy and Pharmacology* 1979; **31**(Suppl): 103P.

139. Cozens-Roberts C, Quinn JA, and Lauffenberger DA. Receptor-mediated adhesion phenomena. Model studies with the Radical-Flow Detachment Assay. *Biophysical Journal* 1990; **58**(1): 107-25.

140. Cozens-Roberts C, Quinn JA, and Lauffenburger DA. Receptor-mediated cell attachment and detachment kinetics. II. Experimental model studies with the radial-flow detachment assay. *Biophysical Journal* 1990; **58**(4): 857-72.

141. Garcia AJ and Gallant ND. Stick and grip: measurement systems and quantitative analyses of integrin-mediated cell adhesion strength. *Cell Biochemistry and Biophysics* 2003; **39**(1): 61-73.

142. Ivanov D, Philippova M, Tkachuk V, Erne P, and Resink T. Cell adhesion molecule T-cadherin regulates vascular cell adhesion, phenotype and motility. *Experimental Cell Research* 2004; **293**(2): 207-18.

143. Woods A and Couchman JR. Syndecans: synergistic activators of cell adhesion. *Trends in Cell Biology* 1998; **8**(5): 189-92.

144. Thyberg J, Blomgren K, Roy J, Tran PK, and Hedin U. Phenotypic Modulation of Smooth Muscle Cells after Arterial Injury Is Associated with Changes in the Distribution of Laminin and Fibronectin. *Journal of Histochemistry & Cytochemistry* 1997; **45**(6): 837-46.

145. Koyama N, Kinsella MG, Wight TN, Hedin U, and Clowes AW. Heparan Sulfate Proteoglycans Mediate a Potent Inhibitory Signal for Migration of Vascular Smooth Muscle Cells. *Circulation Research* 1998; **83**(3): 305-13.

146. Roy CS. The elastic properties of the arterial wall. *Journal of Physiology (London)* 1880-1882; **3**: 125-59.

147. Brossollet LJ and Vito RP. An alternate formulation of blood vessel mechanics and the meaning of the in vivo property. *Journal of Biomechanics* 1995; **28**(6): 679-87.

148. Durante W, Liao L, Reyna SV, Peyton KJ, and Schafer AI. Physiological cyclic stretch directs L-arginine transport and metabolism to collagen synthesis in vascular smooth muscle. *FASEB Journal* 2000; **14**(12): 1775-83.

149. Goldschmidt ME, McLeod KJ, and Taylor WR. Integrin-mediated mechanotransduction in vascular smooth muscle cells: frequency and force response characteristics. *Circulation Research* 2001; **88**(7): 674-80.

150. Smith PG, Garcia R, and Kogerman L. Mechanical strain increases protein tyrosine phosphorylation in airway smooth muscle cells. *Experimental Cell Research* 1998; **239**(2): 353-60.

151. Yano Y, Geibel J, and Sumpio BE. Cyclic strain induces reorganization of integrin $\alpha_5\beta_1$ and $\alpha_2\beta_1$ in human umbilical vein endothelial cells. *Journal of Cellular Biochemistry* 1997; **64**(3): 505-13.

152. Oguchi S, et al. Monoclonal antibody against vascular cell adhesion molecule-1 inhibits neointimal formation after periadventitial carotid artery injury in genetically hypercholesterolemic mice. *Arteriosclerosis, Thrombosis & Vascular Biology* 2000; **20**(7): 1729-36.

153. Castillo JL, Delgado V, Ramirez J, and Urdaneta K, Biofluid dynamics of cardiopulmonary bypass surgery, in *Congress on Biofluid Dynamics of Human Body Systems* 2003. Miami, FL.

154. Lyon M and Gallagher JT. Bio-specific sequences and domains in heparan sulphate and the regulation of cell growth and adhesion. *Matrix Biology* 1998; **17**(7): 485-93.

155. Sumpio BE and Banes AJ. Response of porcine aortic smooth muscle cells to cyclic tensional deformation in culture. *Journal of Surgical Research* 1988; **44**(6): 696-701.

156. Wiersbitzky M, Mills I, Sumpio BE, and Gewirtz H. Chronic cyclic strain reduces adenylate cyclase activity and stimulatory G protein subunit levels in coronary smooth muscle cells. *Experimental Cell Research* 1994; **210**(1): 52-5.

157. Li W, Chen Q, Mills I, and Sumpio BE. Involvement of S6 kinase and p38 mitogen activated protein kinase pathways in strain-induced alignment and proliferation of bovine aortic smooth muscle cells. *Journal of Cellular Physiology* 2003; **195**(2): 202-9.

158. Liu X, Hymel LJ, and Songu-Mize E. Role of Na+ and Ca2+ in stretch-induced Na+-K+-ATPase α-subunit regulation in aortic smooth muscle cells. *American Journal of Physiology - Heart & Circulatory Physiology* 1998; **274**(1): H83-89.

159. Songu-Mize E, Liu X, and Hymel LJ. Effect of mechanical strain on expression of Na+,K+-ATPase α-subunits in rat aortic smooth muscle cells. *American Journal of the Medical Sciences* 1998; **316**(3): 196-9.

160. Songu-Mize E, Liu X, Stones JE, and Hymel LJ. Regulation of Na+,K+-ATPase α-subunit expression by mechanical strain in aortic smooth muscle cells. *Hypertension* 1996; **27**(3): 827-32.

161. Sevieux N, Alam J, and Songu-Mize E. Effect of cyclic stretch on α-subunit mRNA expression of Na+-K+-ATPase in aortic smooth muscle cells. *American Journal of Physiology - Cell Physiology* 2001; **280**(6): C1555-60.

162. Hung CT and Williams JL. A method for inducing equi-biaxial and uniform strains in elastomeric membranes used as cell substrates. *Journal of Biomechanics* 1994; **27**(2): 227-32.

163. Schaffer JL, et al. Device for the application of a dynamic biaxially uniform and isotropic strain to a flexible cell culture membrane. *Journal of Orthopaedic Research* 1994; **12**(5): 709-19.

164. Li L, et al. Regulation of syndecan-4 expression with mechanical stress during the development of angioplasty-induced intimal thickening. *Journal of Vascular Surgery* 2002; **36**: 361-70.

165. Chen Q, Li W, Quan Z, and Sumpio BE. Modulation of vascular smooth muscle cell alignment by cyclic strain is dependent on reactive oxygen species and P38 mitogen-activated protein kinase. *Journal of Vascular Surgery* 2003; **37**(3): 660-8.

166. Wijnen JA, et al. Vessel wall properties of large arteries in trained and sedentary subjects. *Basic Research in Cardiology* 1991; **86**(Suppl 1): 25-9.

167. Glagov S, Zarins C, Giddens DP, and Ku DN. Hemodynamics and atherosclerosis. Insights and perspectives gained from studies of human arteries. *Archives of Pathology and Laboratory Medicine* 1988; **112**(10): 1018-31.

168. Stanley MJ, Liebersbach BF, Liu W, Anhalt DJ, and Sanderson RD. Heparan sulfate-mediated cell aggregation. Syndecans-1 and -4 mediate intercellular adhesion following their transfection into human B lymphoid cells. *J Biol Chem* 1995; **270**(10): 5077-83.

169. Villena J, Berndt C, Granes F, Reina M, and Vilaro S. Syndecan-2 expression enhances adhesion and proliferation of stably transfected Swiss 3T3 cells. *Cell Biology International* 2003; **27**(12): 1005-10.

170. Munesue S, et al. The role of syndecan-2 in regulation of actin-cytoskeletal organization of Lewis lung carcinoma-derived metastatic clones. *Biochemical Journal* 2002; **363**(Pt 2): 201-9.

171. Cheng GC, et al. Mechanical strain tightly controls fibroblast growth factor-2 release from cultured human vascular smooth muscle cells. *Circulation Research* 1997; **80**(1): 28-36.

172. Dobrin PB. Mechanical properties of arteries. *Physiological Reviews* 1978; **58**(2): 397-460.

173. Brighton CT, et al. The proliferative and synthetic response of isolated calvarial bone cells of rats to cyclic biaxial mechanical strain. *Journal of Bone and Joint Surgery* 1991; **73**(3): 320-31.

174. Williams JL, Chen JH, and Belloli DM. Strain fields on cell stressing devices employing clamped circular elastic diaphragms as substrates. *Journal of Biomechanical Engineering* 1992; **114**(3): 377-84.

175. Banes AJ, Gilbert J, Taylor D, and Monbureau O. A new vacuum-operated stress-providing instrument that applies static or variable duration cyclic tension or compression to cells in vitro. *Journal of Cell Science* 1985; **75**: 35-42.

176. Gorfien SF, Winston FK, Thibault LE, and Macarak EJ. Effects of biaxial deformation on pulmonary artery endothelial cells. *Journal of Cellular Physiology* 1989; **139**(3): 492-500.

177. Winston FK, Macarak EJ, Gorfien SF, and Thibault LE. A system to reproduce and quantify the biomechanical environment of the cell. *Journal of Applied Physiology* 1989; **67**(1): 397-405.

178. Leung DY, Glagov S, and Mathews MB. A new in vitro system for studying cell response to mechanical stimulation. Different effects of cyclic stretching and agitation on smooth muscle cell biosynthesis. *Experimental Cell Research* 1977; **109**(2): 285-98.

179. Meikle MC, Reynolds JJ, Sellers A, and Dingle JT. Rabbit cranial sutures in vitro: a new experimental model for studying the response of fibrous joints to mechanical stress. *Calcified Tissue International* 1979; **28**(2): 137-44.

180. Hasegawa S, Sato S, Saito S, Suzuki Y, and Brunette DM. Mechanical stretching increases the number of cultured bone cells synthesizing DNA and alters their pattern of protein synthesis. *Calcified Tissue International* 1985; **37**(4): 431-6.

181. Brown TD, Bottlang M, Pedersen DR, and Banes AJ. Loading paradigms--intentional and unintentional--for cell culture mechanostimulus. *American Journal of the Medical Sciences* 1998; **316**(3): 162-8.

182. Howe A, Aplin AE, Alahari SK, and Juliano RL. Integrin signaling and cell growth control. *Current Opinion in Cell Biology* 1998; **10**(2): 220-31.

183. Giancotti FG and Ruoslahti E. Integrin signaling. *Science* 1999; **285**(5430): 1028-32.

184. Fuller B. Tensegrity. *Portfolio Artnews Annual* 1961; **4**: 112-27.

185. Stamenovic D, Fredberg JJ, Wang N, Butler JP, and Ingber DE. A microstructural approach to cytoskeletal mechanics based on tensegrity. *Journal of Theoretical Biology* 1996; **181**(2): 125-36.

186. Ingber DE. Tensegrity: the architectural basis of cellular mechanotransduction. *Annual Review of Physiology* 1997; **59**(1): 575-99.

187. Chicurel ME, Chen CS, and Ingber DE. Cellular control lies in the balance of forces. *Current Opinion in Cell Biology* 1998; **10**(2): 232-9.

188. Chicurel ME, Singer RH, Meyer CJ, and Ingber DE. Integrin binding and mechanical tension induce movement of mRNA and ribosomes to focal adhesions. *Nature* 1998; **392**(6677): 730-3.

189. Ingber DE. The architecture of life. *Scientific American* 1998; **278**(1): 48-57.

190. Ingber DE. Cellular basis of mechanotransduction. *Biology Bulletin* 1998; **194**(3): 323-7.

191. Pourati J, et al. Is cytoskeletal tension a major determinant of cell deformability in adherent endothelial cells? *American Journal of Physiology - Cell Physiology* 1998; **274**(5): C1283-89.

192. Ingber DE, Heidemann SR, Lamoureux P, and Buxbaum RE. Opposing views on tensegrity as a structural framework for understanding cell mechanics. *Journal of Applied Physiology* 2000; **89**(4): 1663-78.

193. Ingber DE. Tensegrity I. Cell structure and hierarchical systems biology. *Journal of Cell Science* 2003; **116**(7): 1157-73.

194. Ingber DE. Tensegrity II. How structural networks influence cellular information processing networks. *Journal of Cell Science* 2003; **116**(8): 1397-408.

195. Theret DP, Levesque MJ, Sato M, Nerem RM, and Wheeler LT. The application of a homogeneous half-space model in the analysis of endothelial cell micropipette measurements. *Journal of Biomechanical Engineering* 1988; **110**(3): 190-9.

196. Sato M, Theret DP, Wheeler LT, Ohshima N, and Nerem RM. Application of the micropipette technique to the measurement of cultured porcine aortic endothelial cell viscoelastic properties. *Journal of Biomechanical Engineering* 1990; **112**(3): 263-8.

197. Sato M, Ohshima N, and Nerem RM. Viscoelastic properties of cultured porcine aortic endothelial cells exposed to shear stress. *Journal of Biomechanics* 1996; **29**(4): 461-67.

198. Sato M, Levesque MJ, and Nerem RM. An application of the micropipette technique to the measurement of the mechanical properties of cultured bovine aortic endothelial cells. *Journal of Biomechanical Engineering* 1987; **109**(1): 27-34.

199. Wang N, Butler JP, and Ingber DE. Mechanotransduction across the cell surface and through the cytoskeleton. *Science* 1993; **260**(5111): 1124-27.

200. Wang N, et al. Cell prestress. I. Stiffness and prestress are closely associated in adherent contractile cells. *American Journal of Physiology - Cell Physiology* 2002; **282**(3): C606-16.

201. Xu J, Tseng Y, and Wirtz D. Strain hardening of actin filament networks. Regulation by the dynamic cross-linking protein α-actinin. *Journal of Biological Chemistry* 2000; **275**(46): 35886-92.

202. Kaverina I, et al. Tensile stress stimulates microtubule outgrowth in living cells. *Journal of Cell Science* 2002; **115**(Pt 11): 2283-91.

203. Putnam AJ, Schultz K, and Mooney DJ. Control of microtubule assembly by extracellular matrix and externally applied strain. *American Journal of Physiology - Cell Physiology* 2001; **280**(3): C556-64.

204. Smith PG, Garcia R, and Kogerman L. Strain reorganizes focal adhesions and cytoskeleton in cultured airway smooth muscle cells. *Experimental Cell Research* 1997; **232**(1): 127-36.

205. Smith PG, Deng L, Fredberg JJ, and Maksym GN. Mechanical strain increases cell stiffness through cytoskeletal filament reorganization. *American Journal of Physiology - Lung Cellular and Molecular Physiology* 2003; **285**(2): L456-63.

206. An SS, Laudadio RE, Lai J, Rogers RA, and Fredberg JJ. Stiffness changes in cultured airway smooth muscle cells. *American Journal of Physiology - Cell Physiology* 2002; **283**(3): C792-801.

207. Jo H, et al. Differential effect of shear stress on extracellular signal-regulated kinase and N-terminal Jun kinase in endothelial cells. G_{i2}- and $G_{\beta\gamma}$-dependent signaling pathways. *Journal of Biological Chemistry* 1997; **272**(2): 1395-401.

208. Li C, Hu Y, Sturm G, Wick G, and Xu Q. Ras/Rac-dependent activation of p38 mitogen-activated protein kinases in smooth muscle cells stimulated by cyclic strain stress. *Arteriosclerosis, Thrombosis & Vascular Biology* 2000; **20**(3): E1-E9.

209. Rubin J, Murphy TC, Fan X, Goldschmidt M, and Taylor WR. Activation of extracellular signal-regulated kinase is involved in mechanical strain inhibition of RANKL expression in bone stromal cells. *Journal of Bone & Mineral Research* 2002; **17**(8): 1452-60.

210. Ge X, Fu Y-M, and Meadows GG. U0126, a mitogen-activated protein kinase kinase inhibitor, inhibits the invasion of human A375 melanoma cells. *Cancer Letters* 2002; **179**(2): 133-40.

211. LoGrasso PV, et al. Kinetic mechanism for p38 MAP kinase. *Biochemistry* 1997; **36**(34): 10422-7.

212. Barr RK, Kendrick TS, and Bogoyevitch MA. Identification of the critical features of a small peptide inhibitor of JNK activity. *Journal of Biological Chemistry* 2002; **277**(13): 10987-97.

213. Bonny C, Oberson A, Negri S, Sauser C, and Schorderet DF. Cell-permeable peptide inhibitors of JNK: novel blockers of β-cell death. *Diabetes* 2001; **50**(1): 77-82.

214. Houston M, Julien MA, Parthasarathy S, and Chaikof EL. Oxidized fatty acids regulate expression and shedding of syndecan 4. *American Journal of Physiology - Cell Physiology* 2005; **288**(2): C458-66.

215. Fitzgerald ML, Wang Z, Park PW, Murphy G, and Bernfield M. Shedding of syndecan-1 and -4 ectodomains is regulated by multiple signaling pathways and mediated by a TIMP-3-sensitive metalloproteinase. *Journal of Cell Biology* 2000; **148**(4): 811-24.

216. Osenkowski P, Toth M, and Fridman R. Processing, shedding, and endocytosis of membrane type 1-matrix metalloproteinase (MT1-MMP). *Journal of Cell Physiology* 2004; **200**(1): 2-10.

217. Blobel CP. Functional and biochemical characterization of ADAMs and their predicted role in protein ectodomain shedding. *Inflammation Research* 2002; **51**(2): 83-4.

218. Moss ML and Lambert MH. Shedding of membrane proteins by ADAM family proteases. *Essays in Biochemistry* 2002; **38**: 141-53.

219. Li Q, Park PW, Wilson CL, and Parks WC. Matrilysin shedding of syndecan-1 regulates chemokine mobilization and transepithelial efflux of neutrophils in acute lung injury. *Cell* 2002; **111**(5): 635-46.

220. Park PW, et al. Syndecan-1 shedding is enhanced by LasA, a secreted virulence factor of Pseudomonas aeruginosa. *Journal of Biological Chemistry* 2000; **275**(5): 3057-64.

221. Reiland J, et al. Heparanase degrades syndecan-1 and perlecan heparan sulfate: functional implications for tumor cell invation. *Journal of Biological Chemistry* 2004; **279**(9): 8047-55.

222. Rioux V, Landry RY, and Bensadoun A. Sandwich immunoassay for the measurement of murine syndecan-4. *Journal of Lipid Research* 2002; **43**(1): 167-73.

223. Favata MF, et al. Identification of a novel inhibitor of mitogen-activated protein kinase kinase. *Journal of Biological Chemistry* 1998; **273**(29): 18623-32.

224. Young PR, et al. Pyridinyl imidazole inhibitors of p38 mitogen-activated protein kinase bind in the ATP site. *Journal of Biological Chemistry* 1997; **272**(18): 12116-21.

225. Endo K, et al. Cleavage of syndecan-1 by membrane type matrix metalloproteinase-1 stimulates cell migration. *Journal of Biological Chemistry* 2003; **278**(42): 40764-70.

226. Asundi VK, Erdman R, Stahl RC, and Carey DJ. Matrix metalloproteinase-dependent shedding of syndecan-3, a transmembrane heparan sulfate proteoglycan, in Schwann cells. *Journal of Neuroscience Research* 2003; **73**(5): 593-602.

227. Black RA and White JM. ADAMs: focus on the protease domain. *Current Opinion in Cell Biology* 1998; **10**(5): 654-9.

228. Primakoff P and Myles DG. The ADAM gene family: surface proteins with adhesion and protease activity. *Trends in Genetics* 2000; **16**(2): 83-87.

229. Holen I, Drury NL, Hargreaves PG, and Croucher PI. Evidence of a role for a non-matrix-type metalloproteinase activity in the shedding of syndecan-1 from human myeloma cells. *British Journal of Haematology* 2001; **114**(2): 414-21.

230. Herren B. ADAM-mediated shedding and adhesion: a vascular perspective. *News in Physiological Sciences* 2002; **17**(2): 73-76.

231. Hernandez-Barrantes S, Bernardo M, Toth M, and Fridman R. Regulation of membrane type-matrix metalloproteinases. *Seminars in Cancer Biology* 2002; **12**(2): 131-38.

232. Seals DF and Courtneidge SA. The ADAMs family of metalloproteases: multidomain proteins with multiple functions. *Genes and Development* 2003; **17**(1): 7-30.

233. Zucker S, Pei D, Cao J, and Lopez-Otin C. Membrane type-matrix metalloproteinases (MT-MMP). *Current Topics in Developmental Biology* 2003; **54**: 1-74.

234. Duffy MJ, Lynn DJ, Lloyd AT, and O'Shea CM. The ADAMs family of proteins: from basic studies to potential clinical applications. *Thrombosis and Haemostasis* 2003; **89**(4): 622-31.

235. Moss ML and Bartsch JW. Therapeutic benefits from targeting of ADAM family members. *Biochemistry* 2004; **43**(23): 7227-35.

236. Schlondorff J and Blobel CP. Metalloprotease-disintegrins: modular proteins capable of promoting cell-cell interactions and triggering signals by protein-ectodomain shedding. *Journal of Cell Science* 1999; **112**(21): 3603-17.

237. Gechtman Z, Alonso JL, Raab G, Ingber DE, and Klagsbrun M. The shedding of membrane-anchored heparin-binding epidermal-like growth factor is regulated by the Raf/mitogen-activated protein kinase cascade and by cell adhesion and spreading. *Journal of Biological Chemistry* 1999; **274**(40): 28828-35.

238. Umata T, et al. A dual signaling cascade that regulates the ectodomain shedding of heparin-binding epidermal growth factor-like growth factor. *Journal of Biological Chemistry* 2001; **276**(32): 30475-82.

239. Xu K-P, et al. A role for MAP kinase in regulating ectodomain shedding of APLP2 in corneal epithelial cells. *American Journal of Physiology - Cell Physiology* 2001; **281**(2): C603-14.

240. Tsakadze NL, et al. Signals mediating cleavage of intercellular adhesion molecule-1. *American Journal of Physiology - Cell Physiology* 2004; **287**(1): C55-63.

241. Charnaux N, et al. RANTES (CCL5) induces a CCR5-dependent accelerated shedding of syndecan-1 (CD138) and syndecan-4 from HeLa cells and forms complexes with the shed ectodomains of these proteoglycans as well as with those of CD44. *Glycobiology* 2004; **In press**.

242. Park PW, et al. Activation of syndecan-1 ectodomain shedding by Staphylococcus aureus α-toxin and β-toxin. *Journal of Biological Chemistry* 2004; **279**(1): 251-58.

243. Reiland J, et al. Pervanadate activation of intracellular kinases leads to tyrosine phosphorylation and shedding of syndecan-1. *Biochemical Journal* 1996; **319**(Pt 1): 39-47.

244. Isales CM, Rosales OR, and Sumpio BE, *Mediators and mechanisms of cyclic strain and shear stress-induced vascular responses*, in Hemodynamic forces and vascular cell biology, Sumpio BE, Editor. 1993, R.G. Landes: Austin, Tex. p. 90-115.

245. Kakisis JD, Liapis CD, and Sumpio BE. Effects of cyclic strain on vascular cells. *Endothelium* 2004; **11**(1): 17-28.

246. Davis R. The mitogen-activated protein kinase signal transduction pathway. *Journal of Biological Chemistry* 1993; **268**(20): 14553-56.

247. Seger R and Krebs EG. The MAPK signaling cascade. *FASEB Journal* 1995; **9**(9): 726-35.

248. Campbell JS, et al. The MAP kinase cascade. *Recent Progress in Hormone Research* 1995; **50**: 131-59.

249. Tibbles LA and Woodgett JR. The stress-activated protein kinase pathways. *Cellular and Molecular Life Sciences* 1999; **55**(10): 1230-54.

250. Kyriakis JM, et al. The stress-activated protein kinase subfamily of c-Jun kinases. *Nature* 1994; **369**(6476): 156-60.

251. Izumi Y, et al. Gene transfer of dominant-negative mutants of extracellular signal-regulated kinase and c-Jun NH2-terminal kinase prevents neointimal formation in balloon-injured rat artery. *Circulation Research* 2001; **88**(11): 1120-26.

252. Sotoudeh M, et al. Induction of apoptosis in vascular smooth muscle cells by mechanical stretch. *American Journal of Physiology - Heart & Circulatory Physiology* 2002; **282**(5): H1709-16.

253. Zou Y, Hu Y, Metzler B, and Xu Q. Signal transduction in arteriosclerosis: mechanical stress-activated MAP kinases in vascular smooth muscle cells. *International Journal of Molecular Medicine* 1998; **1**(5): 827-34.

254. Cizmeci-Smith G, Langan E, Youkey J, Showalter LJ, and Carey DJ. Syndecan 4 is a primary-response gene induced by basic fibroblast growth factor and arterial injury in vascular smooth muscle cells. *Arteriosclerosis, Thrombosis & Vascular Biology* 1997; **17**(1): 172-80.

255. Bausch AR, Moller W, and Sackmann E. Measurement of Local Viscoelasticity and Forces in Living Cells by Magnetic Tweezers. *Biophysical Journal* 1999; **76**(1): 573-79.

256. Caelles C, Gonzalez-Sancho JM, and Munoz A. Nuclear hormone receptor antagonism with AP-1 by inhibition of the JNK pathway. *Genes and Development* 1997; **11**(24): 3351-64.

257. Lee HY, Walsh GL, Dawson MI, Hong WK, and Kurie JM. All-trans-retinoic acid inhibits Jun N-terminal kinase-dependent signaling pathways. *Journal of Biological Chemistry* 1998; **273**(12): 7066-71.

VITA

Mathéau A. Julien, son of Antoine and Mabel, was born in August of 1974 in a quiet suburb of Philadelphia, Pennsylvania, where spent his youth and adolescence. He attended high school at Chestnut Hill Academy, and during those years, he was heavily involved in soccer and swimming, as well as a number of honors classes and societies, including *cum laude*. He graduated second in his class from CHA in 1992, but not without first being bitten by the biomedical research bug. Mathéau was first exposed to this vector of Eastern Pennsylvania Encephalitis through his AP Biology class. This well-known condition is characterized by a chronic and progressive pursuit of scientific discovery. As a result, over the course of two summers while in high school, he worked in the laboratory of Drs. Brian Balin and Sidney Croul at the Medical College Pennsylvania-Hahnemann University Department of Pathology and Lab Medicine, investigating the attributes of an entirely different brain pathology – namely the characteristics of neurofibrillary tangles in Alzheimer's disease.

Mathéau then decided to come to Emory University for college, where he was selected into the Emory Scholars Program. At Emory, he focused his studies on a Biology and Physics double major, while remaining an avid soccer player and participating in various organizations, including Residence Life, Student Government and Voices of Inner Strength Gospel Choir. Of critical importance early in his time at Emory was his decision to seek membership to Alpha Phi Alpha Fraternity, Inc. Through his contribution to and experiences with the brotherhood of ΑΦΑ, he nurtured his appreciation of the true meaning of service to others. Throughout these swiftly passing college days, the fever associated with his encephalitis persisted. Mathéau therefore continued research in various labs at MCP-Hahnemann, Cornell, and Emory, and graduated Phi Beta Kappa from Emory College in 1996 with *high honors* for his thesis project involving the investigation of osteochondral lesions in the knee.

In time, as the neurological condition became systemic, Mathéau realized that his choice was simple. So he applied for and accepted an MD/PhD trainee position at Emory School of Medicine and Georgia Institute of Technology. And despite the relapsing fevers, he has enjoyed running 10K's, skydiving, and hiking. He embarked on his graduate work in the Bio-Molecular and Biomaterials Laboratory of Dr. Elliot Chaikof, which culminated in the successful defense of his doctoral thesis in Bioengineering in July 2004. Before embarking on this journey, Mathéau had the opportunity to perform in the Opening Ceremonies of the Atlanta Olympic Games. He and a small group were subsequently asked to perform again in London.

Fortunately, the natural history of EPE is such that it often manages to spare the heart. So while completing his undergraduate degree, Mathéau was able to realize when he had found the woman who would eventually become his wife. Mathéau married Pamela Daniels on Cape Cod, Massachusetts in June of 2001. In February of 2004, he and Pamela were blessed with the birth of their first child, Kéleb Daniels Julien; and they happily anticipate the arrival of the newest addition to their family in June of 2005.

Mathéau still checks his temperature every day.